Establishment of new human and mouse liver cancer models and their use to uncover the role of RNF43 and ZNRF3 in liver homeostasis and repair

Gianmarco Mastrogiovanni

Department of Genetics

University of Cambridge

This dissertation is submitted for the degree of

Doctor of Philosophy

Darwin College

May 2017

ABSTRACT

Primary liver cancer (PLC) is the second most common cause of cancer death worldwide, preceded only by lung cancer. Current models for PLC either fail to fully recapitulate tumour histology and architecture or are expensive, time consuming and do not allow for personalised drug testing.

During the first part of my PhD, I have collaborated with Dr. Laura Broutier in order to established a new 3D *in vitro* model system for liver cancer. Based on the current knowledge on organoid cultures, we have managed to establish a system to grow primary human liver cancer cells long-term (Broutier *et al.*, in press). Interestingly, the tumour-derived organoids (tumoroids) recapitulate the original tumour histology and genetic alterations and are also able to generate tumours in an *in vivo* xenograft mouse model after long-term expansion. Furthermore, we have shown that tumoroids can also be successfully used for drug testing, suggesting their use to devise new targeted therapy as well as personalised treatment strategies.

Current models to investigate the role of genes in cancer rely mostly on animal studies, which can be very time consuming and cost demanding, especially if resulting in negative outcomes. To overcome this issue, I have set up a protocol for introducing mutations in healthy human liver organoids using the CRISPR-Cas9 technology. Interestingly, after mutating *TP53*, *RNF43* and *ZNRF3* either alone or in combination, human organoids undergo genetic alterations and phenotypic changes that partially resemble the ones observed in tumoroids. This data suggests that this system could be used as a screening platform to study gene function before using animal models.

In the last part, I have further explored the role of RNF43 and ZNRF3 (R&Z) - two newly identified WNT pathway negative regulators mutated in many cancer types - in the liver using an *in vivo* mouse model. Interestingly, conditional deletion of *R&Z* specifically in adult mouse hepatocytes results metabolic changes that eventually lead to extensive liver damage. However, when the liver is challenged to regenerate in a chronic damage model, *R&Z* mutated livers fail to fully repair and show presence of multiple regenerative nodules. Later, livers develop either focal nodular hyperplasia and/or early hepatocellular carcinoma. These data suggest that R&Z have an important role in both liver metabolic homeostasis and liver regeneration and that their alteration can eventually lead to cancer formation.

To my family

Declaration

This dissertation is the result of my own work and includes nothing which is the outcome of work done in collaboration except as specified in the text and under “External contributions”.

Also, it is not substantially the same as any that I have submitted, or, is being concurrently submitted for a degree or diploma or other qualification at the University of Cambridge or any other University or similar. I further state that no substantial part of my dissertation has already been submitted, or, is being concurrently submitted for any such degree, diploma or other qualification at the University of Cambridge or any other University or similar institution.

This dissertation does not exceed the prescribed limit of 60.000 words.

Gianmarco Mastrogiovanni

May 2017

External contributions

The details about external contribution to the work presented in this thesis are as follow:

Dr. Laura Broutier performed isolation of all tumoroid lines (Figure 3.1) and IWP2 and Gefitinib drug testing experiments (Figure 3.5).

Mikel McKie performed preliminary analysis of human steatosis and NASH datasets for Figure 5.11.

Robert Arnes performed H&E staining.

Table of Contents

Table of Figures

List of Tables

Abbreviations

Acaa1a	Acetyl-Coenzyme A acyltransferase 1A
Acaa2	Acetyl-CoA Acyltransferase 2
Acadl	Acyl-CoA Dehydrogenase, Long Chain
Acot4	Acyl-CoA Thioesterase 4
AMP	adenosine monophosphate
Aqp9	Aquaporin 9
Akr1b10	Aldo-Keto Reductase Family 1 Member B10
Alb	Albumin
APC	Adenomatous polyposis coli
Aqp9	Aquaporin 9
ARID	AT-rich interactive domain
ARID1A	AT-rich interactive domain-containing protein 1 A
ARID1B	AT-rich interactive domain-containing protein 1 B
ARID2	AT-rich interactive domain-containing protein 2
ATCC	American Type Culture Collection
ATP	Adenosine triphosphate
ATR	Ataxia Telangiectasia And Rad3-Related Protein
AXIN1	Axis inhibitor 1
BAF	BRG1-associated factor
BPTF	Bromodomain PHD finger transcription factor
BRG1 / SMARCA4	SWI/SNF related, matrix associated, actin dependent regulator of chromatin, subfamily a, member 4
Cas9	CRISPR associated
Cas9n	CRISPR associated nickase
CCl4	Carbon tetrachloride
CHC	Combined HCC/CC
CK1	Casein kinase 1
CR	Chromatin remodelling
CRE	Causes recombination
CRISPR	Clustered Regularly Interspaced Short Palindromic Repeat
CTNNB1	Catenin (cadherin-associated protein), beta 1
Cyp2c39	Cytochrome P450, family 2, subfamily c, polypeptide 39

Cyp2e1	Cytochrome P450 2E1
Cyp7a1	Cytochrome P450 Family 7 Subfamily A Member 1
CV	Central vein
DDC	3,5-diethoxycarbonyl-1,4-dihydrocollidine
DEN	Diethylnitrosamine
Dkk	Dickkopf
DMSO	Dimethyl sulfoxide
DSB	Double-strand brake
DTT	DL-Dithiothreitol
EGF	Epidermal growth factor
ER	Estrogen receptor
EZH2	Enhancer of Zeste Homolog 2
Fads2	Fatty Acid Desaturase 2
Fasn	Fatty Acid Synthase
FGF10	Fibroblast growth factor 10
Fgf21	Fibroblast growth factor 21
FGFR1	Fibroblast growth factor receptor 1
FSK	Forskolin
Fz	Frizzled
GEM	Genetically engineered model
GFAP	Glial Fibrous Acidic Protein
GFP	Green fluorescence protein
gRNA	Guide RNA
GS	Glutamate synthetase
GSK3β	Glycogen synthase kinase 3-beta
CC	Cholangiocarcinoma
HCC	Hepatocellular carcinoma
HDR	Homology directed repair
HGF	Hepatocyte growth factor
Hmgcs	Hydroxymethylglutaryl-CoA synthase
HNF4α	Hepatocyte nuclear factor 4 alpha
Hsp90	Heat shock protein 90
IDH1	Isocitrate dehydrogenase 1
IRF2	Interferon regulatory factor 2
KO	Knock-out
KRAS	V-Ki-ras2 Kirsten rat sarcoma viral oncogene homolog
LEF/TCF	Lymphoid enhancer factor/ T-cell factor

LGR4/5/6	Leucine-Rich Repeat-Containing G Protein-Coupled Receptor 4/5/6
LoxP	Locus of crossing (x) over, P1
LRP5/6	Low Density Lipoprotein Receptor-Related Protein 5/6
MCDE	Methionine choline-deficient diet supplemented with ethionine
MDM2	Mouse double minute homologue 2
MLL3	Mixed-lineage leukemia 3
NAFLD	Non-alcoholic fatty liver disease
NASH	Non-alcoholic steatohepatits
NHEJ	Non-homologous end joining
Nic	Nicotinamide
NICD	Notch intracellular receptor domain
PAM	Protospacer adjacent motif
PBAF	Polybromo-associated BAF
PEG3	Paternally-expressed gene 3
PLC	Primary liver cancer
Porcn	Porcupine
PTEN	Phosphatase and Tensin Homolog
PV	Portal vein
R&Z	RNF43 and ZNRF3
Rb1	Retinoblastoma protein 1
RNF43	Ring finger protein 43
RSPO1	R-spondin 1
ROBO2	Roundabout homolog 2
ROS	Reactive oxygen species
sFRP	Secreted frizzled-related protein
Slc17a2	Solute Carrier Family 17 Member 2
SMAD4	Mothers against decapentaplegic homolog 4
Sox9	Sry-related HMG box 9
SWI/SNF	SWItch/Sucrose Non-Fermentable
TACE	Transarterial Chemoembolization
Tbx3	T-Box3
TCF4	Transcription Factor 4
Tcf7l2	Transcription Factor 7 Like 2
TERT	Telomerase reverse transcriptase
TGFβ	Transforming growth factor beta
TP53	Tumour protein p53
VEGFR	Vessel endothelial growth factor receptor

Wls	Wntless
WNT	Wingless/Integrated
WT	Wild type
ZNRF3	Zinc and ring finger 3

1. INTRODUCTION

1.1 Liver anatomy

The adult liver, the largest internal organ in the human body, performs a wide variety of functions ranging from metabolism and detoxification of harmful substances to protein synthesis and bile and urea production. The liver has two epithelial cell types, hepatocytes and cholangiocytes. The hepatocytes compose approximately 80% of the liver parenchyma and are responsible for most of its functions. Alternatively, cholangiocytes, or biliary duct cells, form the lining of the bile ducts. The role of the bile ducts is to collect and modify the bile produced by the hepatocytes and to transport it to the gallbladder for storage (Yoo, Lim, and Choi 2016).

Structurally, the liver is organized into hepatic lobules which represent the structural and functional unit of the tissue (Figure 1.1a, b) (Gehart and Clevers 2015). At the centre of the hepatic lobule there is the central vein (CV). The area surrounding the CV, or perivenous area, is also defined as zone 3 (Figure 1.1a, b). Here, perivenous hepatocytes surround the CV and expand radially up to the portal triads in an ordered fashion to form a roughly hexagonal shape. Portal triads can be found at the edges of the hexagon, are composed by the portal vein (PV), hepatic artery and bile duct. The area surrounding the PV, or periportal area, is identified as zone 1 (Figure 1.1a, b). The bile ducts connect to the liver parenchyma through the canal of Hering, which is lined by both cholangiocytes and hepatocytes and it is where progenitor cells are thought to reside (Figure 1.1b) (Lukacs-Kornek and Lammert 2017).

Of note, the liver lobule is also defined by distinct metabolic zonation with divergent hepatic function (Figure 1.1c) (Gebhardt 2014). For instance, gluconeogenesis and β-oxidation are performed in the periportal area, whereas glycolysis and lipogenesis are carried out in the perivenous area. Hepatocytes within these regions also show unique gene expression patterns reflecting their diverse functions. The molecular basis of the metabolic zonation is not fully understood, however, the CV has been described as a source of WNT ligands (Gebhardt 2014). This CV secreted WNT causes expression of common WNT target genes such as *Axin2*, but also liver-specific ones, such as Glutamate Synthetase (*GS* – responsible for the synthesis of glutamine) and Cytochrome p450 (*Cyp2e1* – involved in the metabolism of drugs and xenobiotics). In

the absence of WNT, *Arginase1* (involved in the synthesis of urea) and *Glutaminase2* (involved in the hydrolysis of glutamine) are exclusively expressed in the periportal region (Benhamouche et al. 2006).

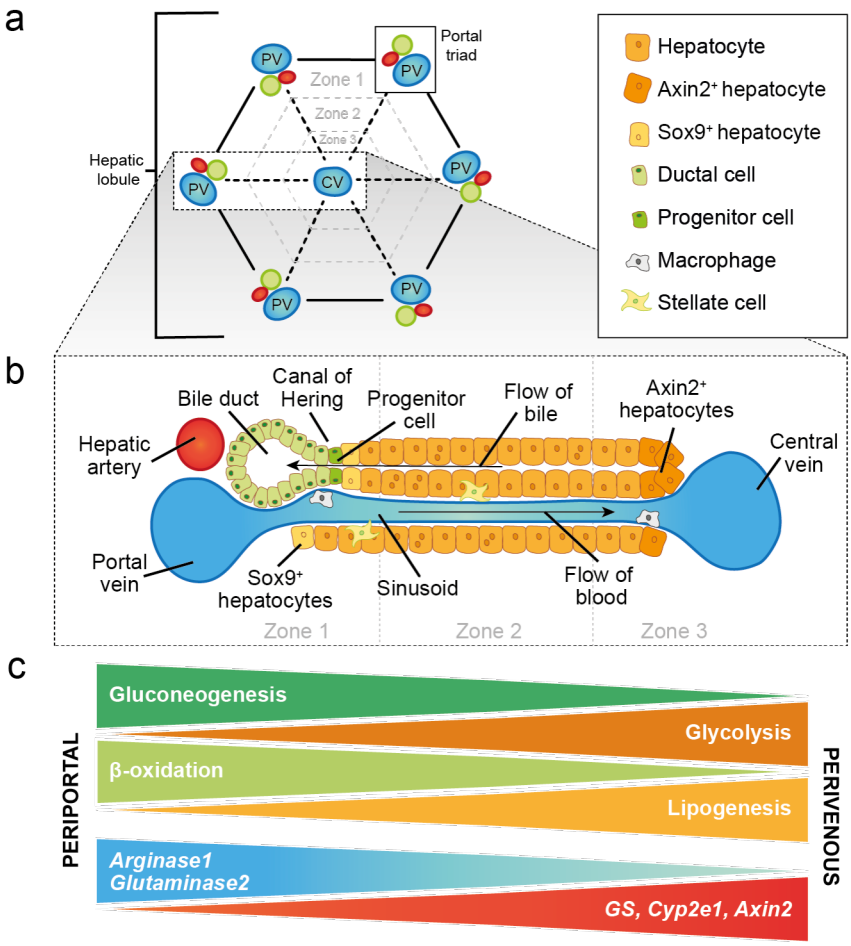

Figure 1.1 Liver structure and zonation. a) Schematic representation of the hepatic lobule, with one central vein and six surroundings portal triads to from a hexagonal shape. PV, portal vein; CV, central vein. Adapted from (Duncan, Dorrell, and Grompe 2009). **b)** Magnification of the region between portal vein and central vein. The portal triad consists of bile duct, hepatic artery and portal vein that connect to the central vein through the sinusoids. The canal of Hering connect hepatocytes to duct cells and it is where progenitor cells are thought to reside. $Sox9^+$ hepatocytes are found in the portal tract while $Axin2^+$ hepatocytes are found in the central tract. Adapted from (Duncan, Dorrell, and Grompe 2009). **c)** Diagram showing difference in metabolic zonation of the liver and differential genes expression between periportal and perivenous area. Adapted from (Birchmeier 2016).

Beyond the cell types described above the liver is home to many other resident cell types with independent roles (Figure 1.1b). These include macrophages, endothelial cells and stellate cells (Hindley, Cordero-Espinoza, and Huch 2016). Liver resident macrophages are also called Kupffer cells and can be usually found in the sinusoids, small blood vessels found widespread throughout the tissue. Endothelial cells form the lining of the blood vessels, including the sinusoids. Finally, hepatic stellate cells are pericytes involved in the scarring process of the tissue.

1.2 Liver regeneration

The adult liver has a very slow turnover, especially when compared to actively dividing tissues, like the intestine. During homeostasis, average mammalian hepatocytes lifespan is estimated to be between 200 and 300 days (Bucher and Malt 1971). A recent report has shown that there is a defined population of hepatocytes, marked by the WNT target gene *Axin2*, which is responsible for hepatocytes turnover during homeostasis (B. Wang et al. 2015). The *Axin2*$^+$ hepatocytes are diploid and located around the WNT rich CV region (Figure 1.1b) (B. Wang et al. 2015). Interestingly, these hepatocytes also express the pluripotency marker *Tbx3* (T-Box3), expression that is then lost in the progeny of these cells. According to Wang et al., *Axin2*$^+$ hepatocytes are able to replenish about 40% of the liver parenchyma in about 1 year in homeostasis conditions. However, it is important to consider how the lineage tracing experiments are performed in this work. The GFP allele used to trace the progeny of the *Axin2*$^+$ hepatocytes are localised inside of the *Axin2* allele itself, thus further validation is needed in order to assess that the expression of the gene is not altered by this modification, thus altering the results of the tracing experiment. Furthermore, the question still remains whether the progeny of these cells is able to replenish the whole liver parenchyma by itself or whether another source for hepatocytes, maybe in proximity of the portal area, exists. In line with this, a recent paper has shown that proliferative cells are not significantly localised around the pericentral area (Planas-Paz et al. 2016), in contrast with the observation of Want et al.. Thus, it is indeed possible for other cells, other than *Axin2*$^+$ hepatocytes, to be the source of newly formed liver cells during homeostasis.

Mechanical injury or chemical and biological agents can alter the normal homeostatic equilibrium of the liver and lead to the activation of several regenerative responses. Several studies have demonstrated the enormous regenerative potential of the liver, being able to regenerate up to 70% of its mass following partial hepatectomy (Michalopoulos and DeFrances 1997). However, liver regeneration is a highly debated field and the scientific community is currently involved in understanding this complex mechanism. Considering the complexity of the regenerative process, tight regulation is essential to prevent liver failure and/or onset of liver diseases such as primary liver cancer.

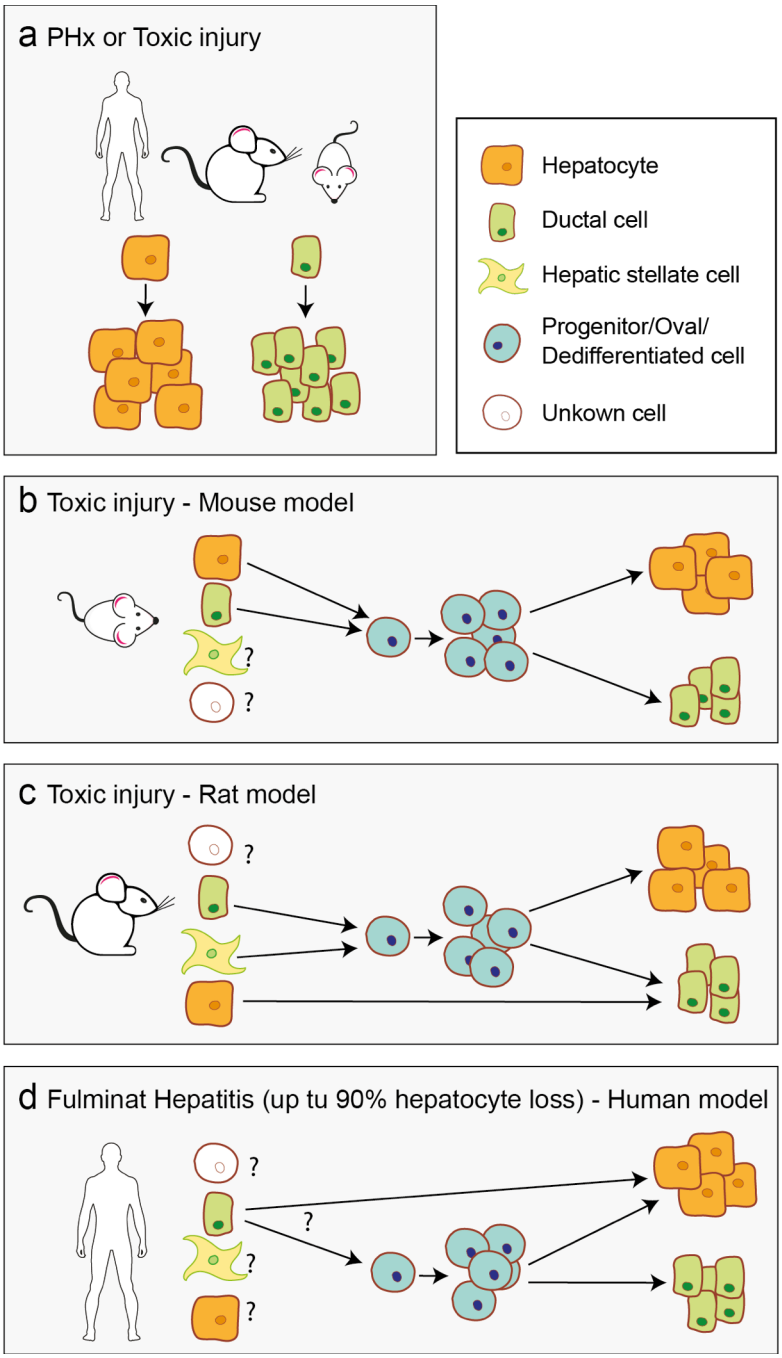

Figure 1.2. Overview of liver plasticity during regeneration in different models. a) Classic view of liver regeneration upon partial hepatectomy (HPx) or toxic injury. **b, c, d)** Alternative model for liver regeneration proposed for mouse, rat and human respectively. Regeneration is achieved by dedifferentiation to progenitor/oval cells and reprogramming to either hepatocytes or ductal cells. Adapted from (Hindley, Mastrogiovanni, and Huch 2014).

Several mechanisms of liver regeneration have been suggested over the years and an overview can be found in Figure 1.2. Several studies have shown that, based on the type of damage model applied, both hepatocytes and cholangiocytes can be activated and can proliferate to compensate for the loss of either hepatocyte or cholangiocytes, respectively (Figure 1.2a) (Yanger et al. 2014; Lu et al. 2015). Further studies have also shown that there is a population of hepatocytes located in the periportal area

expressing both hepatocyte (HNF4α) and cholangiocyte (SOX9) markers - thus named hybrid hepatocytes – that accounts for about 5% of the hepatocyte population (Font-Burgada et al. 2015). Interestingly, although these cells do not seem to contribute to damage repair after acute damage, they are able to replenish two-third of the entire liver parenchyma after mild chronic damage (Figure 1.1b) (Font-Burgada et al. 2015).

Despite the vast regenerative potential of the hepatocyte compartment described above, it has been shown that cholangiocytes or progenitor cells of biliary origin can also be a potent source of regeneration, especially when hepatocytes proliferation is impaired (Figure 1.2) (Lu et al. 2015). Such a response, termed ductular reaction, is characterised by expansion of the ductal compartment. Moreover, it has been shown that upon treatment with the toxic agent carbon tetrachloride (CCl4), *Lgr5*$^{+}$ (Leucine-Rich Repeat-Containing G Protein-Coupled Receptor 5) cells arise from the ductal compartment and are able to generate both hepatocytes and cholangiocytes in the mouse liver (Huch, Dorrell, et al. 2013). CCl4 is a known toxic agent that induces death to the hepatocytes around the CV after being metabolized by the cytochrome p450 and have been extensively used to model liver damage in mouse models (Beer et al. 2008). Interestingly, *Lgr5* was also found to be a stem cell marker in intestine, colon, stomach, hair follicle and other tissues (Barker et al. 2007, 2010; Jaks et al. 2008). Similar activation of Lgr5^{+} cells was also observed when damaging the liver using MCDE (methionine choline-deficient diet supplemented with ethionine) or DDC (3,5-diethoxycarbonyl-1,4-dihydrocollidine) diet (Huch, Dorrell, et al. 2013). While the MCDE diet cause damage due to lack of two essential factors for the formation of phosphatidylcholine, thus altering very low density lipoprotein production, DDC causes the formation of porphyrin crystals within periportal hepatocytes and in small bile ducts (Delire, Stärkel, and Leclercq 2015). Both approaches and are known for triggering an oval cell response in the liver (Akhurst et al. 2001; Preisegger et al. 1999). Oval cells are bipotential transit amplifying cells thought to arise from progenitor cells residing in the canal of Hering and also capable of generating both hepatocytes and cholangiocytes (Figure 1.1b and Figure 1.2b, c, d) (Fausto and Campbell 2003).

Finally, a novel player in liver regeneration has been recently identified in the rat liver. After partial hepatectomy, hepatic stellate cells have been shown to be able to undergo dedifferentiation, regeneration is then driven by re-differentiation of these cells into both hepatocytes and cholangiocytes (Figure 1.2c) (Kordes et al. 2014). Here, experiments were performed by transplanting fluorescently labelled stellate cells from

the bone marrow to the liver, and contribution to regeneration was assessed by analysis of the fluorescent progeny (Kordes et al. 2014). Due to the nature of this system it is still not possible to rule out a contribution of resident hepatic stellate cells to liver regeneration. Mouse hepatic stellate cells have also been suggested to give rise to hepatocytes after damage by employing Glial Fibrous Acidic Protein (GFAP) - Cre lineage tracing (L. Yang et al. 2008). However, further studies have revealed that GFAP it is not specifically expressed in hepatic stellate cells but also in bile duct cells, thus invalidating the result of Yang et al. (Mederacke et al. 2013). Furthermore, by generating a hepatic stellate cells specific Cre line, Mederacke et al. also found no contribution of these cells to liver regeneration after several types of damage models (Mederacke et al. 2013).

Taken together, all these data show how difficult as been trying to understand liver regeneration over the years. However, it is clear that the liver is a highly plastic organ capable of regenerating after several types of insults using distinct mechanisms. Also, the adult liver seems to not be relying on a well-defined stem cell compartment, but rather on the ability of mature cell types to proliferate and/or dedifferentiate to replenish and repair the organ. The question still remains whether other, still unknown, cells could be involved in the regenerative program of the liver (Figure 1.2b, c, d).

1.3 Primary Liver Cancer

Primary liver cancer (PLC) is the second most common cause of cancer death worldwide, preceded only by lung cancer (Siegel et al.; Bosch et al. 2004). The vast majority of adult liver cancers are split between two cancer types, hepatocellular carcinoma (HCC) and cholangiocarcinoma (CC). HCC and CC are both morphologically and genetically distinct malignancies. HCC is a solid tumour that grows in the liver parenchyma, it presents a hepatocyte-like phenotype and it is the most common type of PLC, representing 85-90% of them (El-Serag and Rudolph 2007). CC arises from the lining of the bile duct and is characterized by a large stromal reaction. This tumour type can form from the bile duct located either inside or outside of the liver, with the intrahepatic CC accounting for 5-10% of PLCs (Guglielmi et al. 2009). A third tumour type, that accounts for 0.5-5% of all PLCs, harbours intermediate features of both HCC and CC, thus called combined HCC/CC (CHC), and it is the rarest but also the most aggressive kind of PLC (Maximin et al. 2014; Moeini et al.

2017). Importantly, incidence and mortality have been increasing for both HCC and CC in the last ten years.

PLCs are often associated to liver cirrhosis, representing the major risk factor for this disease, with or without hepatitis B or C infection, liver diseases and alcoholic and non-alcoholic fatty liver disease (El-Serag and Rudolph 2007; Khan et al. 2005). Although these risk factors are shared among all PLCs, especially HCC and CHC, only a small percentage of CCs is known to arise as a consequence of chronic liver damage/ cirrhotic background due to hepatitis C or B infection (Pinter et al. 2016). On the other hand, parasitic infections, primary sclerosing cholangitis, biliary-duct cysts and toxins seem to play a greater role in the establishment of CC, with differences between intra- or extra-hepatic tumours (Tyson and El-Serag 2011). Although related to different etiological agents, both HCC and CC are linked to chronic liver damage. The persistence of chronic diseases and constant tissue and cell damage results in increased cell turnover, favouring the chances of errors during the repair process. These errors can lead to fibrosis and eventually to development of cirrhosis. In this setting, tumours can arise and proliferate (Figure 1.3a), while advanced tumours can metastasise to other tissues, with the lungs representing the primary metastatic site for PLCs (Marquardt, Andersen, and Thorgeirsson 2015).

1.3.1 Non-alcoholic fatty liver disease and HCC

As previously mentioned, non-alcoholic fatty liver disease (NAFLD) is one of the risk factors for the establishment of PLC, especially HCC. NAFLD is the most common liver disease, affecting between 25 to 35% of people in Europe and United States (Bellentani 2017). The disease is established when fat is accumulated in the liver, a condition defined as hepatic steatosis. Steatosis has been considered to be not pathological relevant for years, however, an increase amount of fat in the tissue is now known to trigger an inflammatory response, causing cell damage and, in some cases, leading to non-alcoholic steatohepatitis (NASH), the most aggressive form of the disease (Lonardo et al. 2017). Fat accumulation and the subsequent damage to the tissue, due to reactive oxygen species and excessive inflammatory response, can promote liver fibrosis and, in about 10-15% of the cases, cirrhosis and eventually PLC (White, Kanwal, and El–Serag 2012). Although cirrhosis is a major risk factor for HCC, recent studies have revealed that in 45% of the cases HCC can also arise in patients

affected by NAFLD without a cirrhotic liver, although with a less aggressive phenotype (Piscaglia et al. 2016). However, the molecular events that link NAFLD to HCC are still not understood. Common risk factors for NAFLD are obesity, type 2 diabetes mellitus and insulin resistance and it is often also related to metabolic syndrome. The disease is usually asymptomatic until cirrhosis is developed and mortality is caused either by the consequent cardiovascular disease or establishment of HCC, which represent the second most common complication of NAFLD (Masuzaki, Karp, and Omata 2016). Due to the increasing incidence of both NAFLD and HCC, further studies on the link between the two diseases are necessary in order to shed a light of the molecular mechanisms underlying the establishment of NAFLD/HCC.

1.3.2 Origin of PLCs

There is still heavy debate surrounding the origin of the PLC subtypes. Due to the histological features of the specific tumour types, mature hepatocytes were originally thought to be the main cell type of origin for HCC, whereas the intrahepatic bile duct epithelium would give rise mainly to CC (El-Serag and Rudolph 2007; Sia et al. 2013). Also, progenitor cells are thought to be the cells of origin for CHC (Figure 1.3b, c). However, more recently there have been reports stating that the situation might not be that simple and that based on the differentiation status of the transformed cell, hepatocytes and cholangiocytes could also both be the source for CHC and hepatocytes could also be the where CC originate from (Marquardt, Andersen, and Thorgeirsson 2015). Also, this theory includes the possibility for all tumour types to arise from a progenitor or a stem cell (Marquardt, Andersen, and Thorgeirsson 2015).

In support of this hypothesis, many murine liver cancer models have been generated introducing mutations in the liver bipotent progenitor hepatoblasts - and consequentially in hepatocyte and cholangiocytes - leading to formation of either HCC or CC. These data suggest that the specific mutation introduced can actually drive formation of a tumour type instead of the other and further support the hypothesis of the importance of the differentiation status of the mutated cells (Saha et al. 2014; Zender et al. 2013; Nantasanti et al. 2016). For instance, mice constitutively overexpressing the intracellular domain of the Notch receptor (NICD) in albumin-expressing cells - thus presenting the over-expression of NICD in both hepatocytes and cholangiocytes - results in CC development during adulthood (Zender et al. 2013).

Similarly, when Tp53 and Rb (Retinoblastoma protein) are mutated instead, HCC, but not CC, is formed after that the liver is challenged to regenerate (Nantasanti et al. 2016). Of note, when both NOTCH and AKT signalling are activated together in hepatocytes, cells are induced to trans-differentiate to a bile duct lineage and then give rise to CC (Fan et al. 2012). Thus, hepatocytes can give rise to CC by first transdifferentiating to cholangiocytes.

This new view reflects very well the concept of plasticity during regeneration, where cells can dedifferentiate to repopulate other compartments in the liver. In line with this, reprograming errors, mutations and/or cell damage can lead to the establishment of a tumour type that differ from the original mature cell.

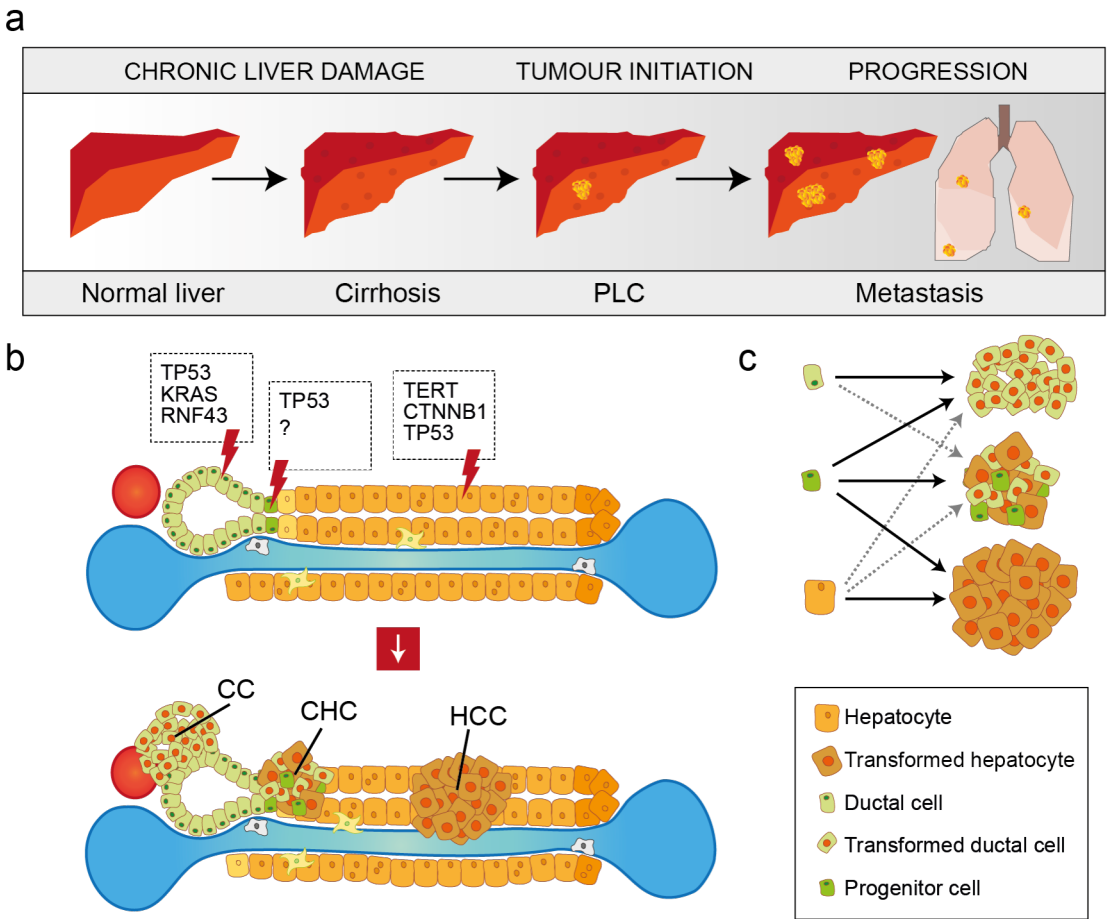

Figure 1.3 Origin and progression of liver cancer. a) Evolution of liver cancer from cirrhosis to establishment of a primary liver tumour and metastasis to the lungs. **b, c)** Schematic representations of the cell of origin of the different tumour types. Upon damage, mutated cells can acquire transformed phenotype and promote cancer formation. Specifically, ductal cells give CC and CHC, and hepatocytes and progenitor cells give both CC, HCC and also CHC. Adapted from (Marquardt, Andersen, and Thorgeirsson 2015).

1.3.3 Therapies for PLCs

Considering the heterogeneity of PLCs, it is very difficult to devise a common therapeutic strategy that would be effective for all tumours. For this reason, each case has to be assessed individually. Current therapies for PLC rely mainly on surgical resection, when possible and/or when liver function is preserved, or on the use of chemotherapy and/or local radiotherapy (Pinter et al. 2016). The gold standard therapy for PLCs is transarterial chemoembolization (TACE) where a blocking material mixed with a chemotherapy drugs is injected into the hepatic artery to block the blood supply of the tumour (Best et al. 2016). Alternatively, in cases where liver function is severely impaired, liver transplantation is also considered, especially to treat HCC. Recently, targeted therapy using the multi-kinase inhibitor Sorafenib has been used to treat advanced HCC resulting in extended survival rate when compared to patients treated with placebo (Llovet et al. 2008). Sorafenib has been shown to act not only on kinases involved in proliferation stimuli and survival (KRAS, BRAF), but also in inhibiting the promotion of vascularization by acting on VEGFR (vascular endothelial growth factor receptor) 2 and 3 (Wilhelm et al. 2004). To date Sorafenib is the only drug that has shown therapeutic potential in treating HCC. The success in using Sorafenib as targeted therapy for HCC has highlighted how important it is to understand tumour biology and genetics, to allow for better drug screening and to selectively target specific deregulated pathways.

1.4 Genetics of PLCs

Due to the higher incidence of HCC over CC, efforts aimed at elucidating the mutational spectra of PLCs have mainly been focused on HCC (Guichard et al. 2012; Fujimoto et al. 2012). However, due to a considerable increase of CC incidence (more than 100%) in the last three decades (Shaib et al. 2004), many studies have been recently made in order to also characterise the genetic background of CC (Jiao et al. 2013; Ong et al. 2012; Zou et al. 2014). These studies have unrevealed the mutational landscape of both HCC and CC (Table 1.1).

The key regulatory genes and pathways mutated in PLCs comprise several known oncogenes and tumour suppressor genes, as well as newly identified chromatin

remodelling (CR) genes involved in cancer (Guichard et al. 2012; Fujimoto et al. 2012; Jiao et al. 2013). Alteration of the Tumour Protein p53 (TP53)/cell cycle pathway seems to play a crucial role in both HCC and CC, as mutations in *TP53* have a frequency of 20.8% and 38.2%, respectively (Guichard et al. 2012; Zou et al. 2014). In line with this, TP53 mutations have also been frequently found in CHC (~27%), where only few studies have been carried out so far due its rarity (Maximin et al. 2014). Recently, TERT promoter mutations have been found very frequently in HCC (60%) suggesting that this could be an early step in the tumorigenesis process (J.-C. Nault and Zucman-Rossi 2016). In CC, the most common mutated gene is *TP53* followed by alterations of Kirsten rat sarcoma viral oncogene homolog (*KRAS*) (16.7%) (Zou et al. 2014). Of note, KRAS is not very commonly mutated in HCC (1.6%) (Guichard et al. 2012). On the other hand, mutations in the Wingless/Integrated (WNT) signalling pathway proteins have mainly been detected in HCC, where β-catenin (*CTNNB1*) is mutated in 32.8% of the cases (Guichard et al. 2012).

Table 1.1. Incidence of mutations in HCC and CC tumours.

Gene	Role	Incidence in HCC	Incidence in CC
TERT	Immortalization	60% (Schulze et al. 2015)	-
TP53	Cell cycle/apoptosis	20.8% (Guichard et al. 2012)	38.2% (Zou et al. 2014)
RB1	Cell cycle/apoptosis	4% (Schulze et al. 2015)	5% (Zou et al. 2014)
SMAD4	Cell cycle/apoptosis	-	16.7% (Ong et al. 2012)
PEG3	Cell cycle/apoptosis	-	5.6% (Ong et al. 2012)
IRF2	Cell cycle/apoptosis	4.8% (Guichard et al. 2012)	-
KRAS	G protein signalling	1.6% (Guichard et al. 2012)	16.7% (Ong et al. 2012)
PTEN	G protein signalling	3% (Schulze et al. 2015)	6% (Zou et al. 2014)
ROBO2	G protein signalling	-	9.3% (Ong et al. 2012)
IDH1	Chromatin remodelling	-	5% (Zou et al. 2014)
ARID1A	Chromatin remodelling	16.8% (Guichard et al. 2012)	6.9% (Zou et al. 2014)
ARID1B	Chromatin remodelling	6.7% (Fujimoto et al. 2012)	-
ARID2	Chromatin remodelling	5.6% (Guichard et al. 2012)	-
MLL3	Chromatin remodelling	4.2% (Fujimoto et al. 2012)	14.8% (Ong et al. 2012)
MLL	Chromatin remodelling	1.7% (Fujimoto et al. 2012)	-
BPTF	Chromatin remodelling	1.7% (Fujimoto et al. 2012)	-
CTNNB1	WNT signalling	32.8% (Guichard et al. 2012)	-
AXIN1	WNT signalling	15.2% (Guichard et al. 2012)	-
APC	WNT signalling	1.6% (Guichard et al. 2012)	-
ZNRF3	WNT signalling	3% (Schulze et al. 2015)	-
RNF43	WNT signalling	-	9.3% (Ong et al. 2012)

Interestingly, *CTNNB1* and *TP53* mutations are mutually exclusive, but mutations of *TP53* and the WNT signalling genes Axis inhibitor 1 (*AXIN1*) (15.2%) and Adenomatous Polyposis Coli (*APC*) (1.6%) are not (Guichard et al. 2012). In addition, mutations of Zinc finger 3 (*ZNRF3*) are also found in HCC at a frequency of 3% (Schulze et al. 2015). ZNRF3 and Ring Finger 43 (RNF43) are two homologous proteins recently found to be negative regulators of the WNT pathway in the mouse intestine (Koo et al. 2012). Interestingly, mutations in *RNF43* (9.3%) can only be found in CC, making this gene the first WNT pathway-relate gene to be mutated in CC identified thus far (Ong et al. 2012).

An interesting similarity between the two tumour types, is the high prevalence of mutations in the chromatin regulator gene AT-rich interaction domain protein 1 A (*ARID1A*) (16.8% in HCC and 6.9% in CC), that again shows mutual exclusivity with *TP53* mutations (Guichard et al. 2012; Zou et al. 2014). Mutations in other CR genes have also been reported for both cancer types and are listed in Table 1.1. Interestingly, although some of the mutations found in CR genes are mutually exclusive, 50% of the tumour samples presented at least one mutation in one of these genes. Therefore, considering the high frequency of mutations in the aforementioned genes, it is reasonable to think that *TP53*, WNT signalling pathway and CR genes could play a critical role in the initiation and progression of liver cancers.

1.4.1 TP53, the guardian of the genome

The high incidence of *TP53* mutations in both HCC and CC suggests that inactivation of the gene is potentially one of the initial steps of liver tumorigenesis. TP53 exerts important roles in both normal and cancerous liver (Meng et al. 2014). Specifically, DNA damage and stress stimuli leads to TP53 activation that in turn promotes cell cycle arrest and/or apoptosis (Meng et al. 2014). TP53 is also important in maintaining the normal number of chromosomes during mitosis. This is especially evident in the liver as hepatocytes show a higher “ploidy” when TP53 is inactivated (Kurinna et al. 2013). More recently, another role for TP53 in tumour prevention has been suggested. TP53 competent hepatic stellate cells would contribute to the formation of a tumour-preventing microenvironment, inhibiting malignant transformation of neighbour cells by recruiting macrophages to supress the proliferation or survival of pre-malignant cells (Lujambio et al. 2013; Chua, Chan, and Tang 2014). Therefore, activation of TP53 is

essential to prevent a tumorigenic state (Vassilev et al. 2004). In addition, TP53 has also been used as target to induce apoptosis in cancer cells harbouring wilt-type copies of the gene. In line with this, the small molecule Nutlin3 is able to induce TP53 activation by blocking its interaction with the inhibitor MDM2 (Mouse double minute homologue 2) (Schug 2009; Hardcastle 2007). However, the use of this drug to target tumours with wild-type copies of TP53 is limited by the possibility of also not cancerous cells to be affected.

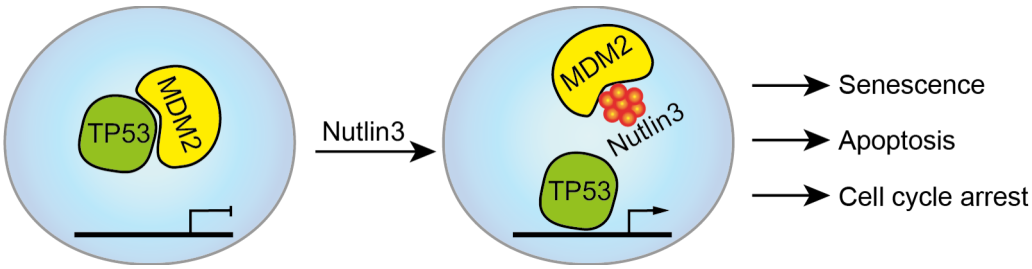

Figure 1.4. **Nutlin3 mediated activation of TP53.** In homeostatic conditions, MDM2 binds to TP53 to prevent activation of TP53-target genes. Nutlin3 prevents the interaction between MDM2 and TP53, allowing TP53 to activate its target genes and promote senescence, apoptosis and/or cell cycle arrest

1.4.2 The ARID family protein

ARID1A, commonly mutated in both HCC and CC, is a member of the chromatin remodelling SWI/SNF (SWItch/Sucrose Non Fermentable) complexes (Helming, Wang, and Roberts 2014; Reisman, Glaros, and Thompson 2009). There are two main complexes in this family, the BAF (BRG1-associated factor) complex and the PBAF (Polybromo-associated BAF) complex. These two complexes differ in protein composition and crucially include different members of the ARID protein family. ARID1A and ARID family protein in general play a crucial role in the proper functioning of the SWI/SNF complexes as the ARID domain confers the ability to bind DNA in a non-specific fashion, thus allowing the complex to exert its role. Some of these functions include promotion of nucleosome remodelling and regulation of many biological processes including proliferation, differentiation, apoptosis and DNA repair.

Mutations in the ARID family members have been initially reported in ovarian clear cell carcinoma and ovarian endometroid carcinoma, whereby *ARID1A* is mutated in 50% and 30% of the cases, respectively (Wiegand et al. 2010; Jones et al. 2010). Subsequently, comprehensive studies have uncovered mutations for these genes in gastric and colorectal cancer (Cajuso et al. 2014). In liver cancer, mutations for

ARID1A have been described for both HCC and CC, whereas *ARID1B* and *ARID2* mutations have only been described in cases of HCC (Schulze et al. 2015). ARID1A and ARID2 have been suggested to have tumour suppressor role in many tissues, whereas the role of ARID1B in cancer is still unclear(J. N. Wu and Roberts 2013; Zhao et al. 2011). Of note, *ARID1A* mutations were more prevalent in tumours related to alcohol intake rather than hepatitis B or C infections, whereas *ARID2* mutations were not significantly associated with any of the risk factor analysed (Guichard et al. 2012). No data for *ARID1B* mutations is available yet.

Interestingly, a recent report has shown that ARID1B expression is essential for survival of ARID1A-deficient cell lines, suggesting a dependence of ARID1A-deficient tumours on ARID1B and highlighting the possibility of using this vulnerability to treat these specific cancer types (Helming et al. 2014). On the same line, pharmacological inhibition of the DNA damage checkpoint kinase ATR (Ataxia Telangiectasia And Rad3-Related Protein) or of the methyltransferase EZH2 (Enhancer of Zeste Homolog 2) has been shown to be lethal for cancer cells harbouring *ARID1A* mutations both *in vitro* and *in vivo* (Bitler et al. 2015; Williamson et al. 2016).

1.4.3 The canonical WNT signalling pathway

The WNT signalling pathway has many important roles, ranging from cell fate decision during embryogenesis to regulation of tissue homeostasis in many adult tissues (Clevers and Nusse 2012). For this reason, it is not surprising that mutations in components of this pathway are observed in tumours originating from a number of tissues, including colon, pancreas, breast, skin and others (Wend et al. 2010). In the liver, members of the canonical WNT signalling pathway are frequently mutated in HCC, whereas only *RNF43* has been found mutated in CC so far (Guichard et al. 2012; Ong et al. 2012).

The WNT signalling pathway starts when the ligand, WNT, binds to the receptor complex composed of Frizzled and its co-receptors LRP5/6 (Low Density Lipoprotein Receptor-Related Protein) the WNT pathway is activated (Figure 1.5a, b). This interaction leads to the inhibition of a complex of protein called the destruction complex, which in turn allows the effector protein β-catenin to accumulate in the cytoplasm first and then translocate into the nucleus (Figure 1.5b). The destruction complex is

composed by several proteins with structural purpose, such as APC and AXIN1, and kinases that mediate recognition and degradation of β-catenin by the proteasome, such as GSK3β (glycogen synthase kinase 3 beta) and CK1 (casein kinase 1) (Figure 1.5a, b). When in the nucleus, β-catenin can associate to the transcription factors LEF/TCF (lymphoid enhancer factor/ T-cell factor) and promote transcription of WNT responsive genes (Figure 1.5b) (Clevers and Nusse 2012). When WNT is not present, the pathway is inactive and β-catenin is targeted for degradation by the destruction complex (Figure 1.5a). Of note, loss of function mutations in members of the destruction complex, like *Apc* or *Axin*, result in constant activation of the pathway even in the absence of the ligand (Sansom et al. 2004). Similarly, mutations that prevent correct ubiquitination of β-catenin by the destruction complex also leads to WNT independent activation of the pathway and can lead to tumour formation (Dong et al. 2015).

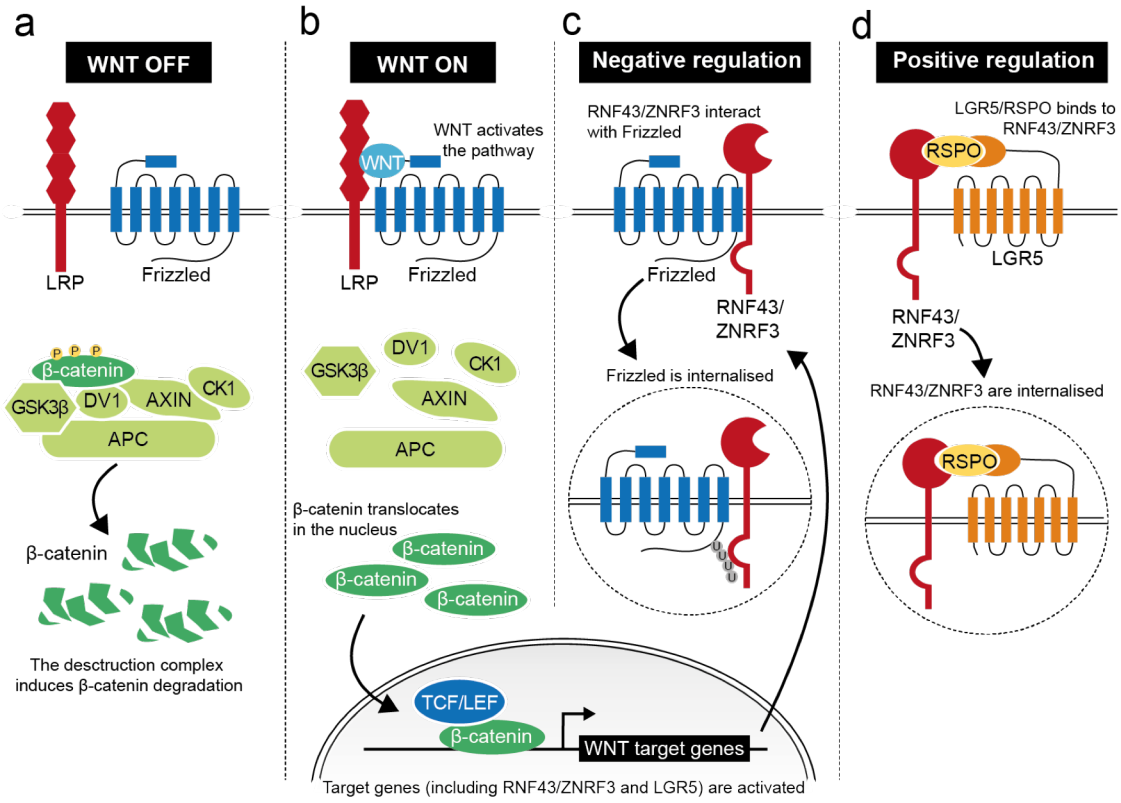

Figure 1.5. The WNT signalling pathway. a) In the absence of the ligand, WNT, the pathway is not active and β-catenin is degraded after being targeted by the destruction complex. **b)** When WNT is present, it binds to Frizzled and LRP preventing the formation of the destruction complex and allowing β-catenin to translocate into the nucleus and drive expression of WNT responsive genes. **c)** Activation of the pathway leads to the expressing and localization of the two homologous E3 ubiquitin ligases RNF43 and ZNRF3 on the cell surface. These proteins induce internalization and ubiquitination of Frizzled, thus negative regulating the WNT pathway. **d)** However, when the WNT agonist RSPO1 is present, it mediates the binding of RNF43 and ZNRF3 to LGR5, which leads to the internalization of this newly formed complex, thus positively regulating the pathway. Adapted from (Yu and Virshup 2014).

The destruction complex is not the only way in which the WNT pathway is regulated. Secreted molecules, like the Dickkopf proteins (Dkks) and the secreted Frizzled-related proteins (sFRPs), are able to bind to Frizzled and/or LRP5/6 and prevent ligand-receptor interaction (Cruciat and Niehrs 2013). More recently, new players involved in regulating the pathway at the receptor level have been identified, namely RNF43 and ZNRF3 (R&Z), two homologous E3 ubiquitin ligases (Koo et al. 2012). R&Z are expressed on the cell surface after activation of the WNT pathway (Figure 1.5b, c). They are single-pass transmembrane proteins with an extracellular PA domain and a cytoplasmic RING domain, that allow substrate-specific recognition for ubiquitination (de Lau et al. 2014) (Figure 1.6). When expressed on the cell surface, R&Z regulate the WNT pathway in a negative-feedback loop manner by promoting internalization and degradation of Frizzled, in a ubiquitination-dependent manner (Figure 1.5c) (Hao et al. 2012). Positive regulation of the pathway is instead achieved when the secreted molecule R-spondin1 (RSPO1) binds to both LGR4/5 and R&Z. The complex is then removed from the cell membrane and R&Z are no longer able to inhibit the pathway (Figure 1.5d) (Yu and Virshup 2014). Thus, RSPO1 acts as a positive regulator of the WNT pathway. Of note, LGR4/5 are also WNT targets, thus they are expressed when the pathway is activated.

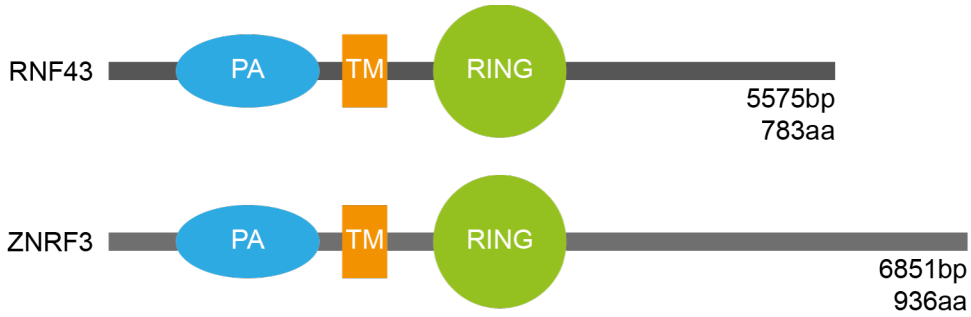

Figure 1.6. Schematic representation of RNF43 and ZNRF3 domains. RNF43 and ZNRF3 share the same structural and functional domains, including the extracellular PA domain and the cytoplasmic RING domain. TM, transmembrane domain. Adapted from (Koo et al. 2012).

Of note, ablation of both RNF43 and ZNRF3 in the mouse intestine induces rapid formation of adenomas with enlargement of the stem cell compartment, suggesting R&Z as another fragile regulatory effector of the WNT signalling pathway (Koo et al. 2012). Interestingly, R&Z intestinal tumours have been found to rely on their paracrine WNT source, the Paneth cells. Indeed, blocking of WNT secretion by porcupine inhibition has shown to strongly inhibit tumour growth *in vivo* without affecting normal crypts homeostasis (Koo et al. 2015). More recently, a new study has shown how

RNF43 and ZNRF3 could also have an important role also in the mouse liver by regulating metabolic zonation (Planas-Paz et al. 2016). Specifically, whole body R&Z deletion (using Rosa-CreERT2 allele) results in increased staining for GS and CYP2E1, two liver-specific WNT target genes involved in metabolism and localised around the CV. In addition, Planas-Paz et al. have also observed a 10% increase in proliferation 10 days after the deletion had been performed. Opposite results were instead observed when performing deletion of LGR4/5, thus confirming an opposite role for R&Z and LGR4/5 in regulating the WNT pathway. Despite the interesting results, further studies are needed to fully understand the consequence of *R&Z* deletion specifically in the liver.

After the identification of RNF43 as tumour suppressor, frequent inactivating mutations have been observed in many tumour types of pancreas, stomach and endometrium (J. Wu et al. 2011; Furukawa et al. 2011; K. Wang et al. 2014; Giannakis et al. 2014). Similarly, mutations in *ZNRF3* have been detected in a number of tumours, albeit less frequently (Wolpin et al. 2014; Zhou et al. 2013; Juhlin et al. 2014). In the liver, *RNF43* mutations have been identified mainly in liver fluke-associated CC (~9.3%) (Ong et al. 2012; Jusakul, Kongpetch, and Teh 2015). Interestingly, a more recent report correlates *RNF43* mutations with poor prognosis between patients with CC and also suggests a possible role for RNF43 in the development of this pathology (Talabnin et al. 2016). On the contrary, *ZNRF3* has been found mutated only in HCC (~3%) in a cohort study where 243 liver tumours were analysed (Schulze et al. 2015).

1.5 Liver cancer modelling

In order to better understand PLCs and to devise better therapies, many cancer models have been generated and used over the years (He et al. 2015; Heindryckx, Colle, and Van Vlierberghe 2009). The use of cell lines has allowed pioneering studies and preliminary drug testing. Animal models have proven to be essential to understand the genetic mechanisms underlying tumour initiation and progression. Also, the use of animal models has enabled the possibility for the development of new cancer treatments. However, considering the histological and genetic complexity of PLCs, it has become clearer that each case of the disease is unique and needs precise and personalised treatment. As a result, there is a growing need of new PLC models that

will also allow for personalized drug testing. Pros and cons of the different model systems are listed in Table 1.2.

Table 1.2. Pros and cons of cancer modelling strategies.

Model system	Pros	Cons
Cell lines	- Inexpensive to maintain - Easy to use for multiple applications - Bulk use for drug testing - Provide reproducible results - Can form spheroids	- Difficult to derive - Do not model microenvironment - Do not recapitulate histology - Frequent mutations at higher passages
Chemically-induced tumour	- Tumours in 6 months - Easy to perform - Tumour progression studies	- Long waiting time to increase efficiency - Variable mutational spectra
Xenograft (cells)	- Unlimited starting material - Can model metastasis - Easy to perform (subcutaneous) - Human tumours modelling - Drug testing	- Poor predictive value - Loss of heterogeneity of starting culture - Cells change when grown *in vitro* - Difficult to perform (kidney capsule)
Xenograft (patient-derived)	- Recapitulate tumour of origin - Recreate tumour heterogeneity - Can model metastasis - Easy to perform (subcutaneous) - Human tumours modelling - Personalised treatment	- Efficiency is low for some tumour types - Lack of standardization - No early tumorigenesis studies - Difficult to reproduce human immune system - Difficult to perform (kidney capsule)
GEMs	- Gene function studies - Early tumorigenesis studies - Temporal and spatial mutagenesis - Tumour progression studies - Gene-specific drug testing	- Expensive - Time consuming to generate - Labour intensive
Organoid cultures	- Human model - Can recapitulate tumour histology - More heterogeneous than cell lines - Genetically stable - Bulk drug testing - Less expensive than animal models	- New model that needs validation - Not available for all tissues - More expensive than cell lines - No microenvironment

1.5.1 Cell lines to model liver cancer

Cancer cell lines have been extensively used to model cancer and have been established from many normal and cancerous tissues, most of which are available and can be found on repository websites such as the American Type Culture Collection (ATCC).

The implementation of cell lines in cancer research has helped not only in increasing our knowledge of the cancer cell itself and its molecular biology, but has also been exploited to test drug sensitivity, resistance and toxicity (Sharma, Haber, and Settleman 2010; Lin and Will 2012). As an example of this, the anticancer drug Sorafenib, currently used as targeted therapy for HCC, has been initially shown to inhibit proliferation and induce apoptosis in two HCC cell lines (Hep2G and PLC/PRF/5) and then also in a tumour xenograft model, proving the usefulness of cancer cell lines for drug testing (Liu et al. 2006). However, it is not always possible to derive stable cell lines from all tumour types. More specifically, only two cancer cell lines from intrahepatic CC have been established so far, thus greatly limiting the use of cell lines to model this disease (Ku et al. 2002; Cavalloni et al. 2016).

Although the use of cell lines has been instrumental over the years, their 2D structure fails to fully recapitulate the *in vivo* counterpart. As a result, the knowledge obtained from studies using cell lines is merely indicative and often will need validation in other cancer models. To overcome this issue, cell lines have been cultured using bioreactors or supporting matrices that allow cells aggregation in a 3-dimensional fashion. These structures, termed spheroids, are more likely to recapitulate tumour physiology *in vivo* and have been able to maintain some of the liver-specific activity and architecture (Mueller, Koetemann, and Noor 2011; Bokhari et al. 2007; Tostões et al. 2012). Nevertheless, they still do not recapitulate the histology and genetics of patient tumours.

1.5.2 Animal models of liver cancer

Animal models have been extensively used to gain insights into tumour biology and responses to drug treatments. To model liver cancer using animal models there are several approaches that have been developed so far, including chemically-induced mutagenesis, xenograft transplants and genetic modification.

Chemical induced hepato-carcinogenesis

The carcinogen diethyl nitrosamine (DEN) is one of the most common chemicals used to induce HCC formation in the liver (Tolba et al. 2015). DEN causes DNA damage and random mutagenesis due to oxidative stress after being metabolised by the cytochrome P450 in the hepatocytes. Administration of DEN results in HCC formation after about a 6 months latency period, with tumour incidence increasing to 100% after longer periods of time (Tolba et al. 2015). Major limitations of this system are the long waiting time to get 100% of adenomas (> 6 months) and the lack of liver fibrosis, usually associated with human HCC. To overcome these issues, new protocols have been implemented using a combination of DEN and CCl4. As previously mentioned, CCl4 is a toxic agent that kills the hepatocytes around the CV but also induce an inflammatory response. Long-term administration of CCl4 have been shown to induce nodule formation in mouse livers, alone or in combination with other agents (Confer and Stenger 1966; Takeki Uehara, Pogribny, and Rusyn, n.d.). When combined with DEN, CCl4 is administered to mice 2 times a week for a total of 17 to 22 weeks after being primed by one injection of DEN. This system has allowed for faster tumour growth in a setting of liver fibrosis, better representing the human tumour counterpart (Takeki Uehara, Pogribny, and Rusyn, n.d.; T. Uehara et al. 2013). Of note, there are currently no models to chemically-induce CC growth.

Xenograft models

Xenograft models consist of inoculating a human cell suspension or a tissue fragment directly into mice either subcutaneously or orthotopic. Engraftment of cells or tissue will generate tumours in the host organism. When cells or tissues are taken directly from a human patient the model is called patient-derived xenograft (PDX). While engraftment of *in vitro* expanded cells has been used to model cancer (Reiberger et al. 2015), they fail to fully recapitulate the histology, genetics and heterogeneity of the original tumour. By contrast, PDX models have the ability of retaining these features also after passaging through mice (Hidalgo et al. 2014). Importantly, a large panel of PDX models of HCC have been recently used to assess the effectivity of Sorafenib, drug commonly used to treat HCC, and Lenvatinib, fibroblast growth factor receptor 1

(FGFR1) inhibitor, proving different responses based on genetic profile (Gu et al. 2015).

Being easy to perform, subcutaneous xenograft models are most commonly used to model HCC. In this model, drugs can be administered either systemically or locally by direct injection into the tumour mass. However, this system lacks the interaction between the forming tumour and the liver tissue. When such interaction is required, orthotropic xenograft models, where cells are injected directly into the hepatic lobes, can be considered instead. This model is also preferred for metastatic studies, as tumour cells are more likely to metastasise to other tissues. Alternatively, kidney capsule xenograft has also been used to model several cancer types, as it provides a good environment for tumour growth and to model metastasis.

Genetically engineered mouse (GEM) models

GEM models are a powerful alternative to the other methods described above. These models rely on the genetic modification of human cancer-related genes (oncogenes and/or tumour suppressor) to induce tumour formation in mice. The increased knowledge of the mutational spectra of liver cancer has also allowed for the use of this system to examine the contribution of newly-found mutated genes to cancer formation. Also, the knowledge of some of the mutations present in the tumour itself has made drug testing for targeted therapy in an *in-vivo* setting easier.

Overexpression of oncogenes and/or deletion of tumour suppressor genes can be performed both constitutively or in a spatial and temporal inducible manner. To generate a GEM model, the desired modification is inserted in the DNA of an embryonic mouse cell which is subsequently injected into an embryo to produce a chimera. When germline transmission is achieved, the genetic modification will be passed to the progeny. In case of constitutive genetic models, all the cells will be affected at all developmental stages. One of the first models of this type used the constitutive expression of Hepatitis B virus x (HBx) protein to rule out the association of Hepatitis B infections with cancer formation (Kim et al. 1991). Of note, this study proved that expression of the HBx protein alone was able to induce adenoma formation at the age of 8-10 months in mouse models (Kim et al. 1991).

In some cases, constitutive DNA modification can affect the proper development of the organism and result in lethality, thus limiting the use of this technology. Many systems have been devised to overcome this issue. One of the most popular strategies is the Cre/LoxP system, that allows to induce the desired modification only in a specific cell population (Zhang et al. 2012). The system relies on the expression of a Causes Recombination (CRE) protein whose gene is located downstream of a tissue-specific promoter. Upon expression, the CRE protein directs the excision of a DNA region of interest previously flanked by loxP sites (floxed) (Figure 1.7) (Zhang et al. 2012). The system has been further improved to allow temporal control of the excision. In the updated system, the CRE protein is fused together with a tamoxifen-dependent version of the estrogen receptor (ERT2). Hence, only when the drug tamoxifen is injected into the mouse, the CRE-ERT2 fusion protein can translocate to the nucleus and drive the DNA excision. This allows to perform DNA modification after birth and removes the lethality problem (Figure 1.7) (Zhang et al. 2012). Over the years, the CRE-ERT2 system has been extensively used to study gene functions and to model cancer. In the liver, one of the most common promoter used to drive liver-specific modification is the albumin promoter. In this case, the genomic modification is exerted only albumin-expressing cells, the hepatocytes, and only in presence of tamoxifen if using the inducible system (Schuler et al. 2004).

Cre/LoxP system has been used to assess genes contribution to cancer either alone or in combination. For instance, hepatocyte-specific knock-out of *Pten* (Phosphatase and Tensin Homolog) has shown to induce adenoma formation and also HCC at lower percentage, proving its tumour suppressor activity in the liver (Horie et al. 2004). Similarly, deletion of both Rb (Retinoblastoma) and Tp53, using a Cre protein whose expression was driven by the Alb (Albumin) promoter, induces HCC formation after DDC diet-induced damage (Nantasanti et al. 2016). Albumin is expressed in hepatoblasts that give rise to both hepatocytes and cholangiocytes in the adult liver, thus Cre mediated modifications will be present in both cell types. In line with this, the use of the AlbCre system has also allowed the generation of models for CC. A few examples includes the overexpression of the intracellular domain of the Notch receptor (NICD) or a mutated form of Idh1, both driven by Albumin-Cre, and resulting in CC development during adulthood (Saha et al. 2014; Zender et al. 2013).

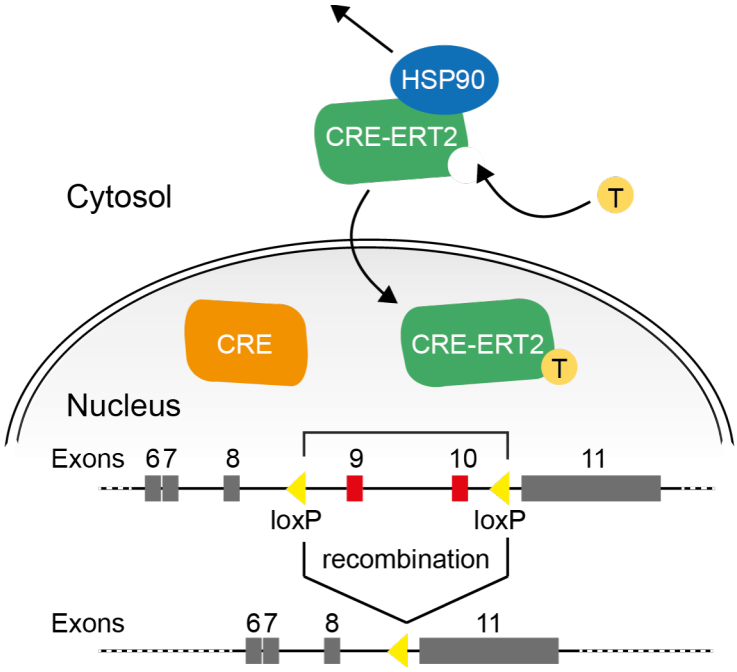

Figure 1.7. Schematic representation of functioning of CRE-loxP system. CRE proteins are always active and translocate to the nucleus once expressed. CRE-ERT2 proteins are trapped in the cytosol by Hsp90. However, the binding with tamoxifen is able to free CRE-ERT2 from HSP90 and allow its nuclear localization. Once in the nucleus, CRE or CRE-ERT2 drives recombination and excision of a DNA region flanked by loxP sites.

1.5.3 Organoid cultures, the new frontier of modelling

Recently, a novel 3D ever-expanding culture system, termed “organoid”, has been established from various mouse and human tissues including small intestine, colon, stomach, pancreas and liver, opening up new possibilities for disease modelling (Sato et al. 2009; Huch, Dorrell, et al. 2013; Huch, Bonfanti, et al. 2013; Stange et al. 2013; Huch et al. 2014; Boj et al. 2014; Bartfeld et al. 2014) (Figure 1.8a). In this system, adult stem cells are harvested from the tissue and then embedded in matrigel, a basement membrane matrix, where they can expand and organize into epithelial structures of the respective organ of origin. Of note, the cells are not transformed, as with established cell lines, but are obtained directly from the original primary tissue. Moreover, the cells preserve their cellular identity *in vitro*, giving rise only to cell types of the tissue of origin (Simmini et al. 2014). Importantly, organoid cultures have been proven to be highly genetically stable, as no abnormalities in chromosomes number have been detected during the culturing periods and single base changes occurred at very low rate (Blokzijl et al. 2016).

The first kind of organoid culture established is from the gut epithelium, where intestinal crypt $Lgr5^+$ stem cells were isolated and seeded in culture. After addition of specific growth factors to activate proliferative pathways (R-spo1, EGF and Noggin), the cells would proliferate, differentiate and organise in 3D structures resembling the *in-vivo* intestinal villus-crypt pattern, still preserving their renewal potential (Sato et al. 2009). After that, similar studies have been performed in order to reproduce these results with other tissue types. In 2013, two studies from the Clevers group were published, presenting their data on organoid cultures from the mouse liver and pancreas (Huch, Dorrell, et al. 2013; Huch, Bonfanti, et al. 2013). Specifically, Huch et al. found that, after damage, Lgr5 also mark a stem cell population in the liver and that these cells can be grown and expanded *in-vitro* indefinitely (Huch, Dorrell, et al. 2013). In order for the adult liver cells to grow and form organoids, they need several stimuli, including FGF (fibroblast growth factor), HGF (hepatocyte growth factor) and EGF (epithelial growth factor) signalling, but also activation of the WNT pathway by addition of the WNT agonist R-spo1. Crucially, the mouse liver organoid culture protocol has been recently adapted to allow long-term expansion of single human liver stem cells (Huch et al. 2014). In addition to the growth factors needed for the culturing of the mouse liver organoids, the human ones also need inhibition of TGFβ (transforming growth factor beta) signalling and addition of FSK (forskolin), a cyclic AMP (adenosine monophosphate) activator, in order to achieve long term expansion. In contrast with the intestinal organoids where different cell types compose the villus-crypt structures *in-vitro*, liver organoids are made predominantly of ductal/progenitor cells assembled in a single layer epithelium to form cystic structures (ductal phenotype). However, both mouse and human liver organoids have been induced to differentiate into hepatocyte-like cells *in-vitro* that retains some of the function of the cells *in-vivo* (e.g. albumin secretion, cytochrome activity) (Figure 1.8b). In addition, liver organoids are able to differentiate into hepatocyte also after transplantation *in-vivo*. To prove the usefulness of this system, Huch et al. have also established organoids from human livers affected by α1-antitrypsin (A1AT) deficiency and Alagille syndrome and used them to model the disease *in-vitro* (Huch et al. 2014).

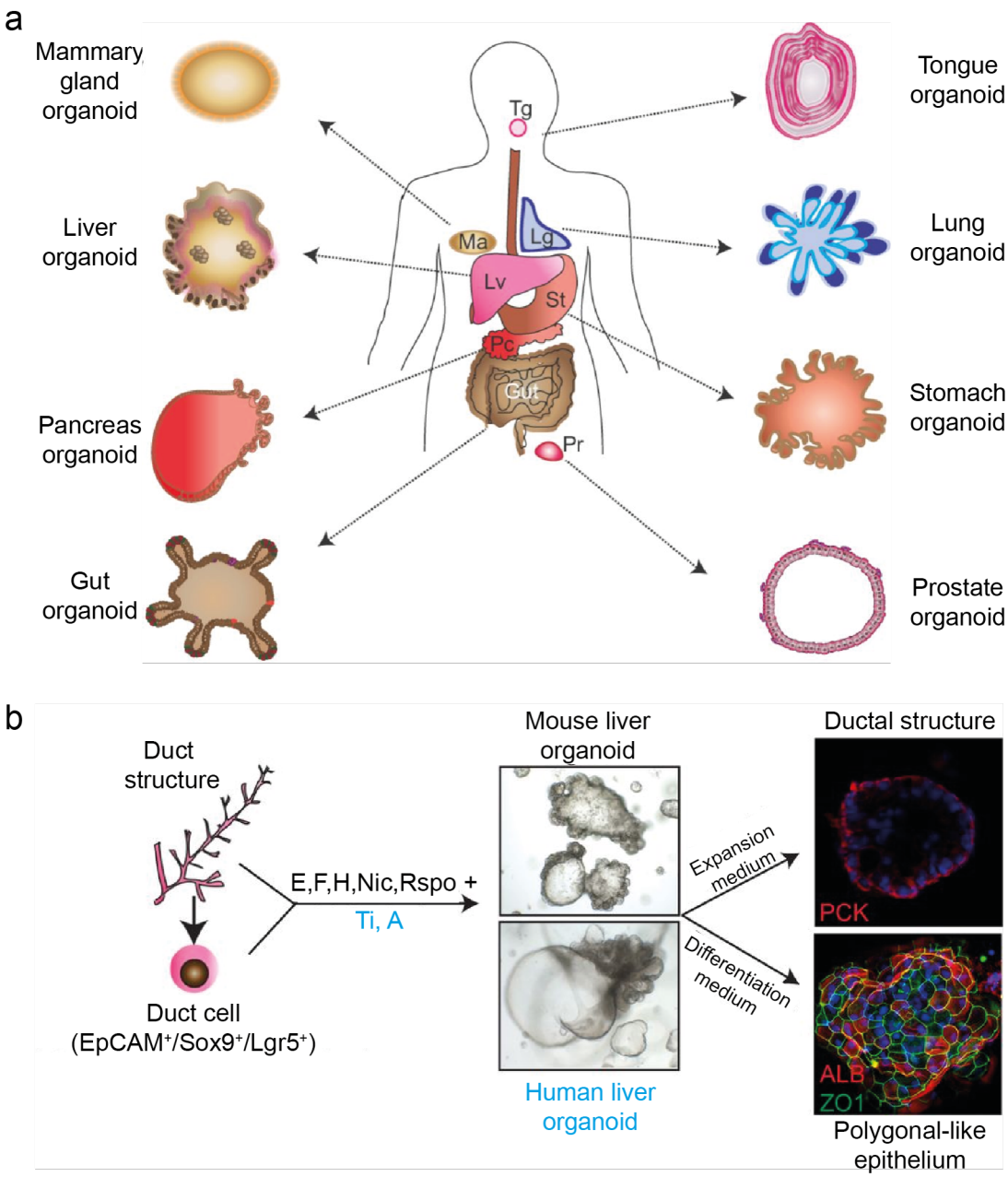

Figure 1.8. Adult stem cell-derived organoid cultures. a) Schematic representation of the different organoids that can be derived from adult human stem cells. Lg, Lung; Lv, Liver; Ma, mammary gland; Pc, Pancreas; Pr, Prostate; St, Stomach; Tg, Tongue. **b)** Mouse and human liver organoids are generated culturing a duct or a duct cell in medium supplemented with E (EGF), F (FGF10), H (HGF), Nic (nicotinamide) and Rspo. Ti (TGFβi) and A (forskolin) (in blue) are required for the growth of human liver organoids. When in expansion medium, cells expand as ductal structures (PCK, pan-cytokeratin, red). When cultured in differentiation medium, cells differentiate into a polygonal-like epithelium expressing hepatocyte markers (albumin, red; ZO1, green). Adapted from Huch and Koo 2015.

Strikingly, the ability of establishing organoid cultures starting from adult stem cells has also made possible the growth of tumour-derived organoid cultures, termed tumoroids. Specifically, tumoroids have been grown from mouse and human colon, pancreas and prostate cancers, but never from liver cancer (Li et al. 2014; Sato et al. 2011; van de Wetering et al. 2015; Boj et al. 2014; Gao et al. 2014). Tumoroids have been shown to closely resemble the tumour of origin, by being able to recapitulate some of the

histological features observed in the original tissue, but also by presenting a matching mutational pattern. The ability of tumoroids of modelling cancer has also been proven upon xenotransplantation *in vivo*, where only tumour-derived organoids, and not healthy tissue-derived ones, are able to engraft, grow, form tumours and, in some cases, give metastasis, thus representing a good new model for cancer *in vitro* and a valuable alternative to cancer cell lines. As tumoroids also recapitulate genetic features of the original tumour, they have also been used for screening of drugs for personalised treatments. Specifically, van de Wetering et al. have established a biobank of 20 tumoroids from human colorectal cancer patient (van de Wetering et al. 2015). After characterisation of the lines to assess their modelling potential, they subjected some of them to drug testing. Interestingly, they observed a good correlation between drug effect and genetic profile of the culture, making this system useful also to devise both new targeted and personalised therapies. However, as tumours are highly heterogeneous and tumoroids originate from a small biopsy of the original tumour, they might not represent the whole heterogeneous population of the tissue of origin. Thus, these data need to be confirmed after validation of the heterogeneity of the tumoroid lines used in order to translate this into a therapeutic approach.

Finally, genome engineering of organoids using the CRISPR-Cas9 technology has further proved the usefulness of this system to model diseases (Matano et al. 2015; Drost et al. 2015) (discussed in next paragraph). These data suggest that organoids not only are a good system to study stem cell physiology but they can also represent a valid tool for disease modelling.

1.5.4 The CRISPR-Cas9 technology

Genome engineering of cells have been made easier and faster by the implementation of the CRISPR-Cas9 technology. Originally discovered to be part of the adaptive immune system that prokaryotic cells adopt to fight viral infections, it has recently been adapted to perform knock-outs and precise gene editing in cells derived from different organisms (Ran, Hsu, Wright, et al. 2013). The acronym CRISPR stands for ‘clustered, regularly interspaced, short, palindromic repeats’, while Cas9 is the CRISPR-associated endonuclease. A single guide RNA (gRNA) is used by Cas9 to recognised a 20bp target sequence downstream of a conserved protospacer adjacent motif (PAM) (Figure 1.9a). In the absence of a DNA template for homologous recombination, the

Cas9 endonuclease generates double-strand breaks that are then ligated back together by the DNA repair machinery via NHEJ (non-homologous end joining). Since this process is inherently error-prone, the insertion or deletion of a nucleotide(s) frequently occurs, resulting in frameshift mutations and inactivation of the target gene (Ran, Hsu, Wright, et al. 2013) (Figure 1.9b). Alternatively, when a donor vector is co-delivered together with gRNAs and Cas9, it is possible for repair to occur via homologous recombination, which therefore allows precise gene editing through knock-in (Figure 1.9b).

Interestingly, recent reports have shown that CRISPR-Cas9 can be used to perform genome engineering of organoid cultures. As originally shown by Schwank et al., human intestinal organoids can be easily genetically manipulated using CRISPR, allowing human disease modelling (Schwank et al. 2013). Two further independent studies have used human intestinal organoid cultures to model colorectal cancer after introducing mutations in cancer-related genes in healthy cultures using the CRISPR technology (Matano et al. 2015; Drost et al. 2015). Using restricted media condition, mutated organoids can easily be selected. For instance, organoids mutated in *Apc*, were selected by removing Rspo1 from media condition, thus allowing only mutated cells to survive. Similarly, only organoids mutated in *Kras* survived after withdrawal of EGF. Interestingly, CRISPR-generated tumoroids acquired feature of malignant transformation and were able to form tumours after subcutaneous injection or implantation in the kidney capsule of mice, suggesting that this could be a new valid method to generate cancer models.

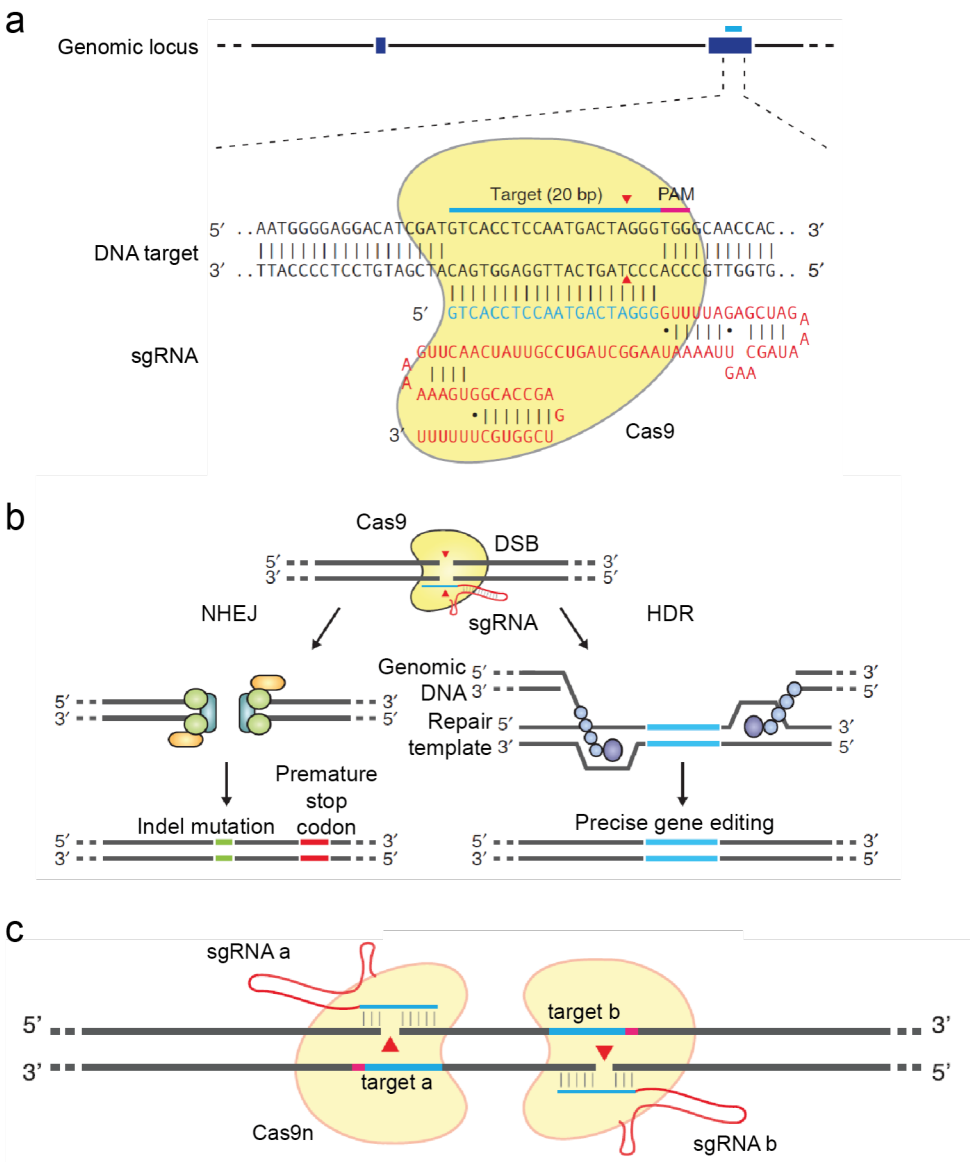

Figure 1.9. The CRISPR/Cas9 technology. a) A single gRNA (red sequence is the gRNA scaffold; blue sequence is 20bp complement to target region) is used by the endonuclease Cas9 (in yellow) to recognize a 20bp region on the DNA target and perform a cut 3bp upstream of a PAM sequence. PAM sequence 5'-NGG is essential in order for the Cas9 to cut the target sequence. A double strand break (DSB) is performed 3bp upstream of the PAM (red triangle) (Ran, Hsu, Wright, et al. 2013). **b)** DSB is repaired either by non-homologous end joining (NHEJ) introducing indel mutations in the sequence or, if a donor template is provided, by homology directed repair (HDR), allowing precise gene editing(Ran, Hsu, Wright, et al. 2013). **c)** More recently, a mutated version of the Cas9, termed Cas9 nickase (Cas9n), able to cut only one strand of the DNA, has been implemented to increase the specificity of the cut (Ran, Hsu, Lin, et al. 2013). Here, DSB is achieved by the use of two adjacent gRNAs that recognize 20bp sequences on opposite strands of the DNA. Off target effect is thus reduced to a minimum as two cutting sites close two each other are required to obtain a DSB. Adapted from Ran et al., 2013 (Ran, Hsu, Wright, et al. 2013).

2. AIMS

Primary liver cancer (PLC) is the second most common cause of cancer death worldwide. Treatment for PLC usually involves surgical resection of the tumour, transplantation and chemotherapy and/or radiotherapy. Current models for PLC either fail to fully recapitulate tumour histology and architecture or are expensive, time-consuming and do not allow for personalised drug testing. The unavailability of specific drugs and the lack of possibility for personalised treatment makes this disease difficult to treat. With this work, I aim at generating new and different approaches to model liver cancer both *in vivo* and *in vitro*, and to use those approaches to investigate the role of genes newly found mutated in this disease.

- To establish a new reliable method for liver cancer modelling, together with Dr. Laura Broutier, I have sought to investigate the possibility of generating liver tumour-derived organoid cultures (tumoroids) from human liver cancer biopsies. Human organoid cultures have been established from many normal and cancerous tissues, proving their usefulness in disease modelling *in vitro*. This system, could allow modelling PLC in a human system *in vitro*, but could also be pivotal for establishing personalised treatment for patients.

- To gain insight about the role of specific genes to cancer initiation and progression, I will generate a protocol for introducing mutations in cancer-related genes in human liver organoid cultures using the CRIPR/Cas9 technology. The use of this *in vitro* tumour model system with a known mutational spectrum could help unravel a specific mutation's contribution to cancer formation. In addition to this, this technology could be used as a screening platform before commencing animal work.

- The last objective of my PhD has been to investigate the role of RNF43 and ZNRF3 (R&Z) in the liver during homeostasis and regeneration, and also to study their role in cancer formation. R&Z are two homologous negative regulators of the WNT pathway and have been found mutated in many cancer types, including liver. Very little is known about the role of these two genes in the liver and this study will help broaden our understanding on the implication of their inactivation in this tissue.

3. RESULTS - PART I

Establishment and characterisation of patient-derived organoid cultures to model primary liver cancer *in vitro*

3.1 Summary

Primary liver cancer (PLC) is one of the deadliest cancer worldwide. There are already several models for PLCs, which include the use of cell lines and animal models. Cell lines have been extensively used for drug testing, although they fail to recapitulate tumour histology and/or genetics. Conversely, animal models, and more specifically PDX models, can very well recapitulate the features of the tumour of origin but they are expensive and not suitable for massive drug screening. New model systems that recapitulate tumour architecture and, at the same time, allow efficient drug testing are currently not available. In this section, I present PLC-derived organoid cultures (tumoroids) as a new model strategy for PLC.

In collaboration with Dr. Laura Broutier, we have found that tumoroids can be established from PLC, including HCC, CC and the combined subtype CHC. Importantly, tumoroids can expand long-term and recapitulate both histological and genetic features of the tumour of origin. For instance, they have high percentage of aneuploidy and present mutations found in the patient's original tumours. Strikingly, the mutational profile of tumoroids can be used to predict drug sensitivity and resistance *in-vitro*. Finally, tumoroids are also able to induce tumour formation that resembles the tumour of origin in mice.

These data show the great potential of this new model system that, not only recapitulates patient's tumours of origin, but can also be used for drug screening as a personalised medicine approach.

3.2 Establishment of patient-derived cancer organoid cultures

I have worked in collaboration with Dr. Laura Broutier to establish a novel system to culture liver tumour cells *in vitro*, by adapting the previously described protocol for culturing human liver cells (Huch et al. 2014). Both normal and cancerous tissues biopsies were obtained from PLC patients with no history of viral-mediated hepatitis. Tissues were dissected and divided into four parts. One part was used for organoids derivation and the remaining ones for histology, genome and expression analysis as shown in Figure 3.1. For organoids derivation, tissue was dissociated to single cells, seeded in BME/2 matrix and monitored for forming organoid structures.

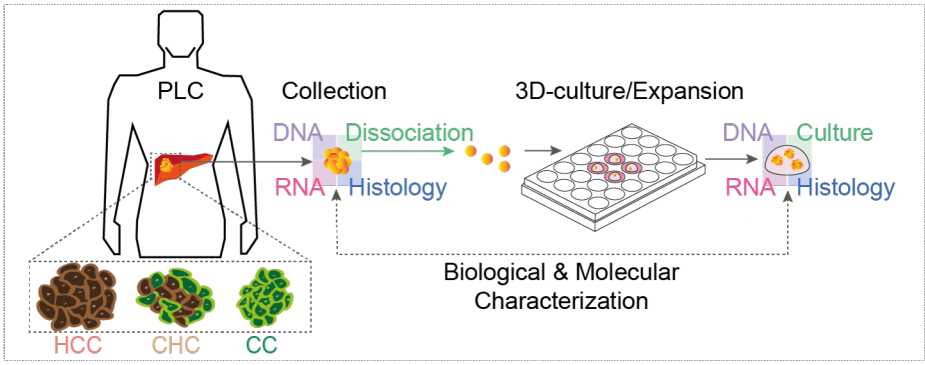

Figure 3.1. Experimental design for establishment of patient-derived tumoroid cultures. Tumour samples were collected from human HCC, CHC and CC tumours. For each tissue, samples were split into 4 parts and processed for histology, RNA and DNA isolation, and for tumoroid derivation. To establish the tumoroid cultures, biopsies were dissociated to single cells and seeded in BME/2 using appropriate medium conditions.

By following the previously established protocol with modified culturing conditions, we have established PLC-derived organoid (tumoroids) cultures from 8 different PLC patients, including moderate/well differentiated HCC (n=3), CC (n=3), and combined HCC/CC (CHC; n=2) (Figure 3.3). Of note, we were unable to establish cultures from well differentiated HCCs, probably due to the very low percentage of proliferative cells in these samples.

Tumoroids were expanded long-term in culture and were passaged weekly at a ratio of 1:4/1:5, CC organoids, or every 10 days at a ratio of 1:3, HCC and CHC organoids, reflecting the proliferative state of the tissue they derive from (Figure 3.2). It was not possible to expand HHC-2 for longer than 1 month due to the elevated presence of fibroblasts, which outcompeted the tumoroids growth (Figure 3.2).

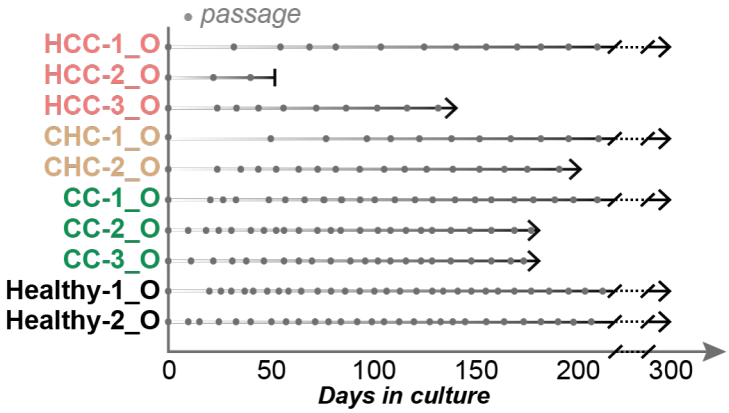

Figure 3.2. Tumoroids can be expanded long-term. After generation of the tumoroid lines, the cultures were expanded and passaged according to their growing potential. Graph indicating the expansion potential of tumoroids cultures established and their correlation to the expansion of healthy-tissue derived organoids. Arrow, continuous expansion. Dot, passage.

At microscopic observation, tumoroids present heterogeneous morphological features (Figure 3.3). Overall, they lost the cyst-like hollow structure of healthy organoids and presented themselves as either compact structures (HCC and CHC) or as irregularly-shaped cyst-like structures (CC). To further corroborate this observation, we performed H&E staining of formalin-fixed paraffin-embedded tumoroids sections. As previously reported, healthy organoids are formed by a single layer of cells and mimic the ductal compartment of the liver (Huch et al. 2014). On the other hand, tumoroids exhibit aberrant structures and features that can also be found on the tissue of origin (Figure 3.3). For instance, CC tumoroids have extensive glandular domains with carcinoma cells invading the lumen. Meanwhile, HCC and CHC tumoroids exhibit a solid and filled structures and, in case of HCCs, also presenting pseudo-glandular domain typical of HCC tissues.

Overall, tumoroids can be established from several liver cancer types, can be expanded long-term and recapitulate histological characteristic of the tissue of origin and cancer subtype.

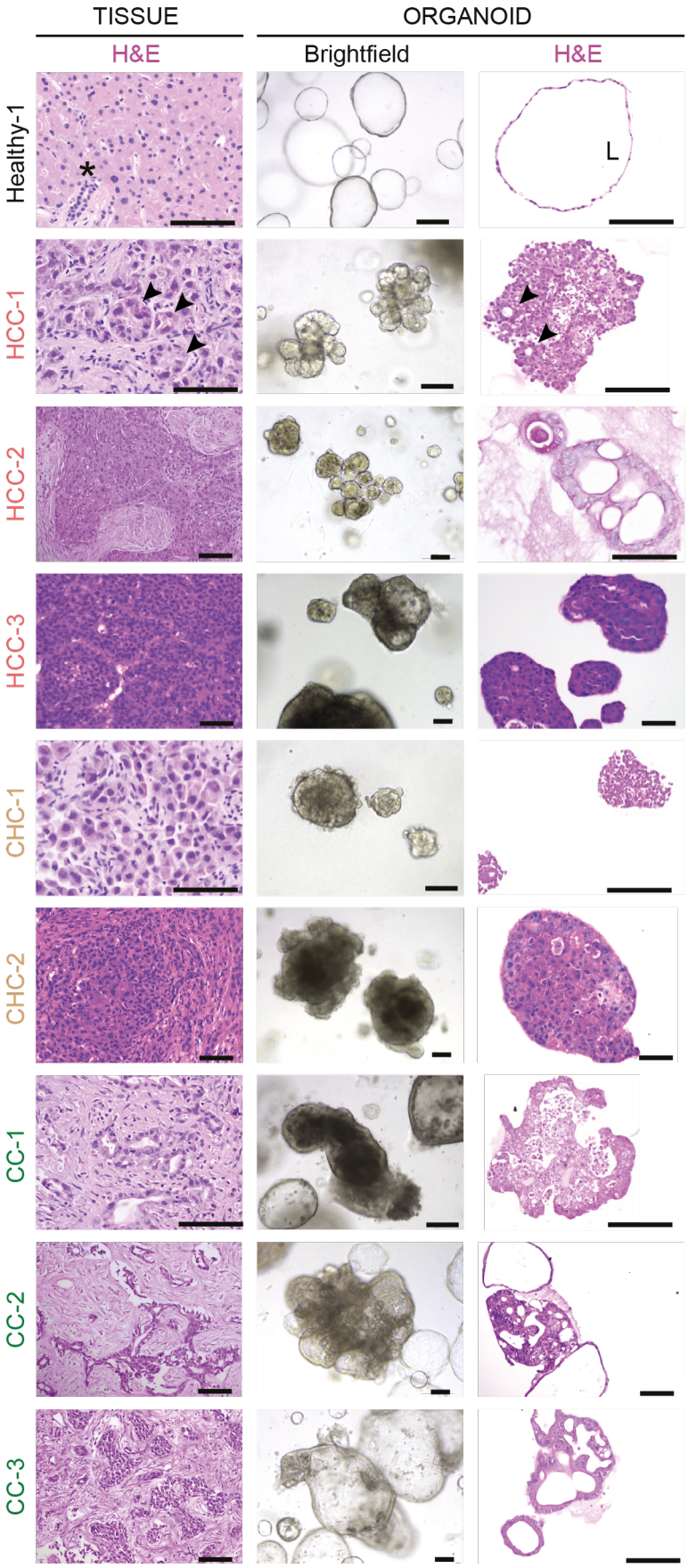

Figure 3.3. Tumoroids recapitulate the histologic features of the patient's tissue of origin. Representative H&E staining of healthy liver tissue and primary tumour (left column), and corresponding bright field microscopy images (middle column) and H&E histological analysis of the organoid lines derived from these (left column). *, duct; L, lumen; arrowheads, pseudoglandular domains. Scale bars, 100µm.

3.3 Tumoroids present genetic alterations and can be used for drug testing

Liver tumours present high percentage of aneuploidy and are characterized by defined genetic alterations. For this reason, we sought to analyse whether tumoroids would also recapitulate genetic abnormalities. As previously described, healthy tissue-derived organoids exhibit normal chromosome number with very low somatic base substitutions in coding regions that arise either *in vivo* or during culture derivation (Huch et al. 2014). Consistently with this, we found no chromosomal alterations in healthy-derived organoids (Figure 3.4a, b). Conversely, all the tumoroids lines we have generated presented multiple chromosomal aberrations with both gain and/or loss of chromosome numbers (Figure 3.4a, b).

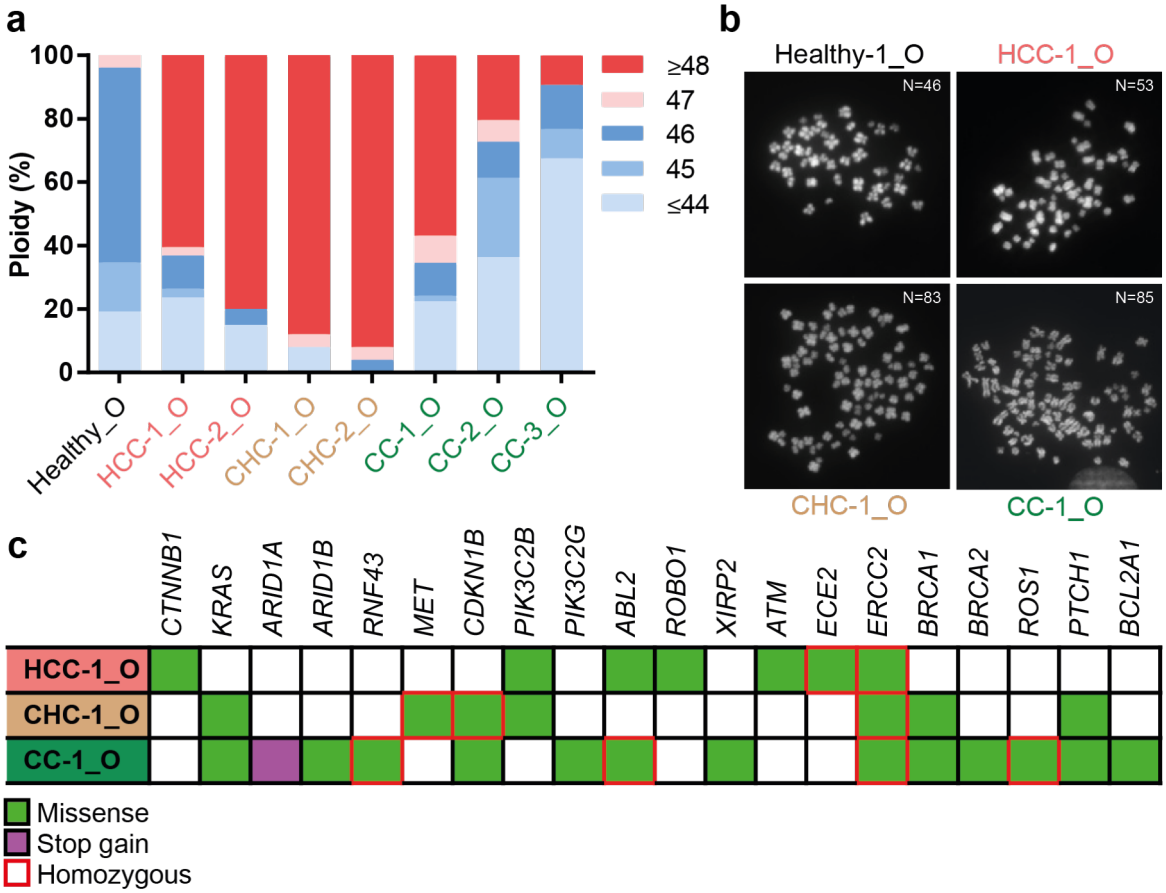

Figure 3.4. Tumoroids are aneuploid and recapitulate the genetic alterations of the patient's tissue of origin. a, b) Healthy organoids and tumoroids were treated with Colcemid reagent to halt proliferation during metaphase and were then processed for chromosome analysis and count. Graph represents ploidy analysis of organoid cultures derived from healthy/donor organoids (n=1), HCC (n=2), CHC (n=2) and CC (n=3) tissues and indicates the % of chromosomes counts present in each sample. Results are expressed as % of ploidy per number of metaphases counted (Healthy_O, n=26; HCC-1_O, n=38; HCC-2_O, n=20; CHC-1_O, n=25; CHC-2_O, n=25; CC-1_O, n=58; CC-2_O, n=44; CC-3_O, n=23). Experiment was performed at least in duplicate. Pictures are representative of organoid metaphases used for the ploidy analysis. **(c)** Whole exome sequencing was performed on DNA extracted from both primary tissue and respective tumoroid cultures. Tables show genes altered in organoid cultures and known to be mutated in liver or gastrointestinal tumours.

To further analyse the genetic alterations of our model system, we have then performed whole exome sequence analysis on one of each subtype of liver tumoroids, namely HCC-1_O, CHC-1_O, CC-1_O and corresponding patient's tissue. Interestingly, tumoroids exhibited different mutational patterns that reflected their subtype of origin (Figure 3.4c). Specifically, HCC tumours have high incidence of mutations in genes belonging to the Wnt signalling pathway and consistently, *CTNNB1* was found mutated in HCC-1_O tumoroids. Instead, homozygous mutations of *RNF43*, the only Wnt pathway-related gene found mutated so far in CCs, and heterozygous mutations of *ARID1A* and *ARID1B*, were found in CC-1_O tumoroids. In addition, *KRAS* (KRAS*G12D*) mutations were also found in CC-1_O and in CHC-1_O, but not in HCC-1_O, consistent with the subtype mutational profile. Importantly, all mutations found in the tumoroids were also found on the patient's tumour of origin, further validating the model system.

Knowing the mutational spectra of HCC-1_O, CHC-1_O and CC-1_O tumoroids, we sought to investigate whether we could use this knowledge to predict tumour drug sensitivity and resistance *in vitro*. To this purpose, we have cultured HCC-1_O, CHC-1_O and CC-1_O with the porcupine inhibitor IWP2 and the epithelial growth factor receptor (EGFR) inhibitor Gefitinib (Figure 3.5a, c).

The porcupine inhibitor IWP2 prevents WNTs secretion, thus it inhibits the WNT pathway and bears death to cells in which the pathway is not constitutively active. In line with this, organoids derived from healthy donors are not able to survive when cultured in presence of IWP2 (Huch et al. 2014). Consistent with the identified mutation in *CTNNB1,* HCC-1 tumoroids were able to survive and expand in presence of IWP2 (Figure 3.5a). On the other hand, Healthy-1_O, CHC-1_O and CC-1_O organoids did not survive the treatment. This data was suggesting that the *RNF43* mutations identified in CC-1_O were not enough to confer Wnt independency, consistent with the results observed in the mouse intestine (Koo et al. 2015). In addition, the IWP2 treatment did not affect the expression of the Wnt target genes *AXIN2*, *LGR5* and *TNSFRS19* only in HCC-1_O tumoroids, suggesting that the CTNNB1 mutation detected in this sample was enough to drive constitutive WNT pathway activation and WNT independency (Figure 3.5b).

Similarly, when HCC-1_O and CC-1_ tumoroids were treated with the EGFR inhibitor Gefitinib, CC-1_O were able to grow and expand, according to their mutations in

KRAS, but not healthy organoids and HCC-1_O tumoroids, where no mutations in the EGF signalling pathway were detected (Figure 3.5c).

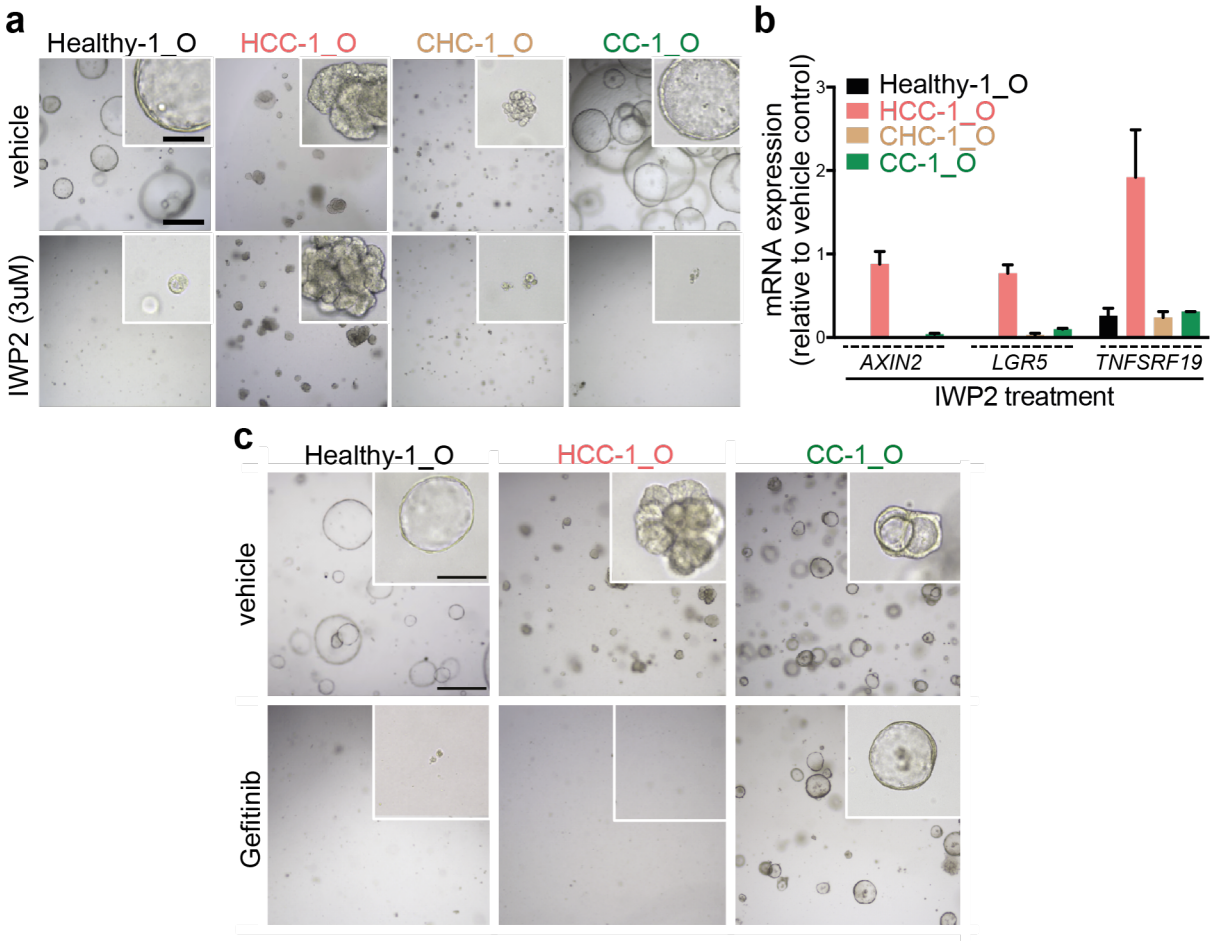

Figure 3.5. Tumoroids can be used for drug testing and to predict drug sensitivity a) Representative bright field microscopy images of organoid cultures derived from healthy-1, HCC-1, CHC-1 or CC-1 tissues tested for their sensitivity to treatment with the porcupine inhibitor IWP2 (3 µM) (1 of 3 independent experiments). Cultures were dissociated to single cells and then seeded in medium containing the drug. Pictures were taken 3 weeks after the seeding. Scale bars, 500µm and 100 µm (insets). **b)** RT-qPCR expression analysis of the Wnt target genes *LGR5*, *AXIN2* and *TNFRSF19* on IWP2 treated cultures. Fold change was calculated relative to the expression on the vehicle-treated control (DMSO control). Results are expressed as mean ± STD of 2 independent experiments. **c)** Representative bright field microscopy images of organoid cultures derived from Healthy-1, HCC-1 and CC-1 tissues tested for their sensitivity to treatment with the EGFR inhibitor Gefitinib (1 µM) (1 out of 2 independent experiments). Cultures were dissociated to single cells and then seeded in medium containing the drug. Pictures were taken 3 weeks after the seeding. Scale bars, 500µm and 100 µm (insets).

Overall, tumoroids show extensive chromosomal abnormalities and recapitulate the genetic spectrum of the tumour subtype of origin. Importantly, tumoroids can be used to predict and test drug sensitivity and resistance according to their mutational profile.

3.4 Tumoroids model tumour subtype and metastasis *in vivo*

To determine whether tumoroids have the potential to give rise to tumours *in vivo* and to recapitulate patient's tumour histology even after long term expansion in culture (>3 months), we performed subcutaneous grafting of HCC-1_O and CC-1_O tumoroids and kidney capsule transplant of CC-1_O tumoroids in immunocompromised NSG mice (Figure 3.6).

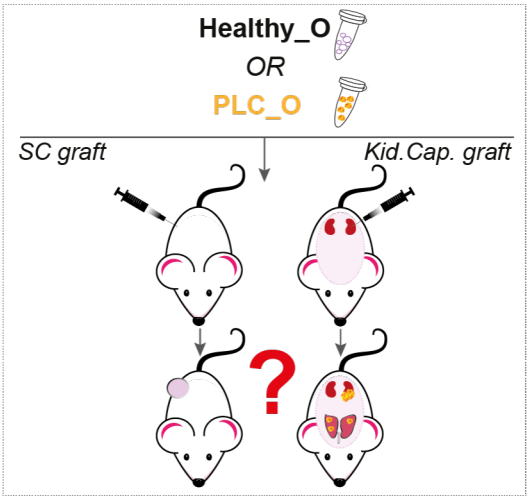

Figure 3.6. Experimental design of xenograft transplant. PLC tumoroids or healthy organoids were transplanted subcutaneously (SC) or under the kidney capsule (Kid.Cap.) of immunocompromised NSG mice and analysed for the presence of tumour growth and metastasis at different time points.

To perform subcutaneous xenograft experiments, a total of ~1 million cells were injected under the skin of immunocompromised mice. Healthy organoids were used as control. Mice were monitored constantly for tumour growth and analysis was performed at 1 and 5 months after the injections. Tumour outgrow was found in animals injected with CC-1_O (6/6) and HCC-1_O (4/6) but not in animals injected with healthy organoids (0/12) (Figure 3.7). Interestingly, CC-1_O derived tumours presented a strong stromal reaction with glands formation and cribriform structures, reminiscent of the CC-1 patient's original tissue (Figure 3.7a). Similarly, pseudo-glandular structure resembling those found in HCC-1 patient's original tissue could also be observed in HCC-1 tumoroid-derived tumours (Figure 3.7b).

To test the metastatic potential of the tumoroid cultures, we injected CC-1_O cells, derived from a patient with history of metastasis, into the kidney capsule of immunocompromised NSG mice (Figure 3.8). Mice were analysed 0.5, 1, 2 and 3 months after injection. In all cases (9/9) mice developed tumours in the kidney, as

confirmed by KRT19 staining (Figure 3.8a, c). Like in the subcutaneous grafting, tumours resembled the original patient's tissue. More importantly, 7 out of 9 mice also developed secondary metastatic nodules in the lungs proving that CC-1_O can retain the metastatic potential of the cells *in vivo* even after long term expansion in culture (Figure 3.8b).

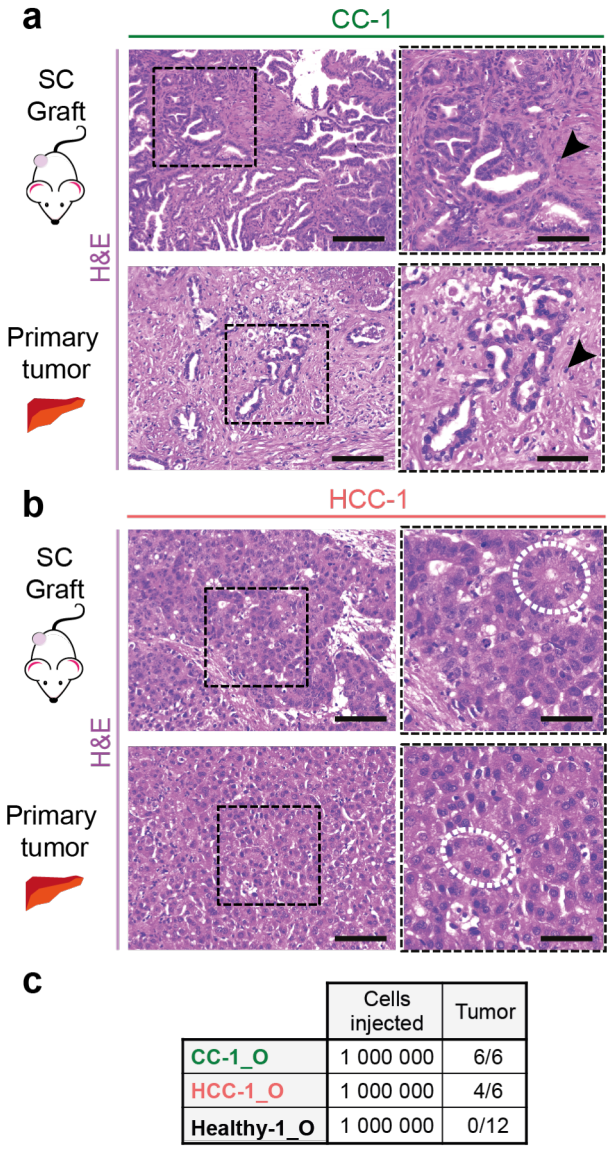

c

	Cells injected	Tumor
CC-1_O	1 000 000	6/6
HCC-1_O	1 000 000	4/6
Healthy-1_O	1 000 000	0/12

Figure 3.7. Tumoroids induce tumour formation *in vivo* maintaining their identity. Tumoroids and healthy organoids were broken into pieces and then injected subcutaneously into nude mice. **a)** Representative H&E staining of CC-1 tumoroids transplanted subcutaneously (top) into NSG mice and corresponding CC-1 patient's tumour sample (bottom). Arrowheads, desmoplasia. Scale bars are top left 250µm; top right 125µm; bottom left 125µm and bottom right 62.5µm. **b)** Representative H&E staining of HCC-1 tumoroids transplanted subcutaneously (top) into NSG mice and corresponding HCC-1 patient's tumour sample (bottom). Dashed circles, pseudoglandular domains. Scale bars are left 125µm and right 62.5µm. **c)** Table summarizing the number of cells injected and the number of tumours formed.

Overall, these data show that tumoroids can give rise to tumours *in vivo* that faithfully recapitulate the tumour subtype histology and retain patient's tissue of origin features, including the metastatic potential even after long-term expansion in culture.

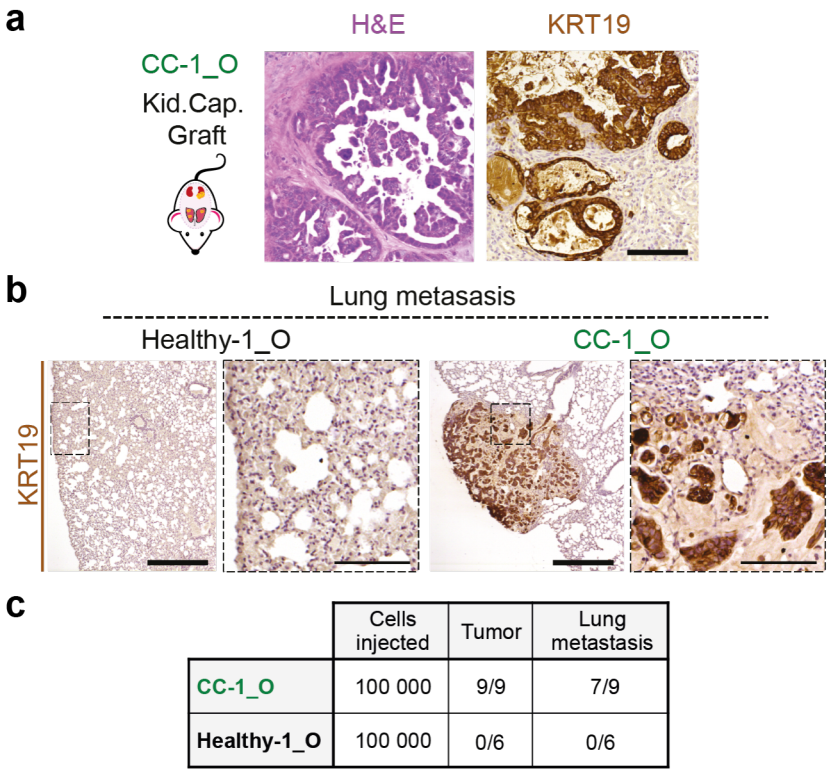

c

	Cells injected	Tumor	Lung metastasis
CC-1_O	100 000	9/9	7/9
Healthy-1_O	100 000	0/6	0/6

Figure 3.8. Tumoroids recapitulate metastatic potential of the tumour of origin. a) Representative H&E (left) and KRT19 (right) immunochemistry analyses of CC-1 tumoroids transplanted under the kidney capsule into NSG mice. Scale bars, 125µm. **b)** Lung metastases derived from the human CC-1 tumoroids transplanted under the kidney capsule cells (right panels) were identified using a human specific KRT19 antibody. Scale bars, 500µm, magnification 125µm. **c)** Table summarizing the number of cells injected and analysis of tumour and lung metastasis.

4. RESULTS - PART II

CRISPR/Cas9 genome engineering of human liver organoid to model liver cancer *in vitro*

4.1 Summary

Tumoroids can have different applications and may contribute to better understanding tumour biology. More importantly, tumoroids may facilitate discovery of new drugs to use as targeted therapeutic strategy. However, their use resents limitation when aiming at studying specific genes and their contribution to cancer formation. To overcome this issue, in this section I will present a different approach, involving the use of CRISPR/Cas9 genome engineering to specifically introduce PLC-related mutations in healthy human liver organoid cultures.

Applying the CRISPR/Cas9 technology to human liver organoids I have successfully introduced indel mutations in *TP53*, *RNF43* and *ZNRF3*. Interestingly, when mutating *TP53*, organoids acquire histology and genetic aberrant features reminiscent of malignant transformation. To test the ability of this system to study less known mutations, I have generated R&Z double mutants organoids, showing for the first time a role for R&Z in the WNT pathway in a human setting and specifically in the liver, similar to what has been previously described in the mouse intestine (Koo et al. 2012). Interestingly, when *TP53* and *R&Z* were mutated together, organoids resembled, in part, the patient's derived tumoroids described in section 3.2.

This data show that while mutations in *TP53* could be driver of cancer in human liver cells, R&Z might instead have a role in tumour progression. Also, this system could represent a new method to test contribution of genetic mutations to cancer formation in human cells before using animal models, thus it may eventually facilitate gene function studies in human cancer research.

4.2 TP53 mutations induce phenotypic changes to healthy human organoids resembling malignant transformation

To study gene functions and identify the contribution of genes to cancer formation, I have established a protocol for introducing indel mutations in healthy human liver organoids using the CRISPR/Cas9 system (Figure 4.1). Briefly, organoid cultures were dissociated to small clumps of 1-3 cells and subsequently transfected with a plasmid containing gRNA, Cas9 and a GFP. GFP^+ transfected cells were sorted and seeded in BME/2 at low concentration to allow for clonal expansion. Clonal organoids were then isolated and screened for mutations. Whenever possible, positive clones were selected either by growth factor withdrawal or drug treatment.

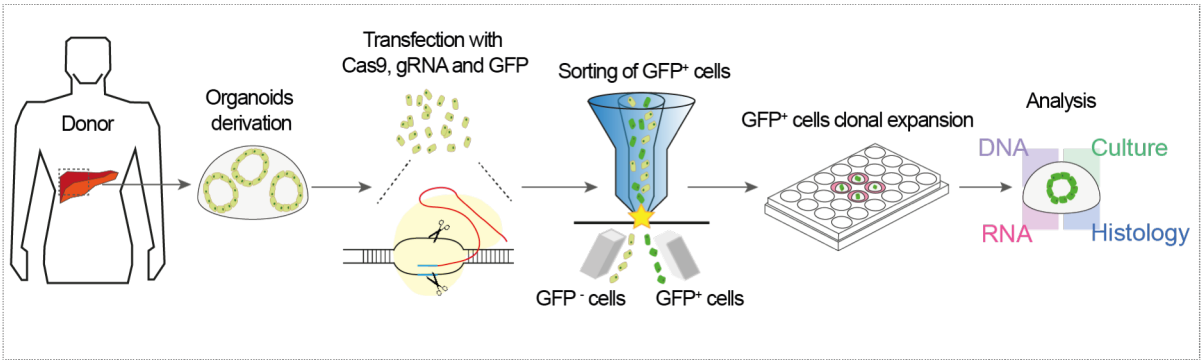

Figure 4.1. Schematic overview of CRISPR/Cas9 genome engineering workflow. Human liver organoids were derived from liver biopsies and then expanded and transfected with gRNA, Cas9 and GFP reporter gene. After 2 days of incubation, cells were sorted for GFP and seeded sparsely for clonal expansion and further analysis.

TP53 is frequently mutated in both HCC and CC and it is thought to be one of the early step in tumorigenesis (Guichard et al. 2012; Zou et al. 2014). For this reason, targeting *TP53* was an obvious choice when trying to recapitulate a tumour phenotype using organoid cultures. To inactivate TP53, I have designed gRNAs targeting the DNA binding domain (DBD), essential to exert its function. After the generation of a plasmid containing gRNA targeting *TP53*, Cas9 and GFP reporter protein, human liver organoid cells were transfected using either lipofectamine 3000 or electroporation. Upon transfection, GFP^+ cells were readily detectable after 24h incubation and were sorted after 48h incubation (Figure 4.2a). Clonally expanding cells were then isolated and maintained as separate cultures. To select for mutant clones with functionally inactive TP53, I have added Nutlin3 to the culture medium. Nutlin3 is a small molecule inhibitor that induces activation of TP53 and thus results in cell cycle arrest and/or apoptosis (Schug 2009; Hardcastle 2007). In this condition, only TP53 mutated cells were

allowed to grow and expand (Figure 4.2b, c). Confirmation of mutation was done by Sanger sequencing analysis (Figure 4.2d). Using this approach, I have generated two independent lines with mutation in *TP53*. Interestingly, also the clone carrying in-frame mutations in *TP53* was resistant to Nutlin3 treatment, suggesting functional inactivation of the DBD. Specifically, organoid formation efficiency of the two clones generated was not affected by the presence on Nutlin3 in the culture (Figure 4.2c). On the other hand, control culture from which the clones have been originated, but that has not been through the full procedure of transfection and sorting, was deeply affected by the treatment (Figure 4.2c). Of note, *TP53* mutant organoids were smaller in size and had a slower growth rate when compared to control healthy organoids (Figure 4.2b). Mutant cultures eventually stopped expanding after a few passages, thus preventing full analysis of the culture. This difference might either be a direct effect of the *TP53* mutation, or a consequence of the stressful procedures the cells have been through. Further data need to be collected in order to rule out this hypothesis.

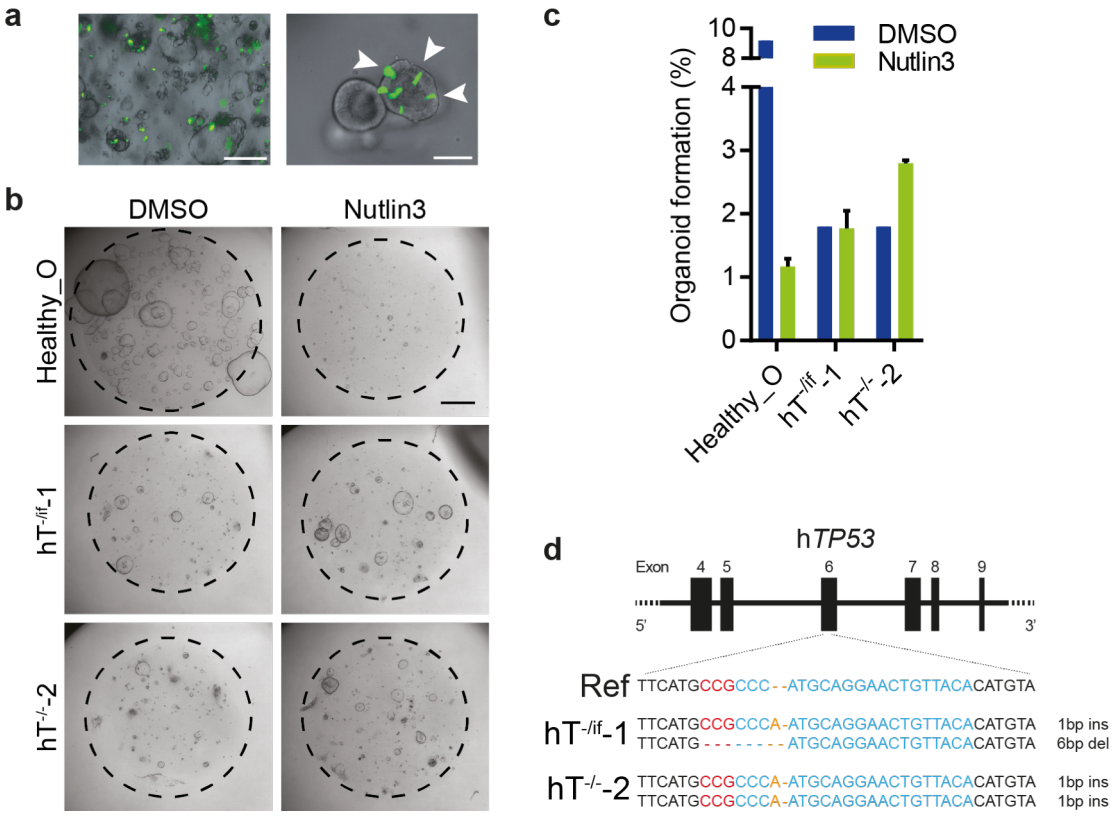

Figure 4.2. *TP53* mutated organoids resist Nutlin3 treatment. a) Pictures of transfected organoids. Arrows, GFP+ cells in an organoid. Scale bar, 250µm (left pictures) and 100µm (right pictures). **b)** Brightfield pictures of healthy and *TP53* mutant organoids with and without Nutlin3 5µm. Scale bar, 1mm. **c)** Graph showing organoid formation efficiency in normal condition and Nutlin3 (5µm) treated cultures. Data represent mean of technical replicates ± SEM. **d)** DNA sequence of mutated clones. RED, PAM sequence; BLUE, gRNA target sequence; ORANGE, insertion; -, deletion. Ref, reference; h, human; T, TP53; ins, insertion; del, deletion.

To further confirm *TP53* inactivation, I have analyzed RNA levels of *CDKN1A*, downstream target of TP53. Strikingly, *CDKN1A* expression levels were highly reduced in both hT$^{-/if}$-1 and hT$^{-/-}$-2 when compared to healthy not-processed TP53 wild-type donor organoids, further confirming successful inactivation of the gene. (Figure 4.3a).

As TP53 is involved in maintaining the correct number of chromosomes during cell division, I have performed karyotype analysis to investigate the presence of chromosomal abnormalities, a hallmark of cancer. Surprisingly, both clones presented aneuploidy with multiple chromosomal gains (Figure 4.3b). This data suggests that the inactivation of TP53 alone is able to induce chromosomal abnormalities in human liver organoid cells. Of note, Healthy_O retained their chromosome number as expected and published in Huch et al. 2014.

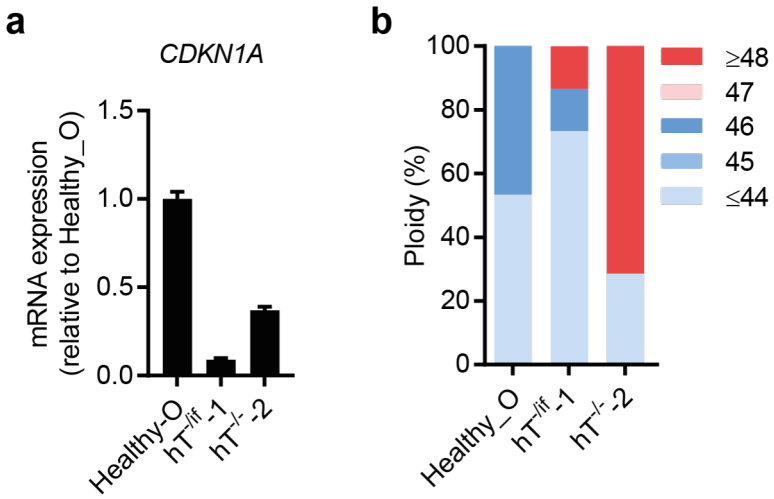

Figure 4.3. *TP53* mutated organoids have low expression of *CDKN1A* and are aneuploid. a) Expression analysis for *CDKN1A* in mutant clones hT$^{-/if}$-1 and hT$^{-/-}$-2 and healthy organoids. Data represent mean ± SEM. **b)** Healthy organoids TP53 clones were treated with Colcemid reagent to halt proliferation during metaphase and were then processed for chromosome analysis and count. Graph represents ploidy analysis of mutant organoid cultures and indicates the % of chromosomes counts present in each sample. Results are expressed as % of ploidy per number of metaphases counted (Healthy_O, n=15; hT$^{-/if}$-1, n=15; hT$^{-/-}$-2, n=7).

At microscopic evaluation, although *TP53*-mutated organoids were still preserving a cyst-like hollow structure typical of healthy organoids, they exhibited a thickening of the outer cell layers (Figure 4.4, brightfield).

To investigate whether these changes were also reflected at histological level, I have performed H&E staining of formalin-fixed paraffin-embedded *TP53*-mutated organoid. Interestingly, CRISPR-mutated organoids presented tumour-like features. Specifically, both clones exhibited abnormal architecture, general thickening and multiple invaginations in the organoids lumen resembling tumour growth (Figure 4.4). These

data suggest that inactivation of TP53 in human liver organoid cells can drive phenotypical and structural changes resembling tumour formation.

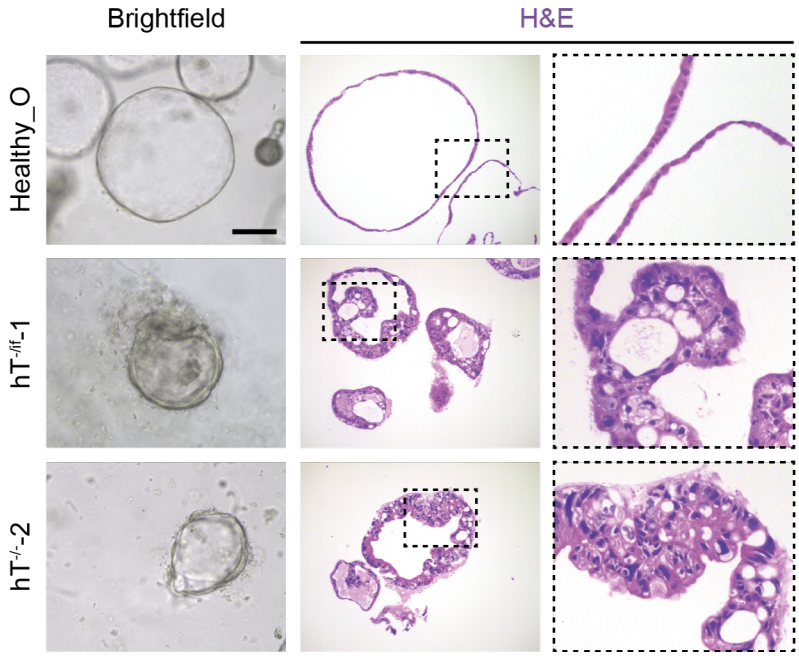

Figure 4.4. *TP53* mutated organoids acquire histologic tumoral features. Representative brightfield microscopy images (left column) and H&E histological analysis (middle column) of the CRISPR-mutated organoid lines. Scale bar, 100µm. Note difference between Healthy_O (single layer epithelium) and TP53 mutated cultures (thick organoid with budding structures).

The phenotypic changes observed in the *TP53*-mutated organoids suggest that these cultures are losing their ductal nature in favour of a hepatocytes/tumour phenotype. To corroborate this hypothesis, I have analyzed the expression of common ductal and hepatocyte markers in the two mutant lines. Remarkably, I have observed a decrease of expression of the ductal marker *SOX9*, but not *KRT19*, and an increase expression of the hepatocyte marker *CYP3A4*, but not *HNF4α* (Figure 4.5). These data might suggest that *TP53*-mutated organoids are changing their differentiation status. However, a more extensive analysis is needed to confirm this hypothesis.

Overall, mutating *TP53* in human liver organoid confer the cultures resistance to Nutlin3 treatment and more importantly, organoids acquire features of malignant transformation, including genetics and histologic alterations. However, as previously mentioned, mutant cultures stopped expanding after a few passages in cultures, making it difficult to confirm the results observed.

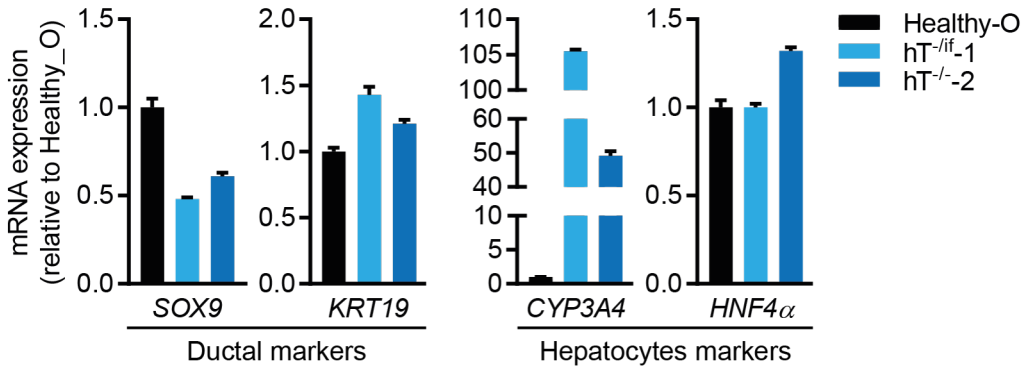

Figure 4.5. *TP53* mutated organoids have altered gene expression of differentiation markers. qRT-PCR expression analysis for ductal and hepatocytes markers in mutant clones $hT^{-/if}$-1 and $hT^{-/-}$-2 and healthy organoids. Data represent mean ± SEM.

4.3 R&Z mutations induce activation of WNT pathway in organoid cultures

Having proved that the CRISPR-Cas9 technology can be applied to human liver organoid cultures, I asked whether this approach could be used to perform preliminary gene function studies of less known genes. To this purpose, I thought to investigate the role of RNF43 and ZNRF3 (R&Z) in liver using human liver organoids, as these genes have recently been associated with cancer and little is known about their role in liver. Of note, R&Z are homologous E3 ubiquitin ligases recently found to be negative regulators of the Wnt pathway and to have tumour suppressor role in the mouse intestine (Koo et al. 2012). Interestingly, *ZNRF3* has recently been found mutated in HCC, meanwhile *RNF43* is the only WNT pathway-related gene found mutated in CC so far (Schulze et al. 2015; Ong et al. 2012; Talabnin et al. 2016).

To inactivate *RNF43* and *ZNRF3*, gRNAs were designed to target a region before the functional RING domain, responsible for Frizzled ubiquitination and degradation. As previously described, cells were transfected with plasmids containing gRNAs, Cas9 and GFP reporter and then were sorted after 48h. Clonally expanding cells were isolated and maintained as separate cultures. I have generated a total of 20 organoid lines that I have then used to select for positive *R&Z* mutations.

I hypothesized that *R&Z* mutant liver organoids would survive R-spondin1 withdrawal, similar to *R&Z* mutated intestinal organoids which are reported to survive in culture without this essential growth factor (Koo et al. 2012). Strikingly, three lines were

resistant to the restricted media conditions and could be expanded for several passages (Figure 4.6a, b, c). The remaining 17 lines died after 2-3 passaging in absence of R-spondin1, suggesting that they were not mutant for *R&Z* (Figure 4.6a).

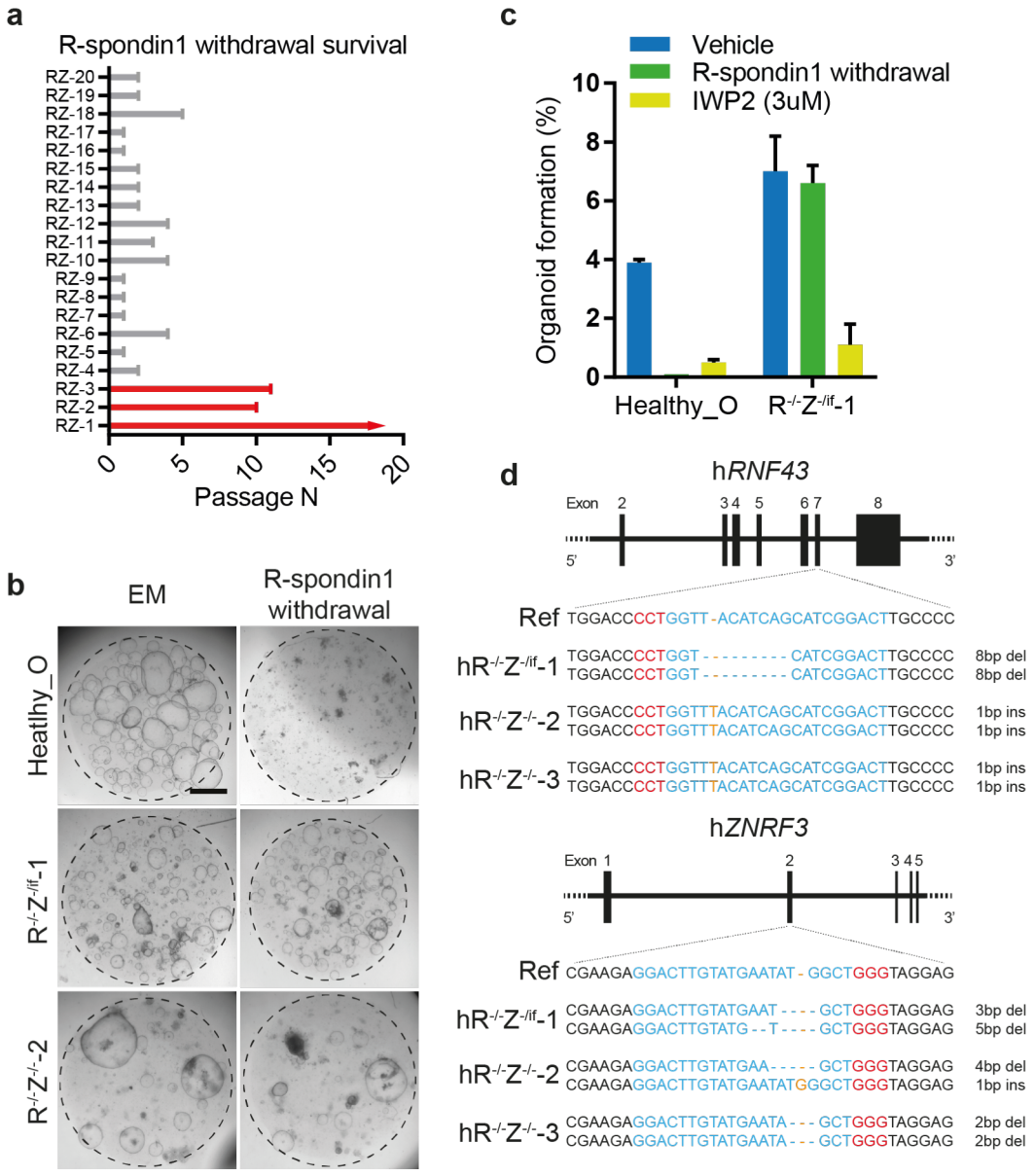

Figure 4.6. ***R&Z* mutated organoids resist R-spondin1 withdrawal and are sensitive to porcupine inhibition. a)** Transfected clones were selected by removal of the growth factor R-spondin1. Graph shows survival of the mutant clones after several passaging. **b)** Brightfield pictures showing R-spondin1 withdrawal resistance of mutated clones. Scale bar, 1mm. **c)** Graph showing organoid formation efficiency in normal condition, R-spondin1 withdrawal and IWP2 (3µm) treated cultures. Experiment was performed twice. Data represent mean ± SEM. **d)** DNA sequence of mutated clones. RED, PAM sequence; BLUE, gRNA target sequence; ORANGE, insertion; -, deletion; Ref, reference; h, human; R, RNF43; Z, ZNRF3; ins, insertion; del, deletion.

As expected, the three resistant lines (hRZ-1, hRZ-2 and hRZ-3) were found to be mutated in both genes after performing Sanger sequencing analysis (Figure 4.6d). Specifically, hRZ-2 and hRZ-3 had frameshift mutations in both genes (hR$^{-/-}$Z$^{-/-}$-2, hR$^{-/-}$Z$^{-/-}$-3), while hRZ-1 had an in-frame mutation in one of the *ZNRF3* alleles and

frameshift mutations in the other alleles (hR$^{-/-}$Z$^{if/-}$-1). Unfortunately, hR$^{-/-}$Z$^{-/-}$-2 and hR$^{-/-}$Z$^{-/-}$-3 stopped expanding when they reached passage 10, while hR$^{-/-}$Z$^{if/-}$-1 was still proliferating and has been expanded up to 19 passages (Figure 4.6a). For this reason, also in this case it has not been always possible to repeat the experiments and to confirm the results observed.

To further confirm functional inactivation of R&Z in hR$^{-/-}$Z$^{if/-}$-1, I have performed an organoid formation assay by dissociating the culture to single cells, culturing them in different conditions and quantifying the number of growing organoids (Figure 4.6c). As expected, I observed no difference in organoid formation efficiency in the mutant clone with or without R-spondin1 (~7%). On the other hand, the organoid formation efficiency of healthy organoids (parental line not subjected to the engineering procedure) dropped to 0% in absence of R-spondin1 as previously reported (Huch et al. 2014). Expectedly, when the porcupine inhibitor IWP2 (that prevents WNT secretion, thus inhibiting the WNT pathway activation) was added to the media, organoid formation efficiency plummeted in both cases, suggesting that *R&Z* mutant organoids still need a WNT ligand source in order to survive.

At microscopic evaluation, I could not observe any significant difference between the mutated cultures and healthy organoids. Similarly, both healthy and mutated organoids presented a one layer cyst-like structures when stained with H&E and did not show any abnormalities (Figure 4.7). This suggests that mutating *R&Z* alone it is not enough to induce tumour-like changes at histological level.

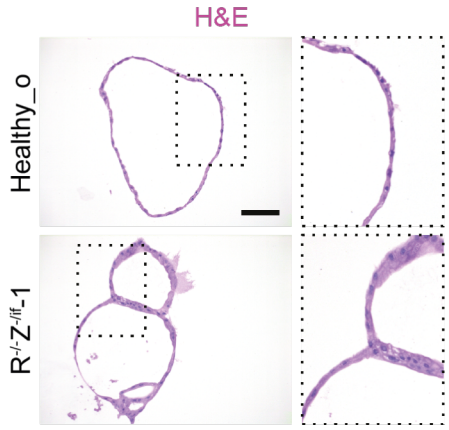

Figure 4.7. *R&Z* mutated organoids do not present histologic alterations. Representative pictures H&E staining of formalin-fixed paraffin-embedded organoids. Scale bar, 100µm.

To further confirm that R&Z inactivation results in WNT pathway activation, I have performed RNA analysis of common WNT target genes. *AXIN2* was upregulated in

both hR$^{-/-}$Z$^{-/if}$-1 and hR$^{-/-}$Z$^{-/-}$-2, whereas *LGR5* was upregulated only in hR$^{-/-}$Z$^{-/-}$-2, suggesting that both *ZNRF3* alleles are required to be inactivated to fully trigger WNT pathway activation in human organoid cultures (Figure 4.8). Interestingly, I have also observed an increase in both ductal and hepatocytes markers, suggesting that R&Z might somehow also play a role in maintaining the differentiation status of the culture (Figure 4.8). Further investigations, including testing the ability of *R&Z* mutated cultures to differentiate into functional hepatocytes, will help to test this hypothesis.

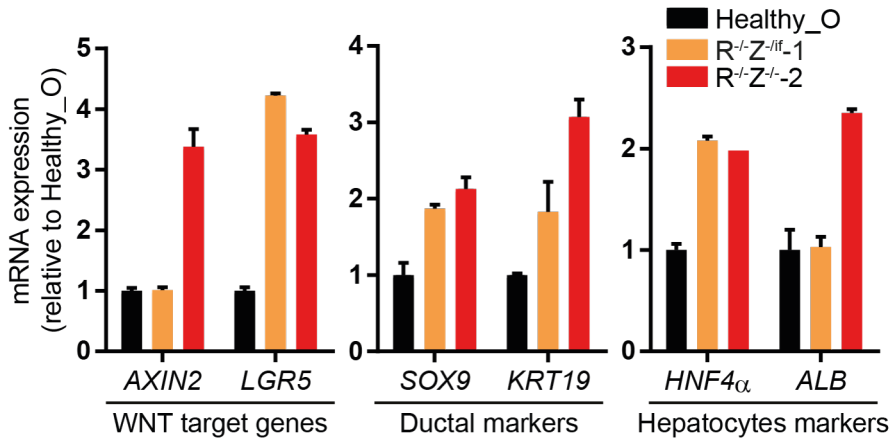

Figure 4.8. *R&Z* mutated organoids show WNT pathway activation and altered gene expression of differentiation markers. qRT-PCR expression analysis for Wnt target genes and ductal and hepatocytes markers in *R&Z* mutant cultures and healthy organoids. Data represent mean ± SEM.

4.4 *R&Z* and *TP53* mutations combined induce a tumoroid-like phenotype in human liver organoids

As demonstrated in section 4.2, *TP53* mutated organoids acquire features of malignant transformation, whereas *R&Z* mutations induce WNT pathway activation in organoid cultures. These data suggest that while mutations in *TP53* could act as driver mutations in cancer, R&Z cannot. To investigate whether R&Z could have a role in promoting tumour progression, I have decided to generate human liver organoid cultures carrying mutations in both *TP53* and *R&Z*.

Cells were transfected with three plasmids containing gRNA for *RNF43*, *ZNRF3* and *TP53* together with Cas9 and then sorted for GFP fluorescence after 48h. Once again, clones were selected by adding Nutlin3 to media condition right after sorting, allowing growth of only *TP53* mutated cells. A total of 16 resistant clones were isolated and expanded. Sanger sequencing analysis revealed presence of mutations predicted to inactivate all three genes in 4 different clones (Figure 4.9).

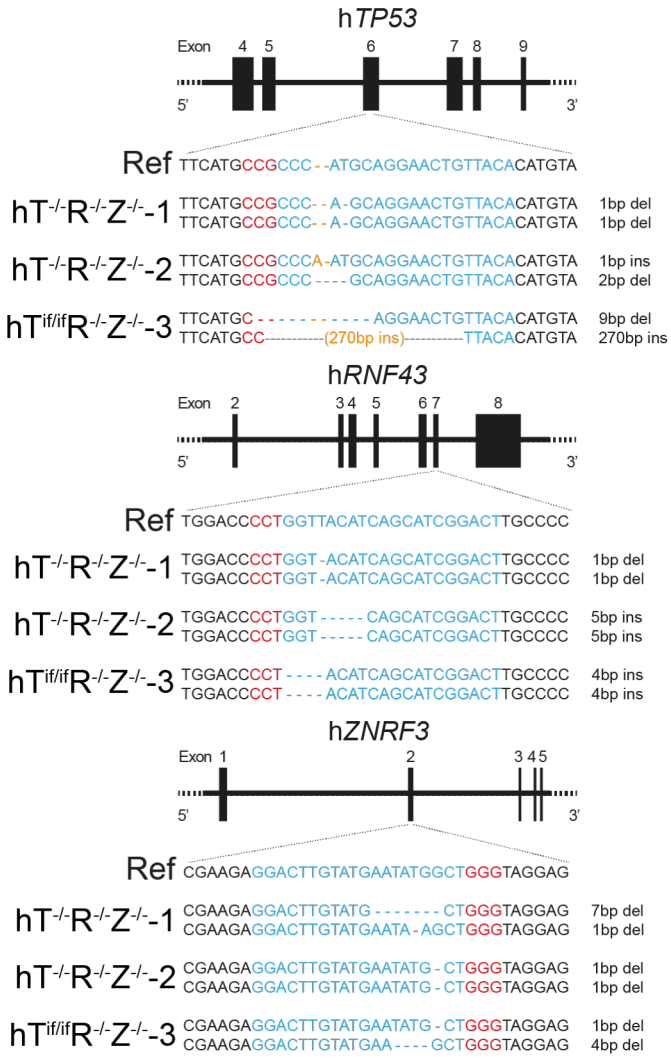

Figure 4.9. DNA sequence of *TP53* and *R&Z* triple mutant clones. RED, PAM sequence; BLUE, gRNA target sequence; ORANGE, insertion; -, deletion; Ref, reference; h, human; T, TP53; R, RNF43; Z, ZNRF3; ins, insertion; del, deletion.

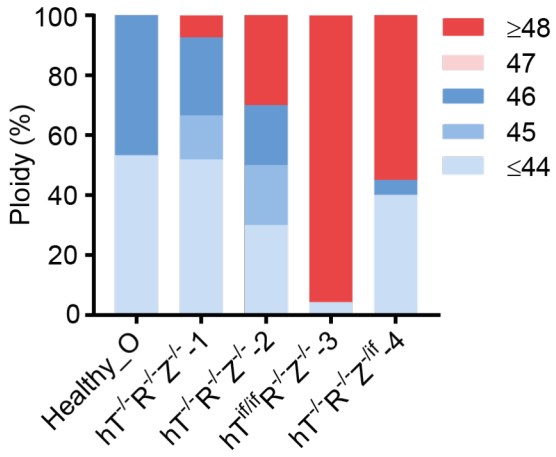

Figure 4.10. *TP53* and *R&Z* triple mutant clones are aneuploid. Ploidy analysis of mutant organoid cultures. Graph indicates the % of chromosomes counts present in each sample. Results are expressed as % of ploidy per number of metaphases counted (Healthy_O, n=15; $hT^{-/-}R^{-/-}Z^{-/-}$-1, n=20; $hT^{-/-}R^{-/-}Z^{-/-}$-2, n=27; $hT^{if/if}R^{-/-}Z^{-/-}$-3, n=23; $hT^{-/-}R^{-/-}Z^{-/if}$-4, n=20).

To test for abnormalities in chromosome numbers, I have performed karyotype analysis. Expectedly, aneuploidy was found in all clones analyzed. Interestingly, one clone, $hT^{if/if}R^{-/-}Z^{-/-}$-3, exhibited more than 90% of chromosomal gains (Figure 4.10).

At microscopic observation, some organoids presented as darker, more compact structures or enlargement of the outer cell layer (Figure 4.11), resembling what we had previously observed with the patients-derived tumoroids. For example, $hT^{-/-}R^{-/-}Z^{-/-}$-1 and $hT^{-/-}R^{-/-}Z^{-/-}$-2 presented pseudoglandular-like structures also observed in HCC-derived tumoroids, whereas $hT^{if/if}R^{-/-}Z^{-/-}$-3 exhibited general thickening and abnormal architecture.

Overall, this data suggests that although mutations in *TP53* alone are able to induce both chromosomal abnormalities and histologic changes to normal organoids, further mutations might be needed to achieve a tumoroid-like state. In addition, *R&Z* mutations seem to be able to further push towards a tumoroid-like phenotype (darker, more compact structures), suggesting a possible role for R&Z in promoting liver cancer progression.

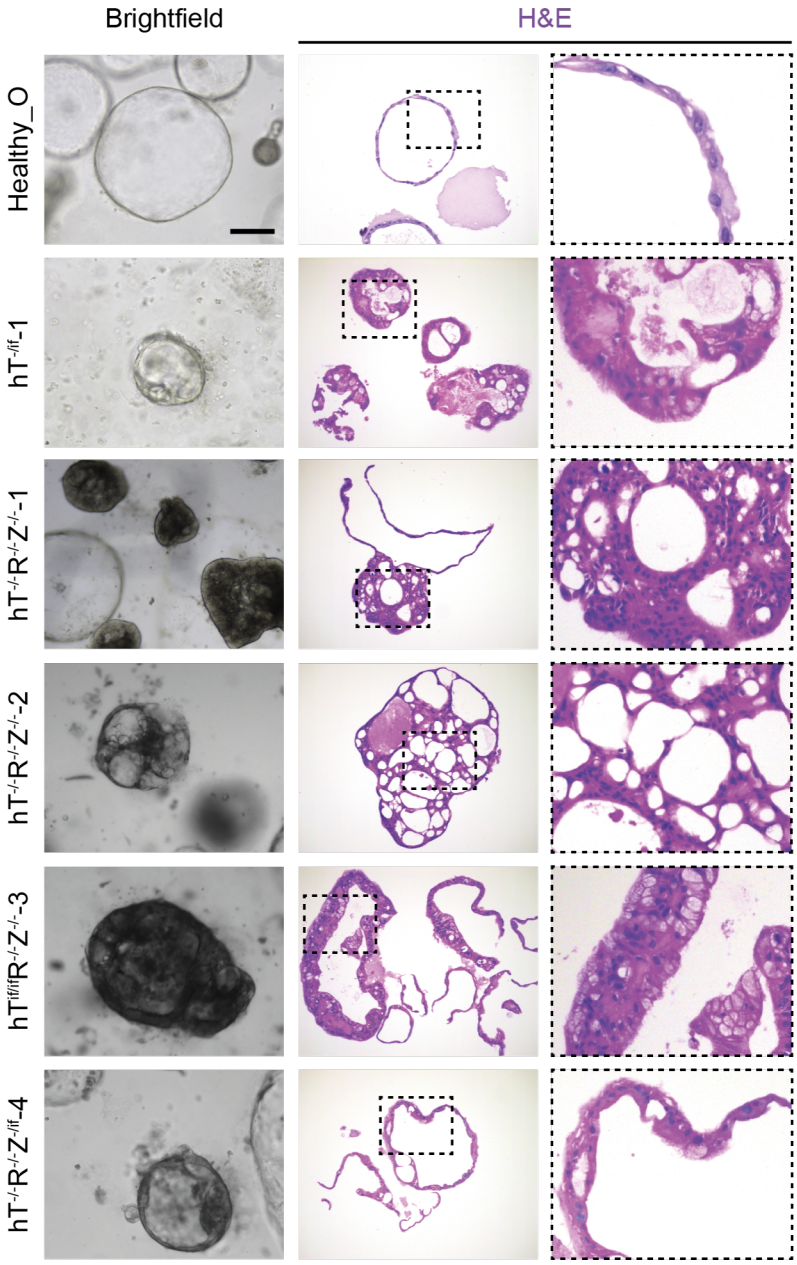

Figure 4.11. *TP53* and *R&Z* triple mutant clones show tumoroid-like features. Representative brightfield microscopy images (left column) and H&E histological analysis (middle column) of the CRISPR-mutated organoid lines. Scale bar, 100µm. Note difference between Healthy_O and mutated cultures.

5. RESULTS PART III

The role of RNF43 and ZNRF3 in adult liver homeostasis and repair

5.1 Summary

RNF43 and ZNRF3 (from here on called R&Z) promote negative regulation of the Wnt pathway by controlling the level of Frizzled on the cell surface. Interestingly they have been found to act as tumour suppressors in the mouse intestine, inducing adenoma formation after few weeks from the deletion (Koo et al. 2012). Of note, *R&Z* have been found to be mutated in several cancer types, including HCC and CC (Guichard et al. 2012; Ong et al. 2012), but their role in liver cancer (or physiology) have not been fully explored yet. Only recently, after R&Z global deletion from the adult mice, they have been suggested to be important in regulating liver metabolic zonation (Planas-Paz et al. 2016).

In this section, I investigate the role of R&Z in the liver by specifically deleting the two genes in either adult hepatocytes or biliary ducts. Firstly, I have analysed and showed the R&Z are both expressed in the liver and, more specifically, in both the hepatocyte and cholangiocyte compartments.

Upon *R&Z* deletion in ductal compartment using a Sox9CreERT2 line, I observed no significant difference between deleted and non-deleted livers both in normal conditions or when mice were fed a DDC diet, known for triggering ductular reaction. However, I have established organoid cultures from the *R&Z* deleted ducts and I have demonstrated that mouse liver organoids lacking R&Z show similar phenotype to what I have observed with the CRISPR-generated *R&Z* mutant human liver organoid, further validating the model system.

When *R&Z* was deleted in hepatocytes, I have observed overexpression of WNT target genes, an increase in liver volume, fat accumulation and alteration of the metabolic pathways of the liver (similar to human livers affected by steatosis), suggesting a

possible role for R&Z in controlling liver metabolism. In addition, the histological features observed resemble human livers affected by non-alcoholic fatty liver disease.

Furthermore, when livers were challenged to regenerate after a chronic damage, they exhibited multiple regenerative nodules and mild fibrosis already at 3 months from induction, while at later stages, focal nodular hyperplasia and early HCCs arose from the liver parenchyma.

All together, these data suggest that although R&Z seem to not be involved in regulating ductular reaction, they play a role in maintaining a balanced metabolism during homeostasis and also are essential to promote correct regeneration following chronic damage.

5.2 *R&Z* are expressed in the liver during homeostasis

First, I have analysed the expression pattern of the two genes during homeostasis in different liver compartments, including hepatocytes, biliary ducts, macrophages, endothelial cells and mouse liver organoid cultures. The strategy for collection of hepatocytes and non-parenchymal cells (ducts, endothelial cells and macrophages) is shown in Figure 5.1a, b.

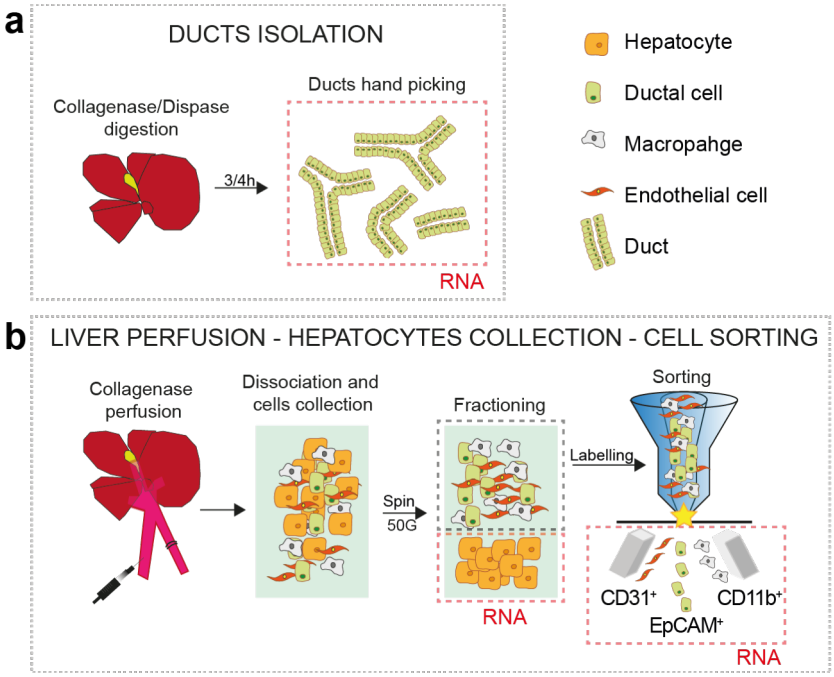

Figure 5.1. Diagram representing strategy for duct isolation and liver perfusion, hepatocytes collection and cell sorting. a) Livers were digested with collagenase and dispase solution for 3-4 hours until clean ducts were visible. Ducts were then isolated by picking manually under a microscope. **b)** Livers were perfused with collagenase and then mechanically dissociated. Hepatocytes were separated from the mixture by centrifugation at 50G. Ductal cells were labelled with anti-EpCAM antibody, macrophages with anti-CD11b antibody and endothelial cells with anti-CD31 antibody and then sorted. RNA was collected from all the isolated cell types.

Upon RNA analysis, expression of both *R&Z* was detected in the total liver, hepatocytes, biliary ducts and at lower level in mouse liver organoids (Figure 5.2a). Low levels of expression of *Axin2* were also found in these compartments, suggesting basal activation of the WNT pathway (Figure 5.2a). Of note, *R&Z* expression was also detected in sorted ductal cells. Here, *Znrf3* levels were higher than *Rnf43*, reflecting the same expression pattern observed in the isolated ducts (Figure 5.2b). Conversely, very low expression was detected in endothelial cells and no expression was found in macrophages (Figure 5.2b).

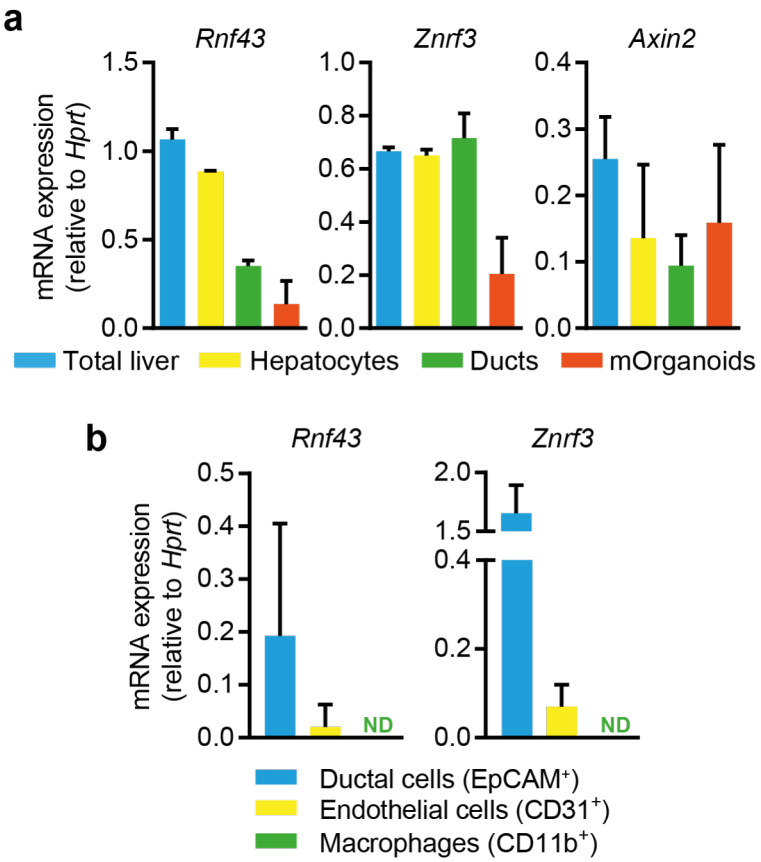

Figure 5.2. *R&Z* expression in liver compartments. a) qRT-PCR expression analysis or *Rnf43*, *Znrf3* and the WNT target gene *Axin2* in total liver, hepatocytes, ducts and mouse liver organoids. Data represent mean ± SEM. n=2 mice/samples per group. **b)** qRT-PCR expression analysis or *Rnf43* and *Znrf3* in sorted ductal cells (EpCAM$^+$), endothelial cells (CD31$^+$) and macrophages (CD11b$^+$). Data represent mean ± SEM. n=1 mouse per group.

Overall, *R&Z* expression can be detected in hepatocytes, isolated ducts, ductal cells and mouse organoids, but not in macrophages and only at very low levels in endothelial cells. Further analysis is needed to confirm this result and to assess the purity of the sorted cells and isolated ducts and hepatocytes.

According to the expression pattern of *R&Z* in the liver, I sought to investigate the role of the two genes in this tissue by conditionally deleting them in either hepatocytes (AlbCreERT2) or bile ducts (Sox9CreERT2). The AlbCreERT2 allele (Schuler et al. 2004) will drive the deletion of the genes of interest specifically in albumin-expressing cells, the hepatocytes. Once CreERT2 is expressed, translocation into the nucleus is achieved by tamoxifen (injected intra-peritoneal). This system is different from the AlbCre allele, in which the Cre is constitutively active and drive recombination already in the embryo and in hepatoblasts, which give rise to both hepatocytes and cholangiocytes in the adult. On the other hand, using a Sox9CreERT2 allele (Kopp et al. 2011), deletion will be introduced in all cells expressing Sox9 after tamoxifen injections. Of note, Sox9 is expressed not only in the ducts form the liver, but also in

the extra-hepatic and pancreas bile ducts. Furthermore, expression of Sox9 is also present in the stomach gland, the intestinal crypts and other tissues. Thus, using this allele will not provide an intra-hepatic bile duct specific model.

5.1 *R&Z*-specific deletion in *Sox9* expressing cells does not affect liver regeneration after DDC-induced damage

RNF43 has been found frequently mutated in CC, subtype of PLC thought to arise mainly from the ductal compartment of the liver (Ong et al. 2012; Jusakul, Kongpetch, and Teh 2015). Importantly, ductal cells have been shown to have a role during liver regeneration, especially when hepatocytes proliferation is impaired (Lu et al. 2015; Huch, Dorrell, et al. 2013). So, to assess whether R&Z might have a role in regeneration or in promoting cancer formation starting from biliary ducts, I have decided to induce deletion of the two genes in the ductal compartment of the liver. Conditional knock-out mice ($R\&Z^{flox}$) carrying the floxed alleles of R&Z were already available in the lab (Koo et al. 2012). $R\&Z^{flox}$ alleles were designed to have loxP sites flanking either one (*Znrf3*) or two (*Rnf43*) of the exons expressing the functional RING domain of the proteins (Figure 5.3a). Mice expressing the CreERT2 protein under the *Sox9* promoter (Sox9CreERT2) were crossed with the $R\&Z^{flox}$ mice to generate Sox9CreERT2-$R\&Z^{flox}$ compound mice (Figure 5.3b). To study the role of R&Z during both regeneration and cancer initiation, I also decided to treat mice with a DDC diet, known to induce liver and bile duct injury and also to trigger a ductular reaction (Preisegger et al. 1999; Fickert et al. 2007).

Experiment plan for Sox9CreERT2 driven deletion is shown in Figure 5.3b, c. When mice were 7-week old, they were injected with tamoxifen multiple times to efficiently drive deletion of the two genes of interest. Tamoxifen allows translocation of the CreERT2 protein in the nucleus that in turn drives excision of the loxP flanked RING domains of R&Z, leading to the expression of deleted non-functional proteins in *Sox9*-expressing cells. Of note, *Sox9* is expressed by cholangiocytes but also by hybrid hepatocytes localised at the portal vein (Font-Burgada et al. 2015). After three injections, mice were either fed a DDC diet or kept on normal diet. Tamoxifen was also injected one last time before the end of the DDC diet treatment. Analysis of the livers was performed 40 days after the first injection (one month after the end of the DDC diet). Liver samples were dissected and pieces were collected for histology, RNA and

DNA analysis and duct isolations. Mice lacking the Sox9CreERT2 allele were used as control.

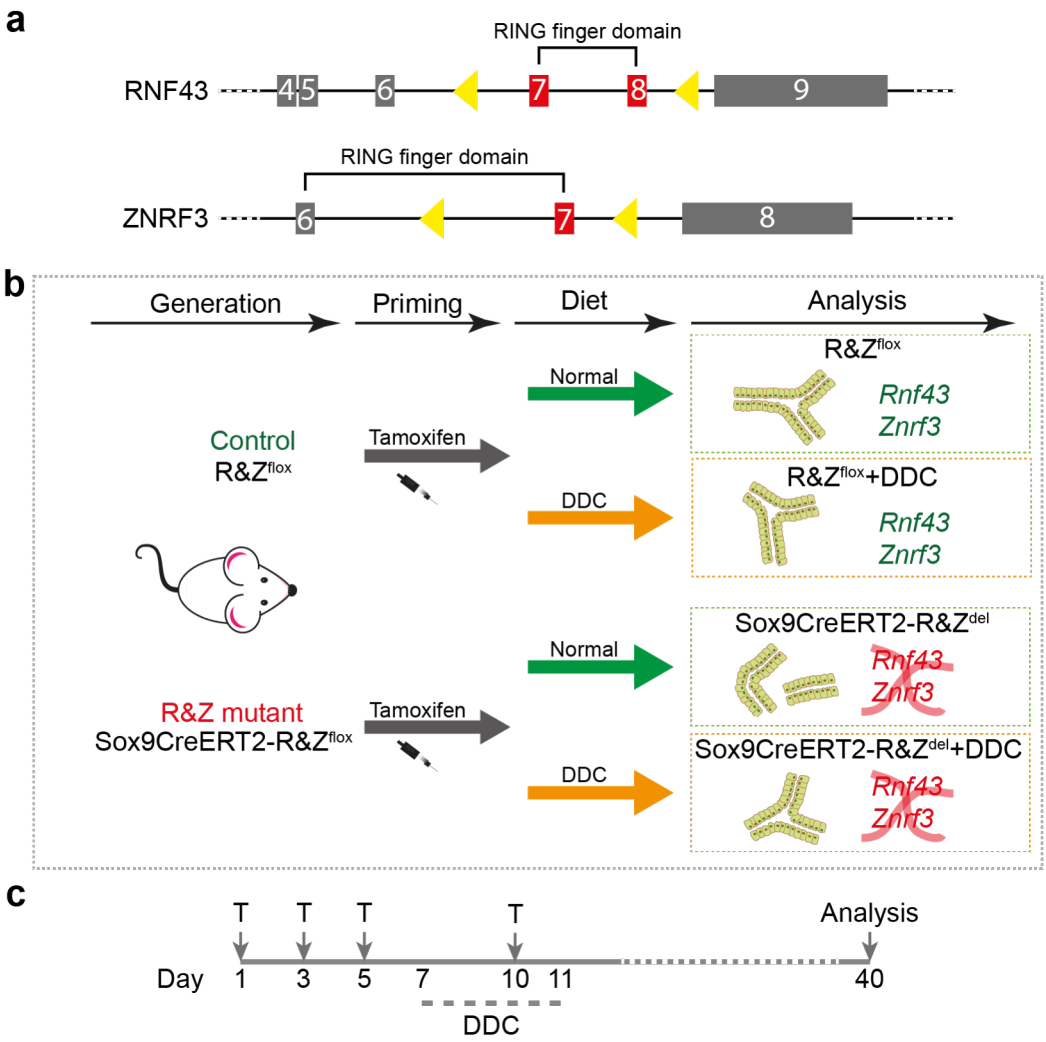

Figure 5.3. Experimental plan for *Sox9*-driven *R&Z* deletion and DDC diet. a) Schematic representation of *Rnf43* and *Znrf3* floxed alleles. Grey boxed, exons; red boxes, exons deleted after recombination; yellow triangles, loxP sites. **b)** Diagrams showing experimental plan. Mice were generated by crossing R&Z^{flox} mice with Sox9CreERT2 mice. After generation, mice were injected with tamoxifen when 7-week old to induce gene deletion. To trigger ductular reaction DDC diet was fed to mice for a total of 5 days. Livers were collected for analysis 1 month after the end of the DDC diet. Ducts were isolated to check for *R&Z* expression. **c)** Timeline of the experiment. T; Tamoxifen.

No gross morphology changes were observed in any of the livers analysed (Figure 5.4a). In addition, I did not observe any significant change in the liver to body weight ratio of the deleted mice compared to the non-deleted littermates (Figure 5.4b). To assess whether the absence of gross morphology changes was due to not efficient deletion of *R&Z* upon tamoxifen injection, I have isolated and extracted RNA from the ducts to perform a quantitative PCR (qRT-PCR) analysis. Primers used for the amplification of *R&Z* were annealing in the deleted region, thus allowing detection only of the wild-type variant. *R&Z* expression was decreased in the deleted livers in both

normal and DDC diet. Specifically, I have observed ~50% of deletion in livers that received normal diet and ~70% in the DDC treated ones (Figure 5.4c).

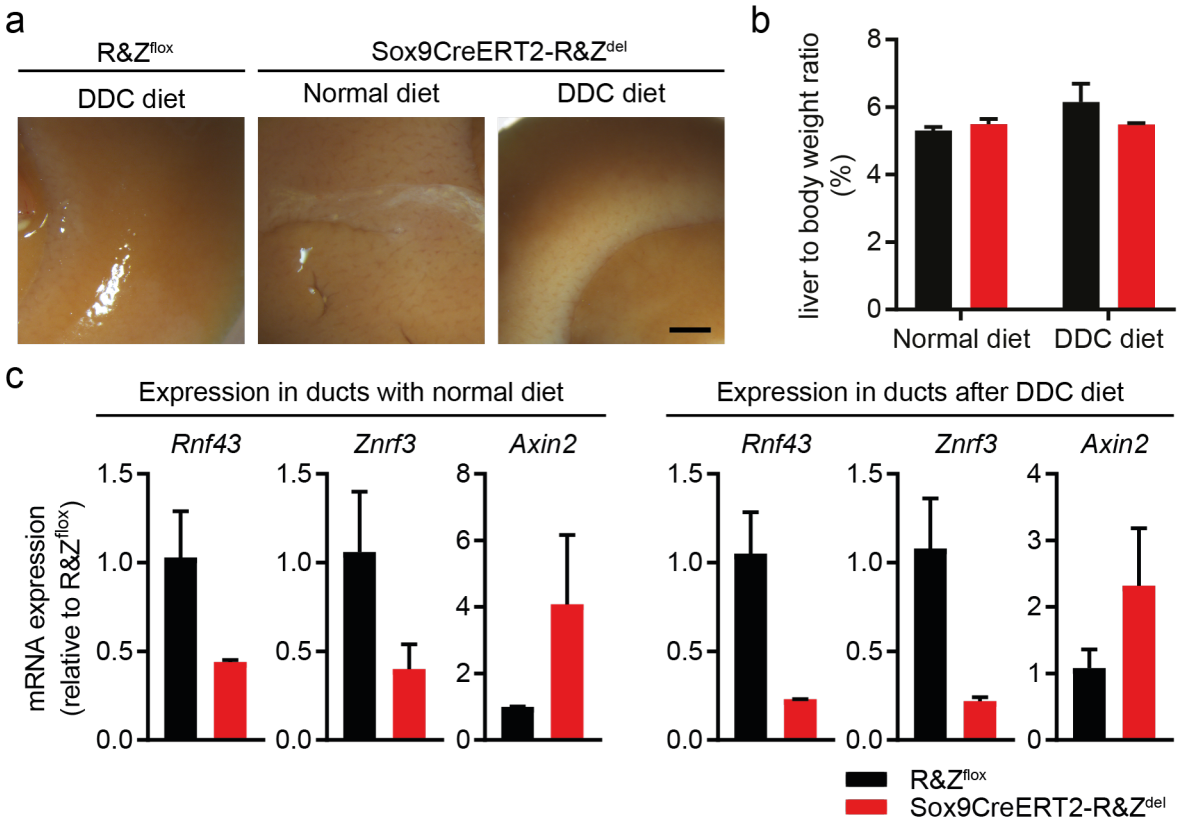

Figure 5.4. Sox9CreERT2 efficiently delete ~50% of R&Z in liver ducts. a) Representative pictures of R&Z^{flox} and Sox9CreERT2-R&Z^{del} livers with and without DDC diet treatment. Scale bar, 2mm. **b)** Graph showing differences in the percentage of liver to body weight ratio. n=2 mice. Data represent mean ± SEM. **c)** qRT-PCR expression analysis of *Rnf43*, *Znrf3* and *Axin2* of ducts isolated from R&Z^{flox} and Sox9CreERT2-R&Z^{del} mice fed with normal or DDC diet. Data represent mean ± SEM. n=2 mice per condition. Statistic was not performed due to low sample size.

In the intestine, *R&Z* deletion drives activation of the WNT pathway (Koo et al. 2012). Also, according to my human *in vitro* CRISPR model, *R&Z* deletion should have a similar effect in the liver. Thus, to test whether the amount of deletion observed was enough to drive WNT pathway activation, I have also checked the expression of *Axin2*. Interestingly, I have observed an increase in *Axin2* expression in both conditions, suggesting possible WNT pathway activation in the ductal compartments upon *R&Z* deletion (Figure 5.4c).

Histologic analysis revealed no structural nor architectural differences between R&Z^{flox} and Sox9CreERT2-R&Z^{del}, as shown by H&E staining (Figure 5.5a). To evaluate whether *R&Z* deletion and DDC-induced damage would result in fibrosis, I have performed Sirius Red staining, which highlights collagen fibres in the tissue. Collagen deposition was observed at the periportal area of mice that received DDC diet but not in mice that were fed with normal diet, with no difference between *R&Z* deleted and

wild type livers (Figure 5.5a). Finally, to assess whether *R&Z* deletion would trigger an increase in ductal cells, I performed a staining for PCK. Again, I have observed an increase in PCK^{+} cells at the periportal area in the DDC-treated mice, with no significant difference between deleted and undeleted *R&Z* (Figure 5.5a, b), however an increased number of samples need to be analysed in order to confirm this observation.

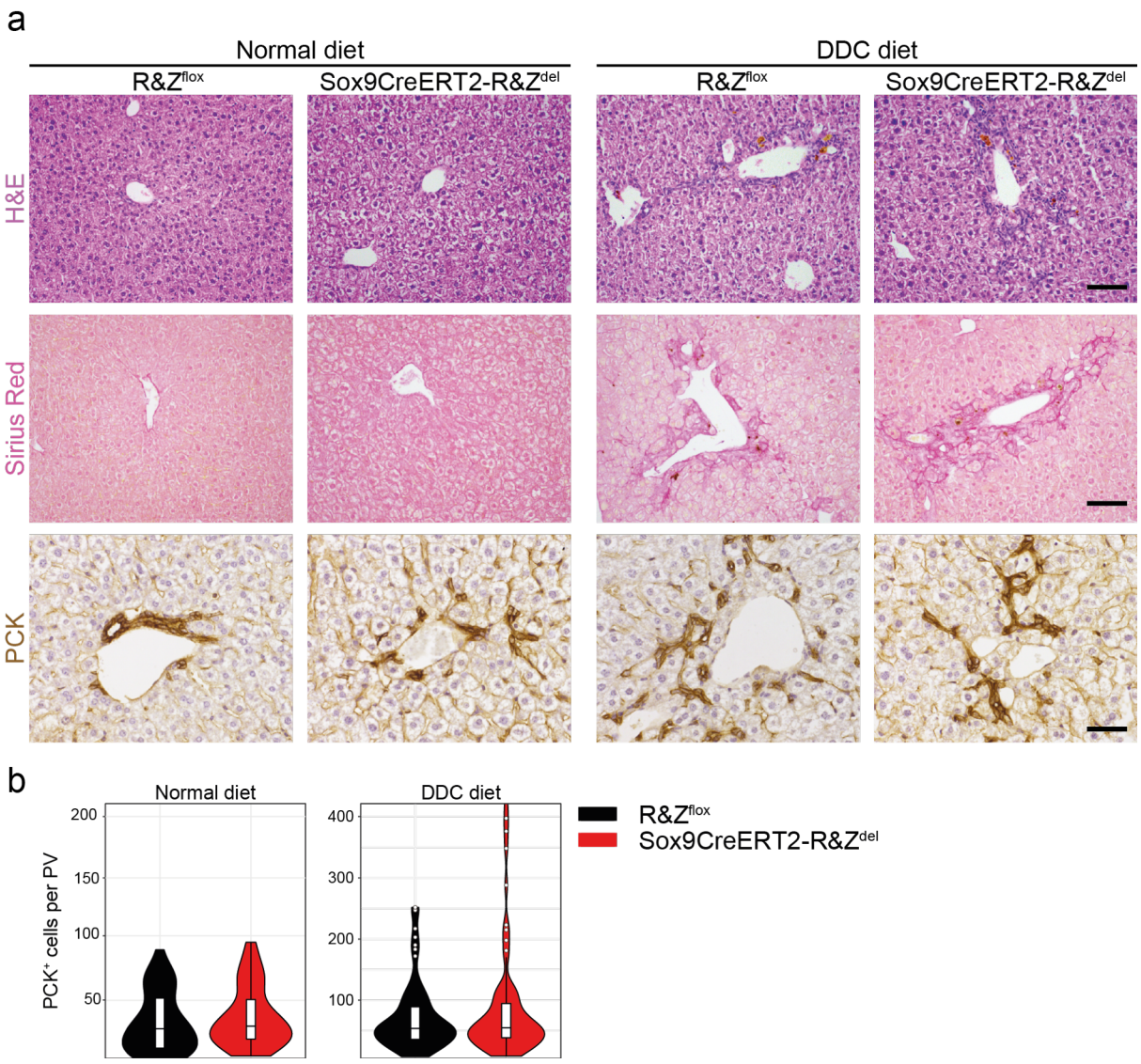

Figure 5.5. *R&Z* deletion in ducts does not affect liver injury repair after DDC treatment. a) Representative pictures of H&E and Sirius Red staining and immunostaining for PCK of R&Z^{flox} and Sox9CreERT2-R&Z^{del} liver sections with or without DDC diet treatment. Scale bar, 100µm (H&E, Sirius Red) and 50µm (PCK). **b)** Quantification of PCK^{+} cells per PV. Graphs represent distribution of cells per PV counted. White circles represent outliners. Bars represent quartile percentile (top is 75% and bottom is 25%). Median is represented as a horizontal line in the bars. PV, portal vein.

Overall, these data suggest that although *R&Z* deletion can drive overexpression of *Axin2* in the duct compartment, it does not affect injury response to DDC diet-induced damage in this model. A new approach that would allow for complete deletion of R&Z

in the ductal compartment is needed in order to rule out the role of these two genes in regulating ductular reaction. For this reason, I have decided to not focus on this model.

5.2 Sox9CreERT2-R&Z^{del} derived organoids exhibit WNT pathway activation

As mentioned in the introduction, liver organoid cultures originate from the ductal compartment of the liver (Huch, Dorrell, et al. 2013; Huch et al. 2014). For this reason, I hypothesized that organoids originated from Sox9CreERT2-R&Z^{del} mice would also show deletion of *R&Z* and thus reduction in their expression. As *R&Z* deletion in the biliary ducts did not show any significant phenotype, I decided to establish organoids from both R&Z^{flox} and Sox9CreERT2-R&Z^{del} mice and use this to validate what I have previously observed in the *R&Z*-mutated human liver organoids. According to my previous data, *R&Z* mutant human liver organoids can grow in absence of R-spondin1 (RSPO1), whereas WT organoids cannot. Thus, to ensure the growth of organoids originated only from *R&Z* deleted cells, I have seeded cells in media lacking RSPO1. Once organoids were formed, I hand-picked two growing clones, thus generating two independent lines. Organoids derived from non-deleted R&Z^{flox} mice were instead cultured in isolation media.

To confirm deletion of *R&Z*, I have performed qRT-PCR analysis on RNA collected from organoid cultured in complete media (CM) or in media lacking RSPO1 (-R). Of note, no expression of either *Rnf43* nor *Znrf3* was detected in the two clones derived from Sox9CreERT2-R&Z^{del} mice, cultured either with or without RSPO1 (Figure 5.6a). Whereas, *R&Z* were both expressed in the wild-type organoids derived from R&Z^{flox} mice and partial reduction in expression was observed when cultured without RSPO1, in line with the decreased WNT pathway activity in absence of this growth factor (Figure 5.6a). Furthermore, I have also detected *Axin2* overexpression in both deleted clones (Figure 5.6a). Interestingly, the expression of *Axin2* was not affected by the removal of RSPO1 from the media condition in the two deleted clones, although it was no longer detectable in the R&Z^{flox} organoids.

To further confirm the phenotype observed, I have performed an organoid formation efficiency experiment in different media conditions. Organoids were dissociated and cultured 500 cell/well in complete media (CM), media lacking RSPO1 (-R), media lacking RSPO1 and with the addition of the porcupine inhibitor IWP2 (-R+I) and finally

media lacking RSPO1 and containing both IWP2 and the GSK3β inhibitor CHIR-99021 (-R+I+CHI). Analysis was performed one week after the seeding. In line with my previous observations, *R&Z* deleted organoids resisted the withdrawal of RSPO1 from the media and showed a similar organoid formation efficiency regardless of the presence of RSPO1 in the medium (Figure 5.6b, c). Expectedly, the efficiency dropped once WNT production was inhibited by IWP2 treatment (-R+I) (Figure 5.6b, c). Finally, this reduction was partially rescued by activating the pathway downstream with CHIR-99021 (-R+I+CHI) (Figure 5.6b, c). Similar pattern was observed in the non-deleted organoids, apart from the -R condition, where the efficiency of organoid formation was reduced, although large organoids could still be observed (Figure 5.6b, c).

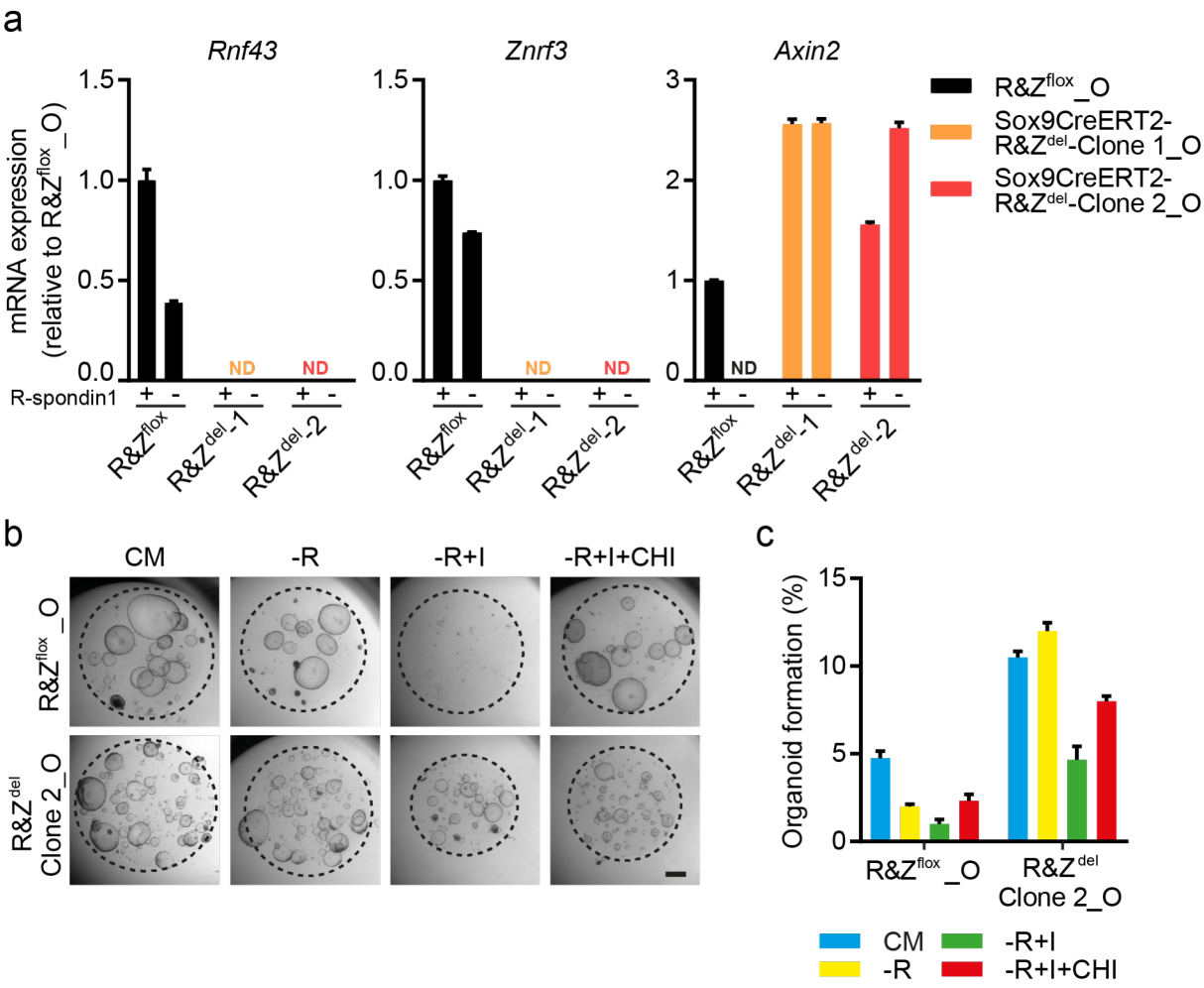

Figure 5.6. *R&Z* mutated mouse organoids have WNT activation and resist RSPO1 withdrawal. **a)** qRT-PCR expression analysis of *RN43*, *Znrf3* and *Axin2* in R&Z^{flox} and Sox9CreERT2-R&Z^{del} derived organoids cultured with or without RSPO1ndin1. Data represent mean ± SEM. Experiment was repeated twice. **b, c)** Organoid formation efficiency of in R&Z^{flox} and Sox9CreERT2-R&Z^{del} derived organoids in different conditions. CM, complete media; R, R-spondin1; P, IWP2 3um (porcupine inhibitor); CHI, CHIR-99021. Scale bar; 2mm. Experiment was performed twice. **c)** Quantification of organoid formation efficiency.

Overall, these data suggest that it is possible to derive organoids lacking R&Z from Sox9CreERT2-R&Z^{del} mice. More importantly, the *R&Z* deleted organoids present the same features observed in the *R&Z* mutated human liver organoids, including *Axin2* overexpression, RSPO1 withdrawal insensitivity and WNT dependency. However, an increased number of samples is needed in order to assess whether these results are statistically significant.

5.3 R&Z KO in hepatocytes induces increased proliferation and expanded GS staining.

As *ZNRF3* is also found mutated in HCC (Guichard et al. 2012), I wondered what would be the role of R&Z in the hepatocyte compartment. Therefore, I proceeded to generate a mouse model to conditionally delete the two genes in the hepatocytes. To this purpose, I have crossed the R&Z^{flox} line with mice expressing the CreERT2 protein under the albumin promoter (AlbCreERT2) to generate AlbCreERT2-R&Z^{flox} compound mice (Figure 5.7b). Tamoxifen was administrated to mice intraperitoneally when they were 7-week old. Upon deletion, livers were harvested for analysis after 3 months (Figure 5.7c). Mice lacking the AlbCreERT2 allele were used as control.

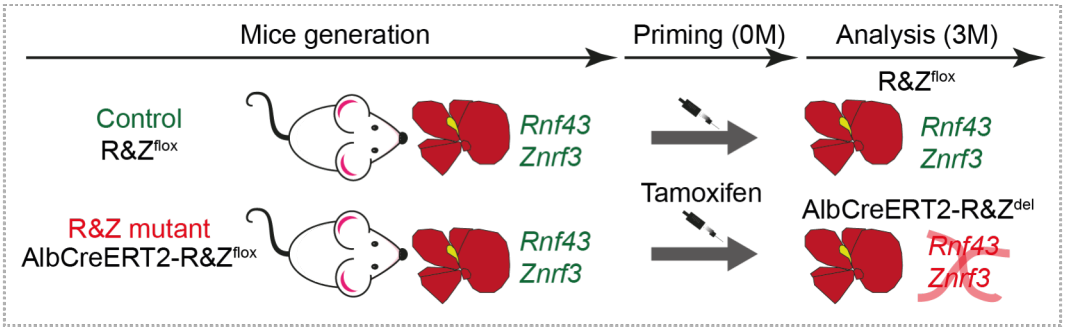

Figure 5.7. Experimental plan for hepatocyte-specific deletion of *R&Z*. Diagrams showing experimental plan. Mice were generated by crossing R&Z^{flox} mice with AlbCreERT2 mice. After generation, mice were injected with tamoxifen when 7-week old (0M) to induce gene deletion and livers were collected for analysis 3 months (3M) after induction.

To assess whether *R&Z* were deleted after tamoxifen injection, I have extracted RNA from the livers and used it for qRT-PCR analysis. In all cases, deletion efficiency was near 100% (Figure 5.8a). To assess whether this deletion would result in Wnt pathway activation as observed in the previous model, I have performed qRT-PCR analysis of common WNT target genes. Expectedly, I have observed overexpression of *Axin2*,

Lgr5 and *Sp5*, suggesting WNT pathway activation and further confirming my previous observation (Figure 5.8a).

Macroscopic analysis of the livers revealed no gross morphological changes (Figure 5.8b). Also, no significant difference was observed in the liver to body weight ratio in the *R&Z* deleted livers when compare to littermate controls, 3 months after inducing the deletion (Figure 5.8c).

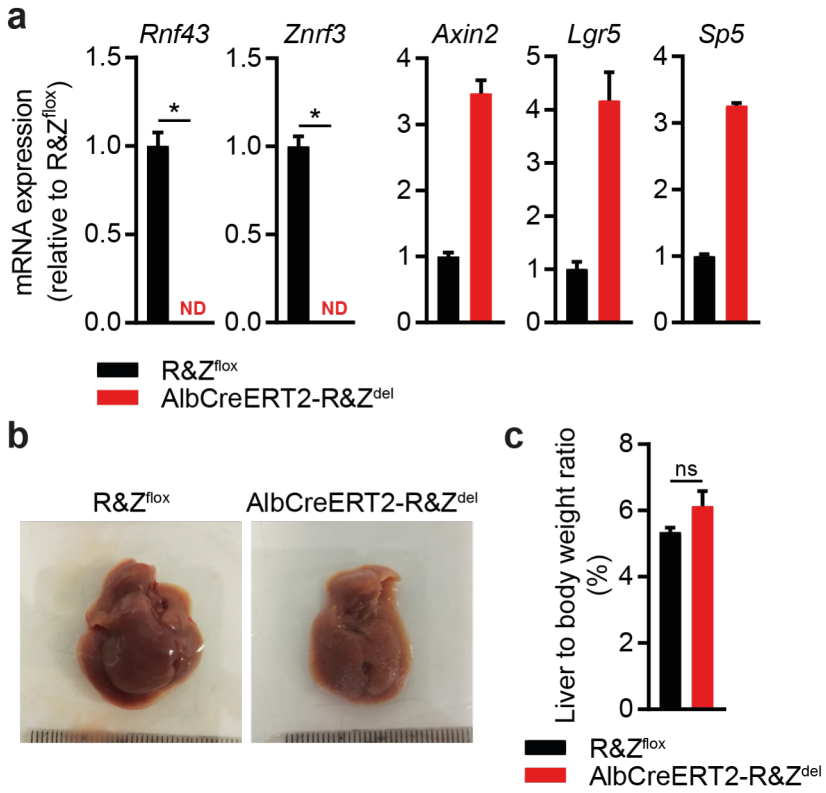

Figure 5.8 *R&Z* hepatocyte-specific deletion results in WNT target genes overexpression. a) qRT-PCR expression analysis or *Rnf43* and *Znrf3* and the WNT target genes *Axin2*, *Lgr5* and *Sp5* in R&Z^{flox} and AlbCreERT2-R&Z^{del} mice. Data represent mean ± SEM. n=2 mice per group. **b)** Pictures of R&Z^{flox} and AlbCreERT2-R&Z^{del} livers. **c)** Graph showing differences in the percentage of liver to body weight ratio. n=2 mice (R&Z^{flox}), 4 mice (AlbCreERT2-R&Z^{del}). Data represent mean ± SEM. ns, not significant; two-tail t-test was used.

Histopathologic analysis revealed that liver tissues did not present any structural abnormalities at 3 months after *R&Z* deletion when compared to littermate controls (Figure 5.9a). A recent paper has shown that upon deleting *R&Z* using a R26CreERT2 line, that induce deletion in the whole body, livers show an increase of staining for glutamate synthetase (GS) and Ki67, 10 days after induction (Planas-Paz et al. 2016). GS is a metabolic and liver-specific WNT target gene, usually expressed only in 1-2 layers of hepatocytes in zone 3 around the CV, source for WNTs (Gebhardt 2014). To confirm that this was true also in my model and at longer periods after induction, I have then performed staining of both GS and Ki67.

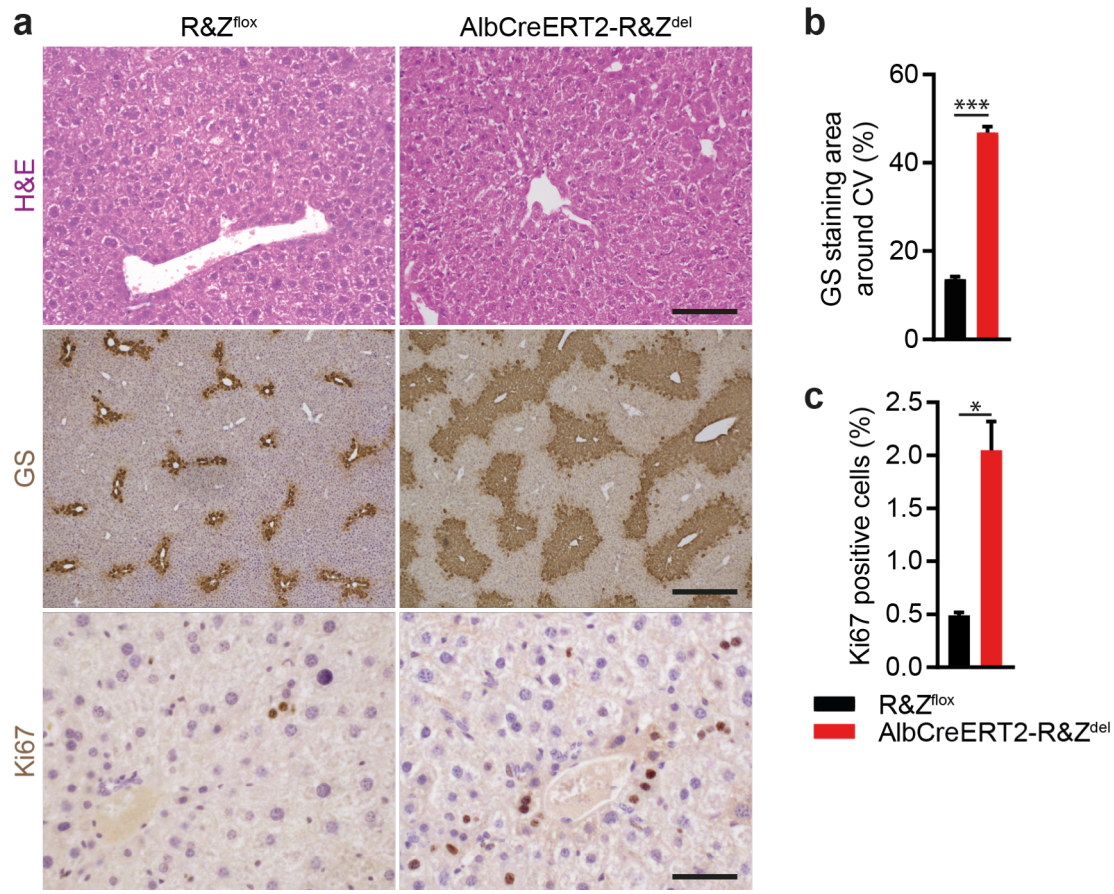

Figure 5.9 *R&Z* hepatocyte-specific deletion causes increase in GS staining area and in Ki67 positive cells. a) Representative H&E and immunostaining for GS and Ki67 of R&Z^{flox} and AlbCreERT2-R&Z^{del} liver sections. Scale bar, 100µm (H&E), 500µm (GS) and 50µm (Ki67). **b)** Quantification of GS positive staining localised around central veins. n=3 mice per group. **c)** Quantification of Ki67 positive hepatocytes. n=3 mice per group. Data represent mean ± SEM; *P<0.05, **P<0.01, *P<0.001; two-tail t-test was used.

Consistent with Planas-Paz et al., I have observed an increased GS stained area. Here, 5 to 16 layers of hepatocytes were stained with this marker, in contrast to the 1 to 2 layers in the control mice (Figure 5.9a). A 3-fold expansion of GS staining around the CV was observed (Figure 5.9b). This increase in GS confirms WNT pathway activation upon *R&Z* deletion and suggests a potential role for R&Z in controlling metabolic liver zonation, like previously reported and similar to *Apc* mutant mice (Benhamouche et al. 2006; Planas-Paz et al. 2016). In addition to this, *R&Z* deleted livers exhibited a significant 4-fold increase in proliferative cells when compared to non-deleted littermate controls, also confirming what observed by Planas-Paz et al. 10 days after *R&Z* deletion (Figure 5.9a, c).

Overall, deletion of *R&Z* in hepatocytes leads to WNT pathway activation and higher proliferation rate. More importantly, this data show that R&Z play a role in controlling liver metabolic zonation, as shown by increased GS.

5.4 Hepatocyte-specific *R&Z* deletion results in metabolic alterations similar to human livers affected by steatosis

The increase in GS staining observed above suggested a role for R&Z in controlling liver metabolism. For this reason, I decided to investigate what other metabolic changes happen in the liver upon *R&Z* deletion. To this purpose, I have analysed the expression of several genes involved in multiple metabolic pathways of the liver (Figure 5.10).

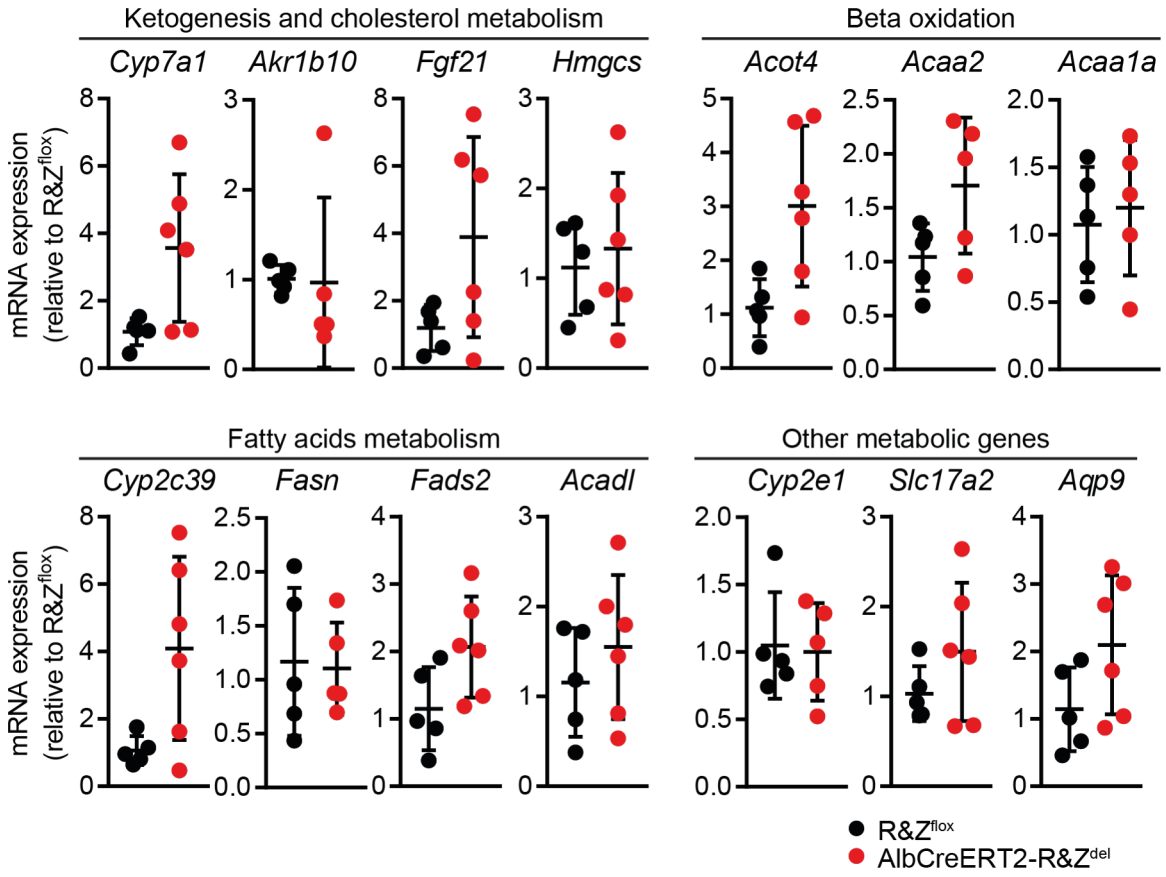

Figure 5.10. *R&Z* hepatocyte-specific deletion induce partial metabolic changes at transcriptional level. RT-qPCR expression analysis of genes involved in fatty acid metabolism, beta oxidation, ketogenesis and cholesterol metabolism and others of R&Z^{flox} control mice and AlbCreERT2-R&Z^{del} mice. n=5 mice (R&Z^{flox}) and 5 or 6 mice (AlbCreERT2-R&Z^{del}). Results represent single events ± SD. two-tail t-test and Holm-Bonferroni correction were used for statistical analysis, data are not significant.

Of note, I have observed an increase in the expression of *Cyp7a1*, *Acot4*, *Cyp2c39*, *Fgf21*, *Acaa2*, *Fads2*, *Aqp9* involved in metabolic processes like beta oxidation, ketogenesis and fatty acid metabolism (Figure 5.10). These data suggest that R&Z might be important in keeping a balanced metabolism in the liver and that their alteration can cause increased expression of enzymes involved in several metabolic

pathways, in agreement with the results published for the TCF4 KO mice, where these genes are downregulated. However, due to high variability between the samples, data are not significant and an increase number of samples need to be tested in order to confirm this observation.

As the changes observed relate to fat metabolism, I sought to explore what are the changes in gene expression observed in human livers presenting pathologies related to fat metabolism alteration. With the help of Mikel McKie, I have analysed the gene expression profile of a cohort of patients affected by steatosis or non-alcoholic steatohepatitis (NASH) published by Arendt et al. 2015. Interestingly, livers affected by steatosis and NASH had a significantly higher expression of the ligand *WNT5A* and the WNT target genes *AXIN2* and *LGR5*, suggesting possible activation of the WNT pathway in these samples. Furthermore, steatotic and NASH livers exhibited a significant increased expression of metabolic genes like *CYP7A1* and *FADS2*, also upregulated after *R&Z* deletion. Whereas, *AKR1B10* was upregulated only in NASH and not in steatosis and *ACOT4* was significantly over expressed only during steatosis. Expression pattern similar to the steatosis one (no change in *Akr1b10* and increase in *Acot4*) was observed in *R&Z* deleted livers.

Overall this data indicates that human livers affected by steatosis and NASH exhibit activation of the WNT pathway similar to *R&Z* deleted livers. In addition, there is a correlation between the increased expression of metabolic genes observed in human livers affected by steatosis and mouse *R&Z* deleted livers. This data suggests that the altered metabolic expression profile observed in the *R&Z* deleted livers might lead to steatosis after long-term deletion.

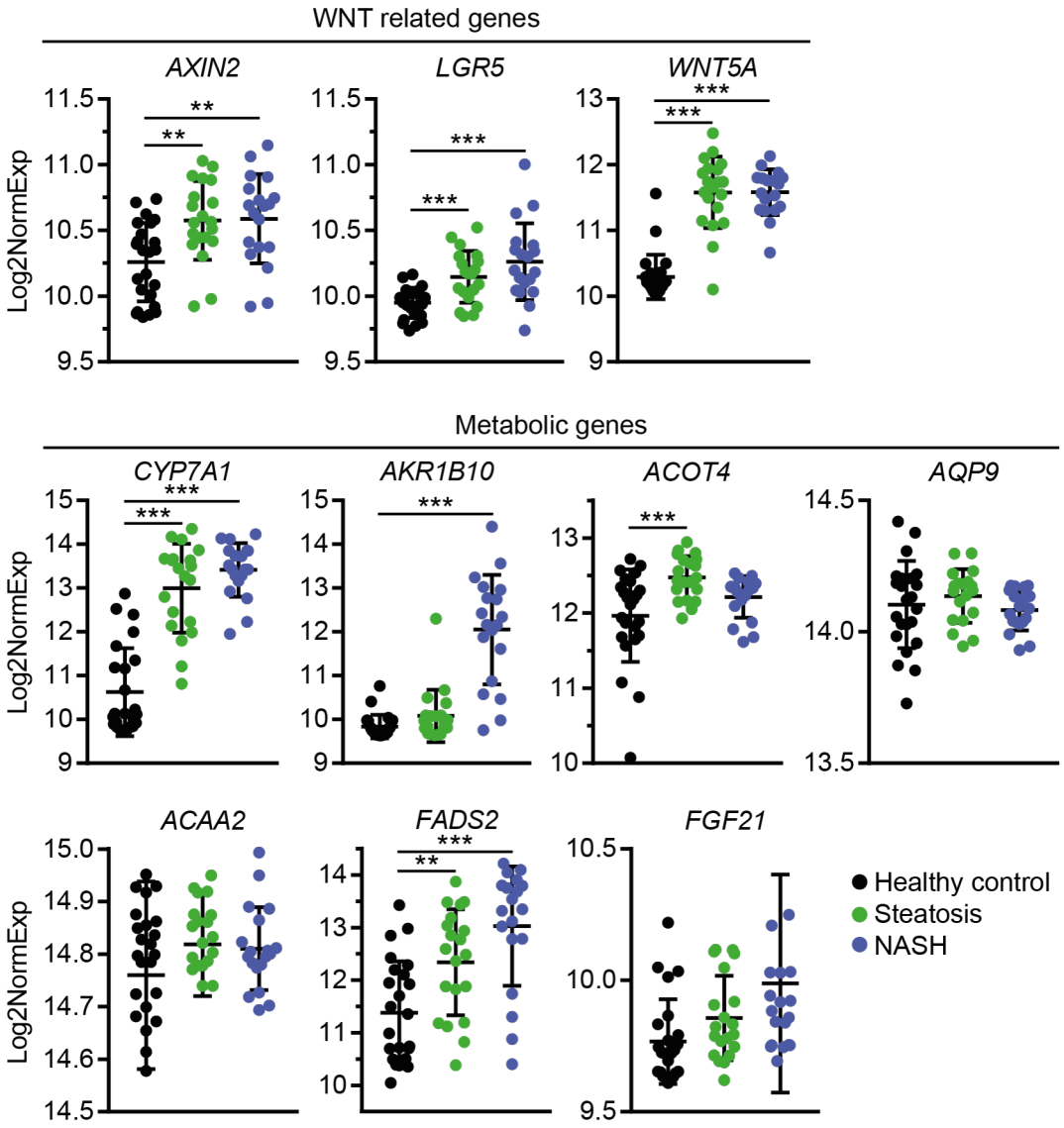

Figure 5.11. Steatosis and NASH expression profiling. Expression of WNT related genes and metabolic genes in a cohort of liver from healthy donors and patients with steatosis and NASH. n=24 (healthy control), 20 (steatosis), 19 (NASH). Results represent single events ± SD. *P<0.05; **P<0.01; ***P<0.001; two-tail t-test and Holm-Bonferroni correction were used. Data were obtained from Arendt et al. 2015.

5.5 Hepatocyte-specific *R&Z* deletion upon acute and chronic liver damage

Liver cancer most commonly arises upon liver damage due to viral infections, chronic diseases and excessive alcohol intake, among others (El-Serag and Rudolph 2007). Specifically, 80 to 90% of hepatocellular carcinomas arise as a consequence of chronic liver damage. For this reason, and also to study the role of R&Z during regeneration, I sought to investigate the effect of their deletion in the liver *in vivo* after acute and chronic damage.

To induce liver damage, I have treated mice with carbon tetrachloride (CCl4). CCl4 is a known toxic agent that induces death in the hepatocytes surrounding the central veins, thus triggering hepatocytes proliferation and a ductal progenitor response to help regenerate the liver (Beer et al. 2008). In the acute damage (AD) model, CCl4 was injected in single dose; whereas for the chronic damage (CD) model CCl4 was injected in lower dose but multiple times over a period of six weeks.

5.5.1 Hepatocyte-specific *R&Z* deletion does not affect liver regeneration upon acute damage

In the acute damage model, mice were first injected with tamoxifen to drive R&Z deletion and, after two days, CCl4 was administered intraperitoneally at high dose (1ml/kg). Also, tamoxifen was injected again after two days to induce deletion in newly formed hepatocytes generated from non-deleted progenitors. Livers were analysed 3 months after the first injection (Figure 5.12a, b).

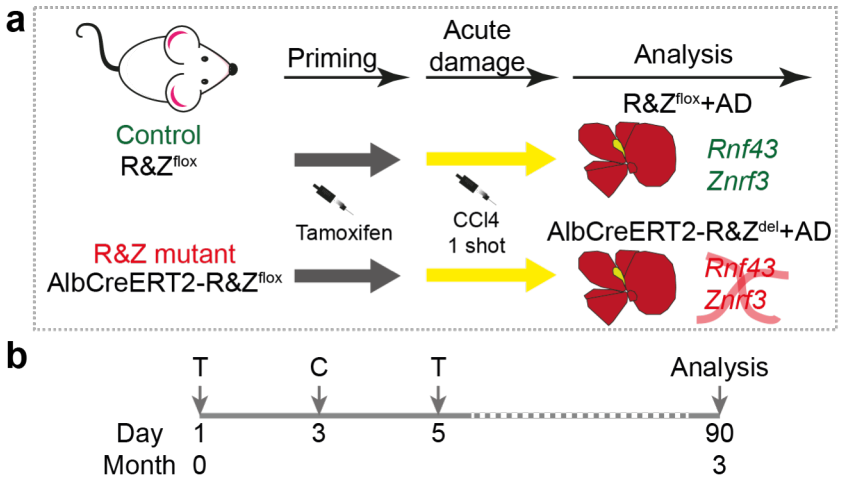

Figure 5.12. Experimental plan for hepatocyte-specific deletion of *R&Z* and acute damage. a) Diagrams showing experiment plan. Mice were injected with tamoxifen when 7-week old, with CCl4 2 days later and tamoxifen again after 2 days. Livers were collected for analysis 3 months after induction. **b)** Timeline of the experiment. T, tamoxifen; C, CCl4.

Upon RNA analysis, complete deletion of both R&Z in all livers analysed was confirmed (Figure 5.13a). In addition, I have also confirmed over expression of the WNT target genes *Lgr5* and *Axin2*, similar to what I had previously observed (Figure 5.13a). Of note, no liver gross morphology abnormalities were observed (Figure 5.13b). Liver to body weight ratio was increased by ~67% in *R&Z* deleted and damaged mice compared to non-deleted but damaged controls (Figure 5.13c). This was in contrast with the undamaged *R&Z* deleted livers, where I had observed no significant difference

on the liver to body weight ratio between *R&Z* deleted and non-deleted livers, suggesting that damaging the liver might results in a hyperplastic phenotype (Figure 5.13c).

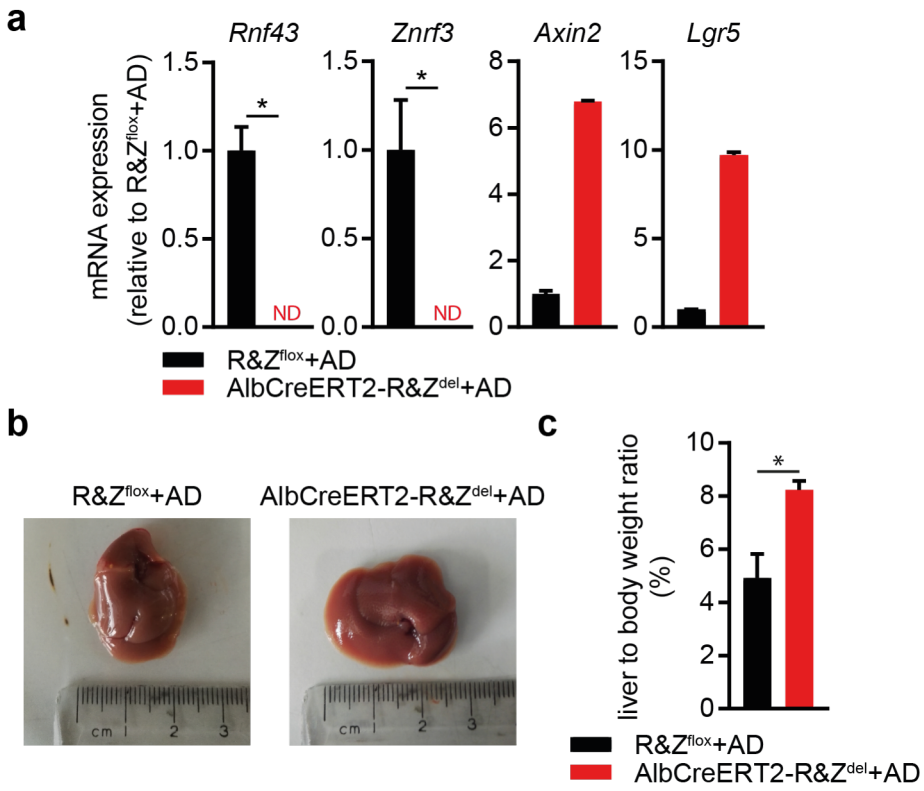

Figure 5.13. *R&Z* hepatocyte-specific deletion results in WNT target genes overexpression and hyperplasia. a) qRT-PCR expression analysis or *Rnf43* and *Znrf3* and the WNT target genes *Axin2* and *Lgr5* in R&Z^{flox} and AlbCreERT2-R&Z^{del} mice. Data represent mean ± SEM. n=2 mice (*R&Z*) and 1 mouse (*Axin2* and *Lgr5*). **b)** Pictures of R&Z^{flox} and AlbCreERT2-R&Z^{del} livers. **c)** Graph showing differences in the percentage of liver to body weight ratio. n=3 mice (R&Z^{flox}) and 4 mice (AlbCreERT2-R&Z^{del}). Data represent mean ± SEM. *P<0.05; two-tail t-test was used.

At histological level, livers were not showing any structural alterations and the pattern of GS staining was very similar to what I had previously described for the R&Z KO non-damaged model, with ~50% of staining around the CV (Figure 5.14a, b). In addition, I also observed an increase in proliferative cells similar to the undamaged livers at the same time point (Figure 5.14a, c).

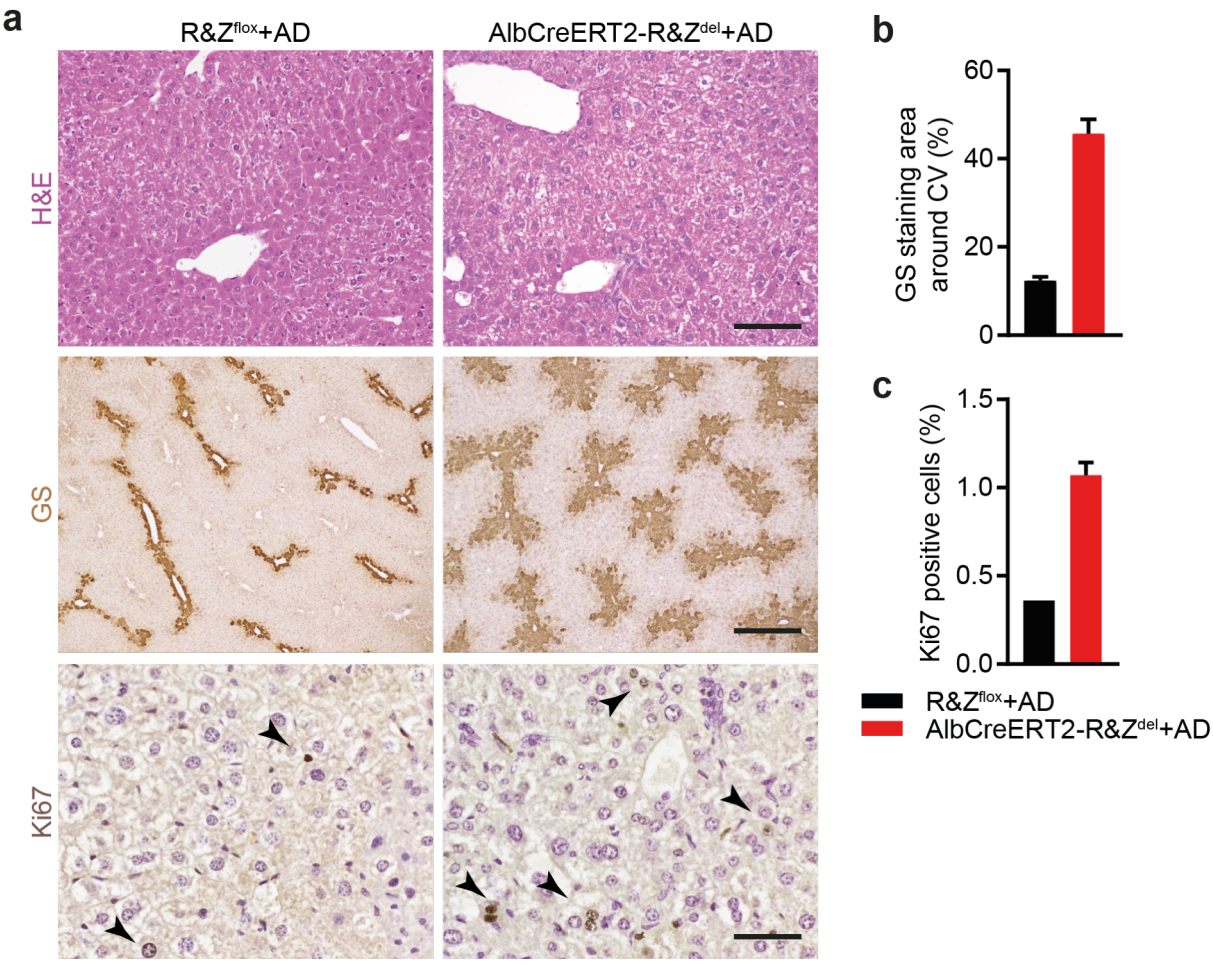

Figure 5.14. *R&Z* hepatocyte-specific deletion does not affect liver regeneration following acute damage. **a)** Representative pictures of H&E and immunostaining for GS and Ki67 of R&Z^{flox} and AlbCreERT2-R&Z^{del} damaged liver sections. Scale bar is 100um for H&E, 500um for GS, 50um for Ki67. Arrowhead, Ki67^{+} cells. **b)** Quantification of GS positive staining localised around central veins. n=2 mice per group. **c)** Quantification of Ki67 positive hepatocytes. n=1 mouse (R&Z^{flox}) and 2 mice (AlbCreERT2-R&Z^{del}). Data represent mean ± SEM. Statistic not performed due to low sample size.

Overall, when challenged by CCl4-induced AD, livers lacking R&Z are able to regenerate without presenting structural alterations. Of note, livers exhibit the same characteristic observed in absence of AD, including activation of the WNT pathway and increased rate of proliferative cells. Of note, a hyperplastic phenotype was observed, although no histological differences were detected when compare to control mice. Considering these preliminary data, I decided to no longer focus on the AD model and therefore no more livers were analysed.

5.5.2 Hepatocyte-specific *R&Z* deletion induces formation of regenerative nodules and mild fibrosis upon chronic damage

As previously mentioned, chronic liver diseases precede HCC establishment in most of the cases. Therefore, to better recapitulate what happens in the human before tumours arise, I also investigated the role of R&Z upon chronic damage (CD).

Mice were injected with tamoxifen to conditionally delete *R&Z* when they were 7-week old. After that, to induce CD mice were injected with CCl4 for a total of 6 weeks. During this period, mice were also injected with tamoxifen two more times the first 2 weeks and one last time at the end of the protocol, to induce *R&Z* deletion in potentially newly formed hepatocytes originated from liver progenitors (Figure 5.15a). Livers were collected for analysis 3 months after the beginning of the protocol (Figure 5.15b).

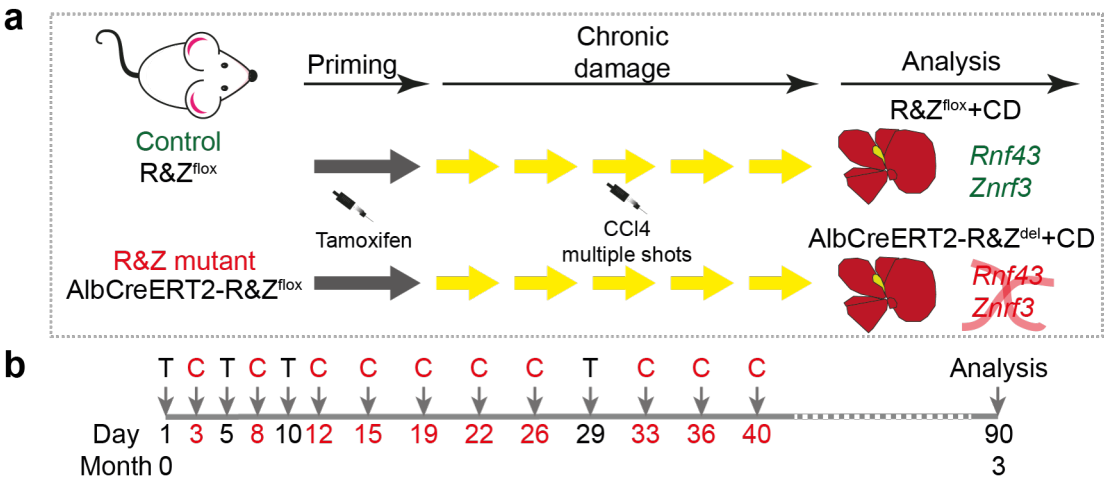

Figure 5.15. Experimental plan for hepatocyte-specific deletion of *R&Z* and chronic damage. a) Diagrams showing experiment plan. Mice were injected for the first time with tamoxifen when 7-week old, the injected again multiple times with CCl4 and tamoxifen. Livers were collected for analysis 3 months after induction. **b)** Timeline of the experiment. T, tamoxifen; C, CCl4.

Upon RNA collection from the total livers, qRT-PCR analysis revealed a reduction in R&Z expression of about 80%, in stark contrast to my previous observation in the undamaged (UD) and AD models where complete deletion was observed. This data suggests that, after the chronic damage, newly formed liver cells (hepatocytes and non-parenchymal cells) had been derived from cells carrying undeleted copies of *R&Z* (Figure 5.16a). Overexpression of the WNT target gene *Axin2*, but not *Lgr5* and *Sp5*, was still present, indicating that complete deletion of *R&Z* is needed to fully activate the pathway (Figure 5.16b).

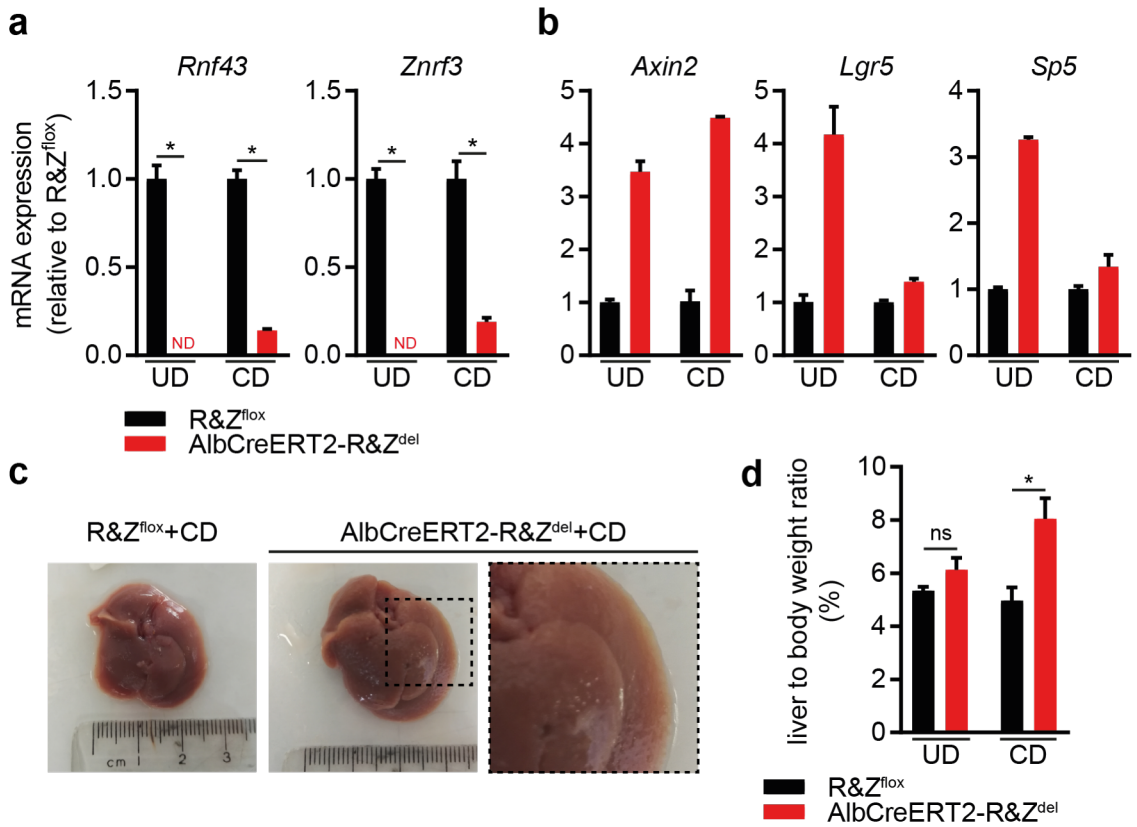

Figure 5.16. In the setting of chronic damage, R&Z deletion induces gross morphology changes, *Axin2* overexpression and hyperplasia in R&Z deleted livers. a) qRT-PCR expression analysis of *Rnf43* and *Znrf3* in R&Z^{flox} and AlbCreERT2-R&Z^{del} livers with and without CD. Data represent mean ± SEM. n=4 mice per group. **b)** qRT-PCR expression analysis of the WNT target genes *Axin2*, *Lgr5* and *Sp5* in R&Z^{flox} and AlbCreERT2-R&Z^{del} livers. Data represent mean ± SEM. n=2 mice per group.**c)** Pictures of R&Z^{flox} and AlbCreERT2-R&Z^{del} livers. Magnification show nodular liver surface. **d)** Graph showing differences in the percentage of liver to body weight ratio. n=2 mice (R&Z^{flox} UD), 3 mice (R&Z^{flox} CD),4 mice (AlbCreERT2-R&Z^{del} UD and CD). Data represent mean ± SEM. *P<0.05; ns, not significant; two-tail t-test was used. ND, not detected; UD, undamaged; CD, chronic damage.

At macroscopic observation, livers were visually larger and exhibited irregular nodular surface (Figure 5.16c). In addition, analysis of the liver to body weight ratio revealed an increase of ~60%, similar to the AD model but in contrast to undamaged mice, where no change was observed (Figure 5.16d). These data suggest that CD is able to induce liver hyperplasia upon *R&Z* deletion.

The histopathological analysis revealed that livers exhibited tissue damage and presence of multiple small nodules, as confirmed by H&E staining (Figure 5.17a). These structures exhibited cells with small nuclei and low nucleus to cytoplasm ratio. Interestingly, immunological infiltrate (lymphocytes and macrophages) and large liver cell changes (giant hepatocytes), usually associated with aging, cirrhosis and/or neoplasia (Park and Roncalli n.d.), were present in these livers, especially in the perinodular area (Figure 5.17a). Considering the histological features of these small nodules and after pathological evaluation by consultant histopathologist Dr. Susan

Davies, these were classified as regenerative nodules. Of note, control livers chronically damaged but WT for *R&Z* did not present any of the alterations described above and were fully regenerated at the time of the analysis.

Increased GS staining around the CV further confirmed activation of the WNT pathway also in this case. Occasionally, GS staining was extending from zone 3 up to zone 1 (around the PV), in stark contrast to undamaged R&Z mutant littermates of the same age, where zone 1 is negative for GS marker (Figure 5.17a, b). Similarly, there was a significant increase of ~9 fold in proliferative hepatocyte cells in the KO livers but not in the WT ones, as confirmed by Ki67 staining (Figure 5.17a, c).

Considering the histological observations in the chronically damaged livers, I thought to investigate whether the failed regeneration would result in deposition of collagen fibres and thus fibrosis due to cell death. To this purpose, I performed a Sirius Red staining that highlights collagen fibres located in the tissue. Interestingly, I have observed deposition of few laces of collagen only in the R&Z chronically damaged livers (Figure 5.17a). In line with the previous findings, this mild fibrosis was located mainly at the perinodular regions, where the most amount of tissue damage was observed.

Overall, deletion of *R&Z* specifically in the hepatocyte compartment results in impaired regenerative potential of the liver. Cells are unable to repopulate the tissue with functional new hepatocytes, probably because they fail to fully activate or complete the regenerative program, thus resulting in formation of regenerative nodules, hepatocytes proliferation and collagen deposition in the tissue.

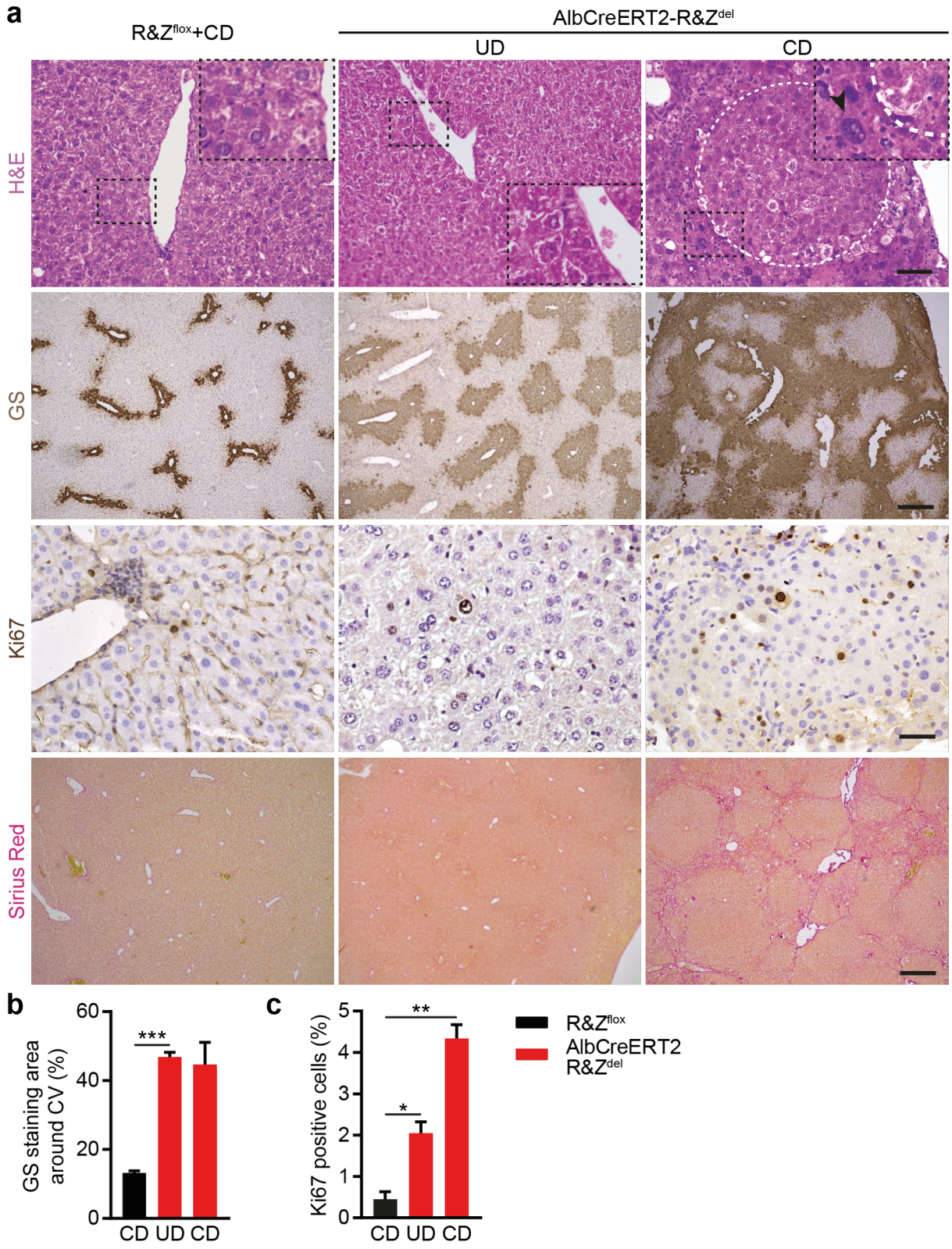

Figure 5.17. In the setting of chronic damage, liver-specific R&Z deletion induces regenerative nodules formation, increase proliferation and mild fibrosis in the liver. a) Representative pictures of H&E and Sirius Red staining and immunostaining for GS and Ki67 of chronically damaged R&Z^{flox} and damaged and undamaged AlbCreERT2-R&Z^{del} liver sections. Scale bar, 100µm (H&E), 500µm (GS, Sirius Red) and 50µm (Ki67). The white dotted circle marks the nodule border. Perinodular area is right outside of the circle. **b)** Quantification of GS positive staining localised around central veins. n=3 mice per group. **c)** Quantification of Ki67 positive hepatocytes. n=3 mice per group. Data represent mean ± SEM; *P<0.05, **P<0.01, ***P<0.001; two-tail t-test was used; CD, chronic damage; UD, undamaged.

5.6 Long-term hepatocyte-specific *R&Z* deletion in adult liver parenchyma induces steatohepatic injury in both undamaged and chronically damaged livers

According to my data, R&Z play a role not only in controlling metabolism during homeostasis, but they also seem to be essential for the liver to properly regenerate after a chronic damage. Therefore, I asked whether the absence of R&Z from the hepatocytes for longer periods could further exacerbate the phenotypes observed or whether livers would finally recover after chronic damage. To tackle this question, I conditionally deleted *R&Z* from livers and collected the tissues after 7 months, either undamaged (UD) or with a chronic damage (CD) (Figure 5.18a). Upon collection, RNA was analysed and used to assess *R&Z* deletion and WNT target genes overexpression. Once again, deletion was total in the UD model and only partial in the CD model, with ~25% of expression still detectable (Figure 5.18b). Overexpression of *Axin2*, *Lgr5* and *Sp5* was observed in both UD and CD livers, suggesting WNT pathway activation (Figure 5.18c).

Morphologically, UD and CD livers were visually larger and, the damaged ones, exhibited several visible nodules with heterogeneous shapes and sizes on the surface (Figure 5.18d). Also, a large nodule was observed on the surface of one of the control UD (1/5) and one of the mutant UD (1/3) mice (Figure 5.18d). Since old mice are known to naturally develop tumours in the liver and, considering the very low frequency of this event, it would be difficult to prove that the nodule on the mutant liver is a direct consequence of the deletion rather than due to the mouse age. For this reason, I have decided to not focus on this specific event.

Although I did not observe an increase in the liver to body weight ratio in the undamaged *R&Z* deleted mice after 3 months, at the later time point both damaged and undamaged livers showed an increase of ~60-70%, suggesting that R&Z deletion eventually result in hyperplasia also during homeostasis and that this effect is not a direct consequence of the damage itself but it is accelerated by it (Figure 5.18e). Once more, this data suggests a regenerative defect of *R&Z* deleted livers.

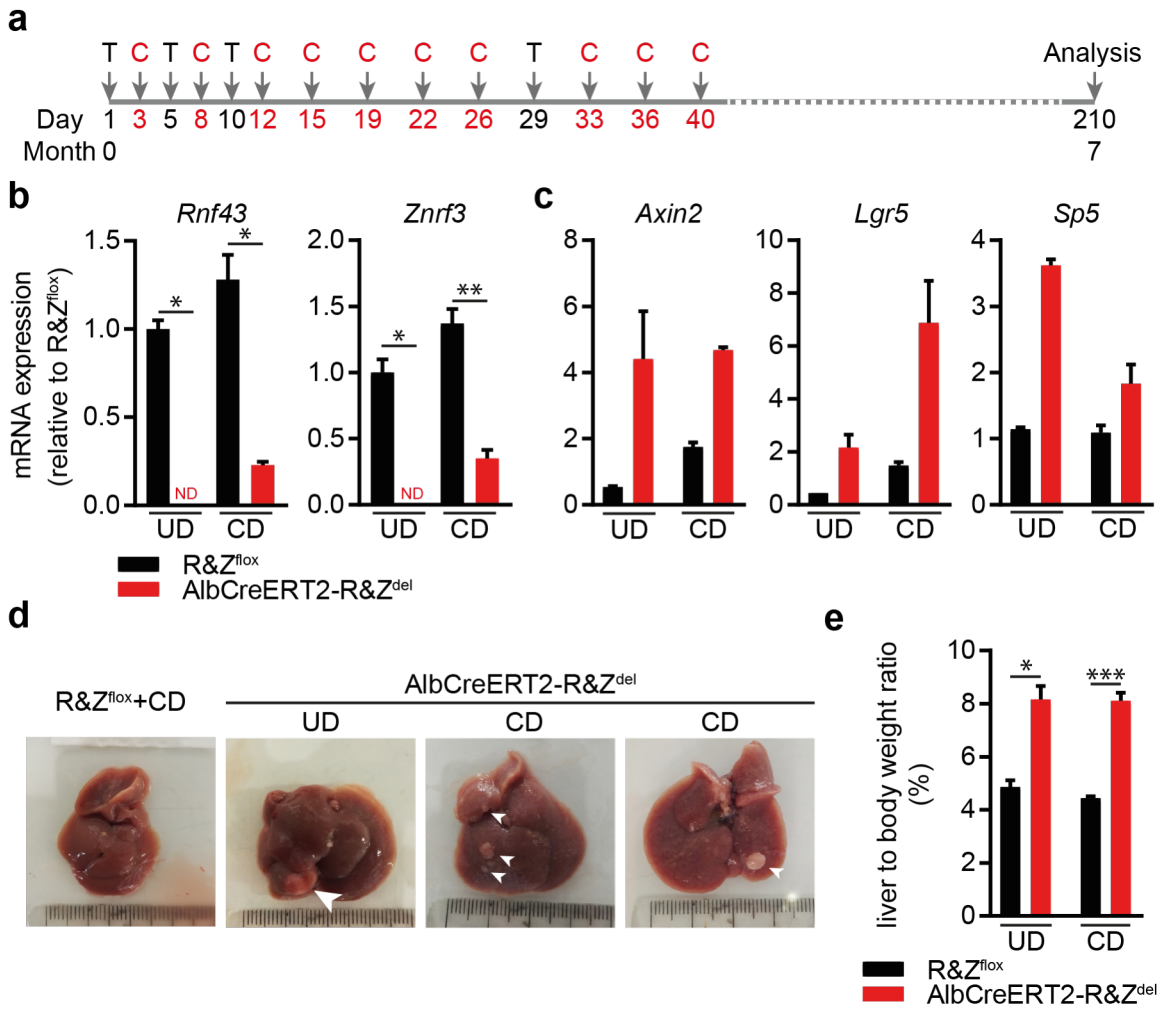

Figure 5.18. Long-term deletion of *R&Z* induces hyperplasia and larger nodules formation on the liver surface after CD. a) Timeline of the experiment. T, tamoxifen; C, CCl4. **b)** qRT-PCR expression analysis of *Rnf43* and *Znrf3* in R&Z^{flox} and AlbCreERT2-R&Z^{del} livers with and without CD after 7 months. Data represent mean ± SEM. n=4 mice per group. **c)** qRT-PCR expression analysis of the Wnt target genes *Axin2*, *Lgr5* and *Sp5* in R&Z^{flox} and AlbCreERT2-R&Z^{del} livers. Data represent mean ± SEM. n=2 mice per group.**d)** Pictures of R&Z^{flox} and AlbCreERT2-R&Z^{del} livers. Arrowheads, larger nodules visible on liver surface. **e)** Graph showing differences in the percentage of liver to body weight ratio. n=4 mice (R&Z^{flox} UD and CD), 3 mice (AlbCreERT2-R&Z^{del} UD), 9 mice (AlbCreERT2-R&Z^{del} CD). Data represent mean ± SEM. *P<0.05, **P<0.01, ***P<0.001; two-tail t-test was used. ND, not detected; UD, undamaged; CD, chronic damage.

At histopathologic analysis, both UD and CD *R&Z* deleted livers exhibited multiple small nodular foci characterized by clear cell changes and due to either fat accumulation or cellular degeneration (Figure 5.19**Error! Reference source not found.**a). Also, livers showed extensive cellular damage characterised by the presence of hepatocytes undergoing ballooning degeneration. All these pathological features are commonly associated to steatohepatic injury and were observed in most of the *R&Z* mutant mice analysed (3/3 for the UD mice and 7/9 for the CD mice), but not in control UD (0/3) or CD (0/4) mice. This data further suggested a possible role for R&Z in regulating liver metabolism. Furthermore, regenerative nodules were still observed in the CD *R&Z* deleted livers after 7 months, although more sparsely.

A significant increase in both GS area staining and cell proliferation was detected in both UD and CD livers, with a ~3 fold increase in GS and ~9 fold increase in Ki67 positive cells in the UD livers and slightly less in the CD ones (Figure 5.19a, b, c). To assess whether the damage observed would result in fibrosis, I have again performed Sirius red staining. No collagen deposition was observed in the undamaged liver, but few laces - less than at the earlier time point - were instead present in the CD model, suggesting an impaired recovery from the damage (Figure 5.19a).

The characteristic features observed in the *R&Z* deleted UD and CD livers after 7 months - steatohepatic injury and ballooning degeneration - highly resembles what has been described for human livers affected by non-alcoholic fatty liver disease (NAFLD) (Takahashi and Fukusato 2014). To assess whether *R&Z* deletion would trigger accumulation of fat in the hepatocytes, I have performed an Oil Red staining. Interestingly, sporadic foci of fat accumulation were present in both UD and CD livers but not in the non-deleted littermate controls (Figure 5.19a).

Overall, deletion of R&Z in hepatocytes after 7 months leads to increase liver volume, higher proliferation rate and WNT pathway activation. More importantly, R&Z seems to play a role in controlling liver metabolism as shown by increased GS staining, the presence of steatohepatic nodules and fat accumulation. Extensive cellular damage was also observed, probably due to the steatohepatic lesions and accumulation of reactive oxygen species (ROS) and/or failed activation or completion of the regenerative mechanism. These data might indicate that R&Z play an important role in maintaining liver homeostasis turnover and metabolism. Also, the presence of regenerative nodules and the mild fibrosis still at the later time point suggest that R&Z are also essential to induce proper regeneration after a chronic damage.

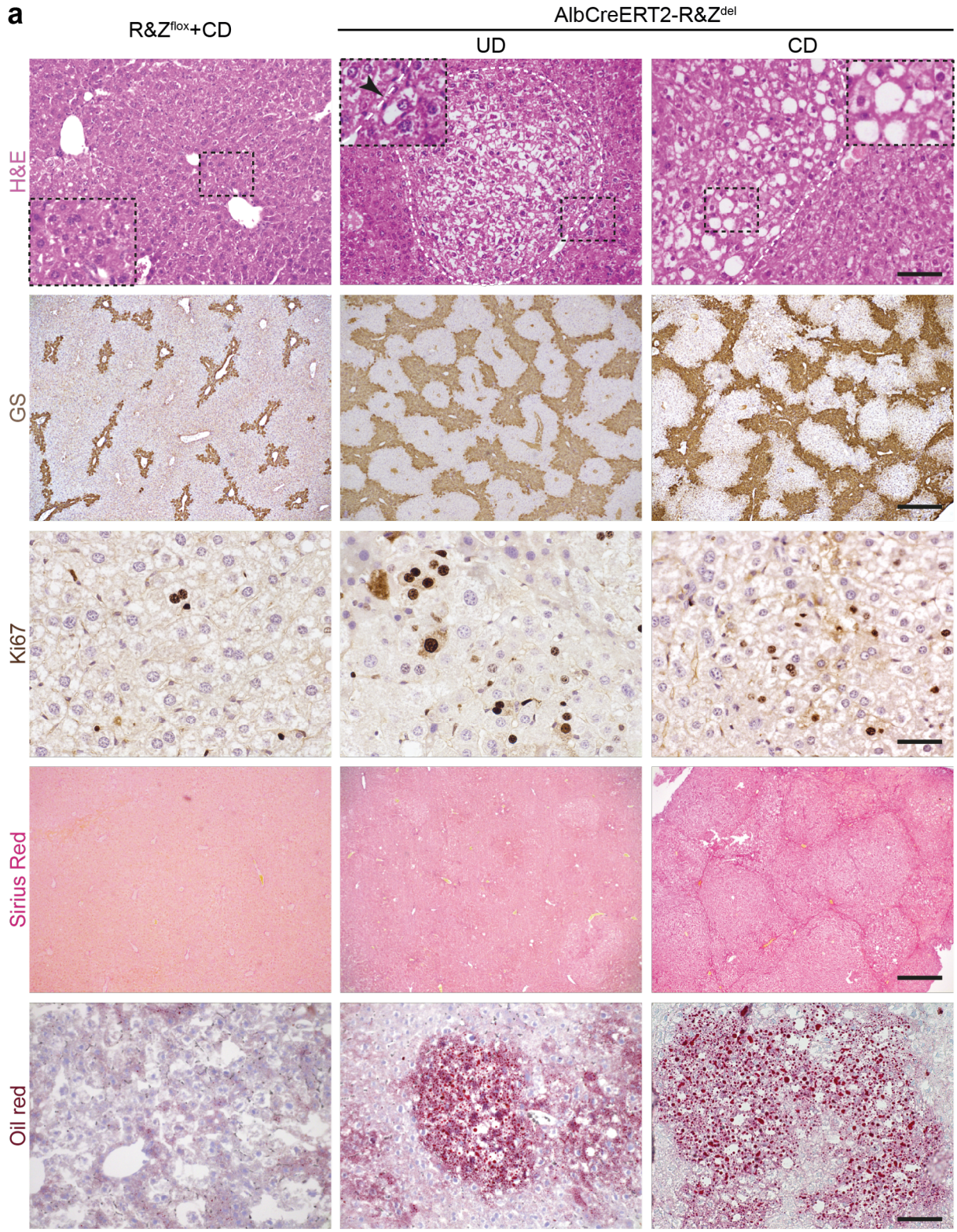
a
R&Z^flox+CD
AlbCreERT2-R&Z^del
UD
CD
H&E
GS
Ki67
Sirius Red
Oil red
b
GS staining area around CV (%)
60
40
20
0
CD UD CD
*
c
Ki67 positive cells (%)
5
4
3
2
1
0
CD UD CD
*
*
R&Z^flox
AlbCreERT2-R&Z^del

Figure 5.19. Long-term deletion of *R&Z* induces steatohepatic foci and fat accumulation in the liver. a) Representative pictures of H&E, Sirius Red and Oil Red staining and immunostaining for GS and Ki67 of chronically damaged R&Z^{flox} and damaged and undamaged AlbCreERT2-R&Z^{del} liver sections. Scale bar, 100μm (H&E, Oil Red), 500μm (GS, Sirius Red) and 50μm (Ki67). Arrowhead, ballooning degeneration. **b)** Quantification of GS positive staining localised around central veins. n=3 mice per group. **c)** Quantification of Ki67 positive hepatocytes. n=3 mice per group. Data represent mean ± SEM; *P<0.05; two-tail t-test was used; CD, chronic damage; UD, undamaged.

5.7 Long-term hepatocyte-specific *R&Z* deletion in adult liver parenchyma leads to early HCC and focal nodular hyperplasia after CD

As previously mentioned, livers were exhibiting several significantly larger nodular structures after CD at the later time point (Figure 5.16c). To characterise these structures, nodules were dissected and divided into three parts. Material for RNA, DNA and histological analysis was collected from two independent nodules, found on two different livers.

Histopathological analysis of the nodules, performed by histopathologist Dr. Susan Davies, identified these as early HCC (eHCC) or focal nodular hyperplasia (FNH) (Figure 5.20). eHCC were dysplastic, presenting abnormal edges that compressed the adjacent tissue, thus resulting in tissue dysplasia, and increased proliferative cells, as shown by Ki67 staining (Figure 5.20). Furthermore, CD34^{+} endothelial cells were also observed inside the nodules, suggesting increased vascularization of the nodule, typical feature of eHCC (Figure 5.20). Finally, cells inside the nodules were smaller and presented a steatohepatic phenotype (Figure 5.20). All these features are characteristic of eHCCs (Kudo 2013), and were used to identify eHCC presence in 6 out of 9 of the mice analysed. On the other hand, FNH is a benign lesion thought to arise from abnormal blood vessels regeneration after liver damage and it is characterised by the presence of an extensive ductular reaction with large septa without pleiomorphic cellular changes (Figure 5.20) (J. Nault, Bioulac–Sage, and Zucman–Rossi 2013). Increased proliferation and vascularization was also present in these nodules (Figure 5.20). A total of 2 mice out of 9 presented FNH growth.

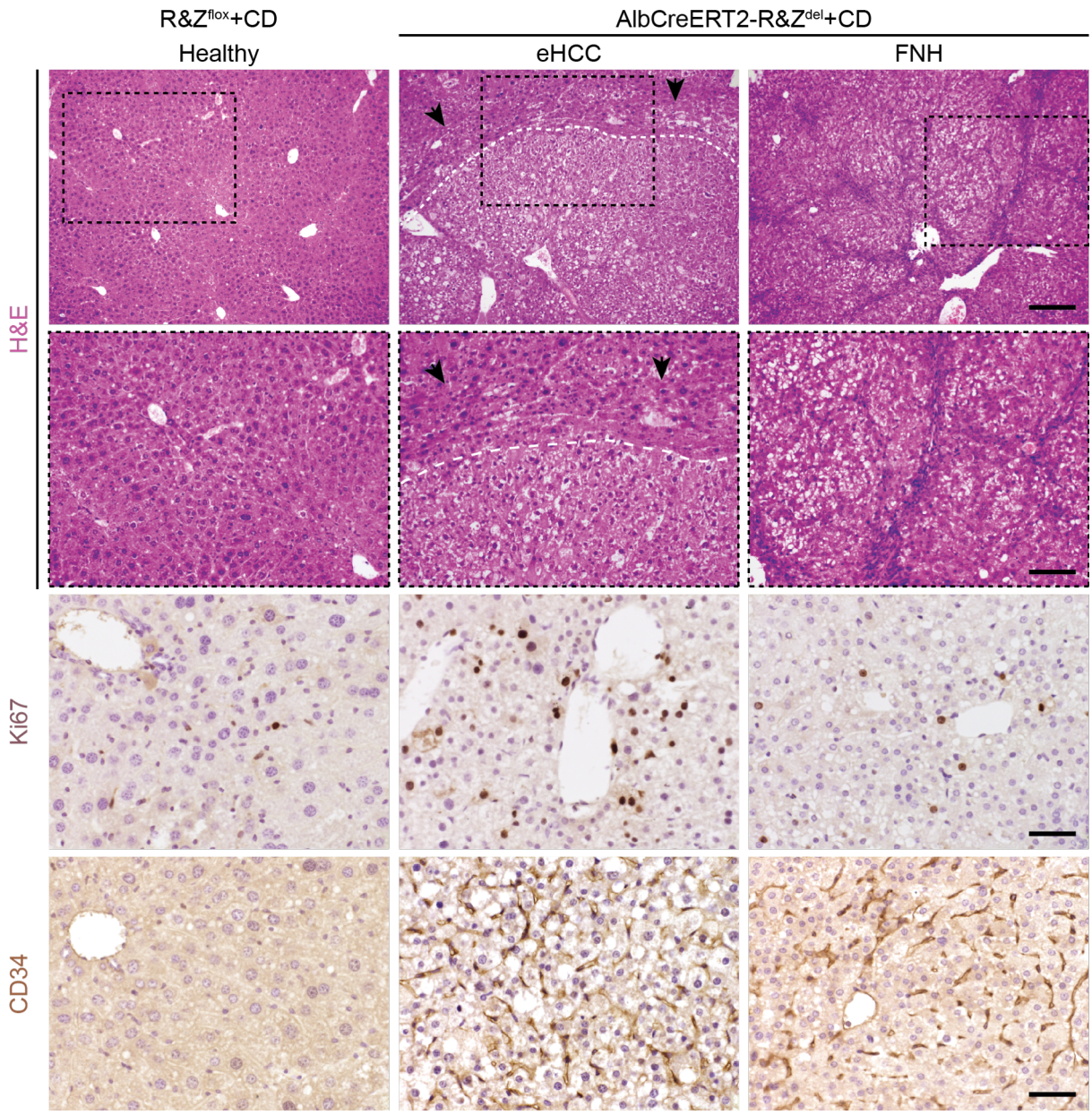

Figure 5.20. Long-term *R&Z* deletion and chronic damage promote eHCC and FNH formation. Representative pictures of H&E staining and immunostaining for Ki67 and CD34 of chronically damaged R&Z^{flox} liver and AlbCreERT2-R&Z^{del} nodules sections. Scale bar, 200µm (H&E top panel), 100µm (H&E bottom panel) and 50µm (Ki67 and CD34). Dotted line, nodules border; arrowheads, tissue compression.

As mentioned, RNA was collected from both eHCC and FNH and the respective total livers, TL^{eHCC} and TL^{FNH}. In line with previous analysis, *R&Z* deletion was observed in both TL^{eHCC} and TL^{FNH} (Figure 5.21). Specifically, ~55% of deletion was observed in TL^{eHCC} and almost complete deletion (~90%) in TL^{FNH}, when compared to undeleted chronically damaged liver TL^{flox}. Strikingly, no expression of either *Rnf43* nor *Znrf3* was detected in either eHCC or FNH, suggesting that either the WNT pathway was not active in these structures or that they had clonally originated from *R&Z* deleted hepatocytes, thus being unable to express the two genes (Figure 5.21). To investigate

whether this result was a consequence of the WNT pathway being inactive, I have checked the expression of the WNT target gene *Axin2* in both nodules and respective total livers. As expected, *Axin2* was upregulated in both TL^{eHCC} and TL^{FNH} with a fold change higher than 7 in both cases (Figure 5.21). Interestingly, eHCC still exhibited a change fold increase of more than 4 in *Axin2* expression when compared to the control, suggesting activation of the WNT pathway in this lesion and more importantly, that the nodule itself might have arisen from an *R&Z* deleted cell (Figure 5.21). However, *Axin2* expression in FHN was highly reduced when compared to the respective liver TL^{FNH} and equal to the littermate control TL^{flox} (Figure 5.21). In this case, WNT pathway was not active in the nodule, thus it cannot be discerned whether the nodule originated from *R&Z* wild type or deleted cells. At this stage, I was only able to collect one nodule of each type, thus further analysis of an increased number of nodules is needed in order to fully understand the origin of these lesions.

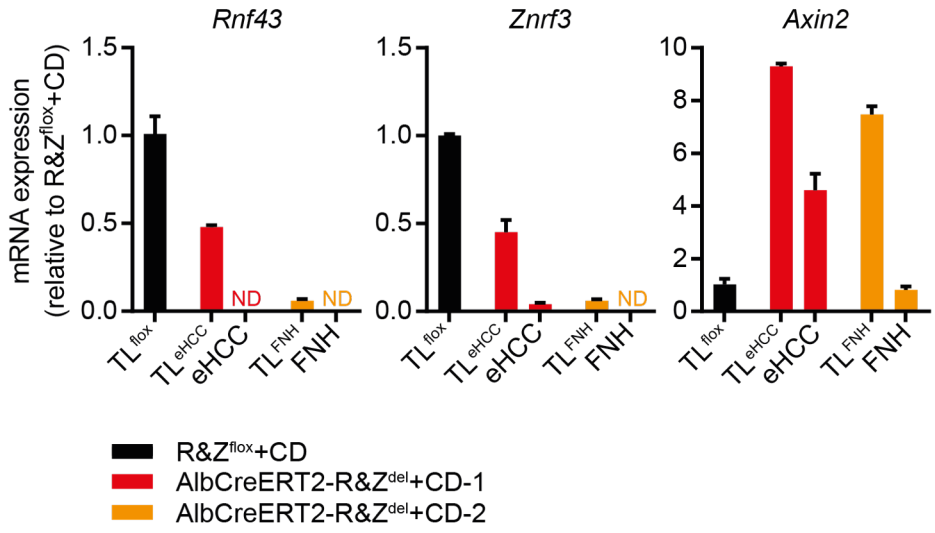

Figure 5.21. eHCC and FNH do not express R&Z. qRT-PCR expression analysis of *Rnf43*, *Znrf3* and *Axin2* in total liver from one $R\&Z^{flox}$+CD mouse and two AlbCreERT2-$R\&Z^{del}$+CD livers with respective nodules. Data represent mean ± SEM. TL, total liver; eHCC, early HCC; FNH, focal nodular hyperplasya. Statistic was not performed due to low sample size.

Overall, these data suggest that due to the metabolic defect caused by *R&Z* deletion and/or combined with the defective regeneration after long-term chronic damage, livers undergo several morphological changes that eventually lead to establishment of FNH and/or eHCC.

6. DISCUSSION

6.1 PLC-derived organoids as a bridging model system between cell lines and animal models

Hepatocellular carcinoma (HCC) is the most frequent and most studied primary liver cancer (PLC), accounting for 85 to 90% of all PLCs (El-Serag and Rudolph 2007). Thus, it is not surprising that many HCC model systems have been already developed. Dozens of cell lines and animal models have been used to better our knowledge about this disease but, more importantly, to help us devise new therapeutic strategies. Despite the recent advancement in the field, treatment strategies are still scarce and PLC remains one of the most lethal malignancies worldwide (Pinter et al. 2016).

Being easy and cheap to handle, cancer cell lines are commonly the first approach used by scientists to test the effect of newly discovered drugs. The efficiency of the drug Sorafenib, was indeed first tested in cancer cell lines (Liu et al. 2006). More recently, this anticancer drug is sometimes used as a targeted therapeutic strategy for HCC (Llovet et al. 2008). However, cell lines lack many of the traits that are found in real tumours, traits that not only include the histology and architectural organisation, but also the interaction between the tumour itself and the surrounding environment. Consequently, it is obvious that all the data gathered using cell lines will need further validation using a more sophisticated system, most commonly animal models. Unfortunately, due to the substantial limitations of cell lines in recapitulating the main features of the tumour, the results first gleaned from their use may be difficult to reproduce in an *in vivo* setting. These difficulties and resulting slowed progress could culminate in a waste of money, energy, time and animal lives. Additionally, although many cancer cell lines have been established for HCC, currently only two have been derived from cholangiocarcinoma (CC) and none from the combined HCC/CC subtype (CHC), two rarer forms of PLC, which account for 5-10% and 0.5-5% of all PLCs respectively.

More recently, the use of patient-derived xenograft (PDX) models has allowed the study of human tumours in an *in vivo* setting, thus not only recapitulating tumour architecture and histology, but also the interaction with the host environment. Importantly, this new experimental strategy has made possible to model tumour

subtypes that lack established cell lines, e.g. CC (Cavalloni et al. 2016). Moreover, as tumours are derived directly from patients, this system has enabled the possibility of testing drugs for personalised treatment strategies. However, although these tumours have been recently shown to be able to be passaged multiple times in mice, retaining the tumour morphological features, their use for large scale drug screening (>20 drugs) has major limitations due to technical difficulties, and has to rely on PDX tumour-derived cultures (Bruna et al. 2016).

Tumoroids could represent the tool that would bridge the gap between cancer cell lines and PDX models. Until now, it has been impossible to derive and propagate primary liver tumour cells *in vitro* from patients into cultures that maintain tumour identity and genetic aberrations. Although cell lines can be aggregated to form spheroid structures that more closely mimic a real tumour, they still cannot recapitulate tumour histology and genetics. Instead, we have shown that PLC-derived tumoroids have histological architecture associated with the tumour of origin. Strikingly, we have managed to establish tumoroid cultures not only from HCC, but also from CCs and CHCs, for which *in vitro* model systems are not readily available. It is clear then, that validating this system as a reliable cancer model may eventually enhance how tumours are studied and treated. In this regard, we have shown that tumoroids retain the same mutational profile of the original tumour tissue. This is a key point if the system is to be used to test personalised treatment strategies. More importantly, we have shown that knowing the mutational profile of tumoroids, can help to predict drug efficiency and sensitivity of the cultures. So not only can tumoroids be used to assess which drug is the best drug to be used for the subject patient, but the same drug could be used to treat patients bearing tumours with a similar mutational profile. However, knowing the mutational profile might not always be enough to know which drugs to use. Nonetheless, tumoroids can be expanded long-term and can be frozen and thawed several times, without affecting their expansion potential. This represents a great advantage of this culture system as it could actually be used to virtually test an unlimited number of drugs, thus removing the intermediate PDX step.

One concern that might arise is whether tumoroids maintain the identity of the tumour of origin after several passages. We have performed xenograft experiments showing that tumoroids cultured for more than 3 months, not only are able to generate tumours *in vivo*, but also retain the same features observed in the tumour of origin. Also, when tumoroids derived from a patient with a history of metastatic disease were injected in

the kidney capsule, mice developed secondary metastatic nodules in the lung, further proving their modelling capabilities.

Data presented here suggests that tumoroids could become a new attractive model to bolster our current arsenal of tools in cancer biology. This could have a monumental impact on how liver tumours are currently handled. Tumoroids exhibit the best features of both cell line and PDXs models whilst avoiding several of their downfalls. For instance, the expansion potential and ease at which large scale experiments can be carried out in cancer cells lines is maintained in tumoroids. However, tumoroids can also histologically and genetically mimic the tumour of origin, a key advantage of using animal models such as PDXs. More importantly, whilst tumoroids seem to represent the best of both worlds they remove some of the limitations that these two systems have. For instance, they retain the tumour identity even after long-term expansion, unlike cancer cell lines, and can be propagated and expanded indefinitely, not possible in PDX models.

Despite several advantages of using tumoroids, they also have limitations of their own. Unfortunately, we were unable to find culture conditions that would allow growth of well differentiated HCC (wHCC) samples, restricting the use of our model to tumours with a poorly or moderate/well differentiation state. Strikingly, we were able to generate tumoroids from all the poorly and moderate/well tumours (100% efficiency) but none from the wHCC (0% efficiency) (Annex, Table 9.1). We have observed that the ability of establishing tumoroids from PLCs, correlates very well with the proliferative rate of the original tissue. In line with this, well differentiated HCCs exhibit a very low number of proliferative cells. Possible solutions to this issue could be to enrich for the proliferative cells in these tissues when deriving organoid cultures. However, surface markers for these tumour proliferative cells have not been identified yet, making this a challenging approach. In addition to this, being an *in vitro* system, tumoroids still lack interaction with the tumour microenvironment. For this reason, validation with animal models might still be required, although in lower numbers. Also, at the current stage, we are unable to say whether our culture condition favours expansions of some cells or clones over the other, thus changing the culture composition over time and resulting in a false positive or false negative when performing drug screening. To investigate this further, we are currently trying to understand whether tumoroids can also recapitulate tumour heterogeneity and whether this feature is maintained after derivation of the line and long-term culture.

These data prove that tumoroids could be a valid new alternative to cell lines and PDX models to faithfully model PLCs *in vitro*. The expansion potential, the histology and genetic features recapitulating the tumour they derive from, make PLC-derived tumoroids a powerful new tool that could change the approach to the treatment of this disease.

Current work and future plans

- Further characterisation of tumoroids lines is currently ongoing or has been already performed by Dr. Laura Broutier and this includes: IHC and IF staining for cancer subtype specific markers, deeper analysis of expression profile and genomic data.
- In collaboration with the Sanger Institute we have performed a drug screening on some of the tumoroids lines to further assess their use as cancer models for therapeutic approaches. We have once again observed a correlation between drug resistance/sensibility and genetic profile.
- Interesting drug candidates have been validated *in vivo* by injecting the drug directly in the tumour mass of xenotransplantated mice. Drug efficiency in killing the tumour was assessed by comparing with vehicle-injected tumours.
- We are now currently investigating the heterogeneity potential of the cultures by performing single-cell RNAseq at early and late passage and comparing the results with data gathered from the original tissue.

This work has been accepted in *Nature Medicine* and further data can be found on the manuscript once published.

6.2 Genetic engineering of human healthy liver organoids to model liver cancer initiation and/or progression *in vitro*

When it comes to study the role of specific genes or specific mutations and their contribution to cancer formation, animal models have become the gold standard. The most common strategy for gene function studies is to either alter (specific mutagenesis) or completely remove (knock-out) the gene of interest from the organism or a specific tissue. The introduction of the Cre-loxP system has overall facilitated the DNA modification of the host genome, and most of gene function studies in cancer research

rely on the use of this system (Horie et al. 2004; Nantasanti et al. 2016; Zender et al. 2013; Saha et al. 2014). From the design of a targeting vector to the generation of a conditional mouse model, it can take up to two years before starting any experiment and obtaining any information on the gene of interest. With the introduction of the CRIPR/Cas9 system, the science community has found other ways that allow for faster results. For instance, viral vectors containing gRNAs can directly be injected into mice expressing a Cas9 protein, thus eliminating the need of crossing multiple mice lines and making it easier to mutate multiple genes at once (Platt et al. 2014).

In the second section of the results, I have shown how human liver organoids can be genetically manipulated to study gene contribution to cancer formation using the CRISPR technology. The whole process takes between four to six months, and this includes not only the generation of the mutant cultures, but also their analysis. Could this system be used as a valid alternative to animal models to study gene functions?

I have generated *TP53*-mutated human liver organoids and shown that while the mutation introduced was efficiently inactivating the gene, the culture was acquiring phenotypical changes reminiscent of malignant transformation. The histologic features of the cultures and the aneuploidy observed, all pointed towards *TP53* mutations alone being already enough to induce cellular transformation. Although *TP53* is a well-known tumour suppressor gene, it was anyway surprising to observe such changes upon its inactivation. In most of the cases, mouse livers do not develop tumours when a single gene is mutated and a second hit is usually required. In line with this, when *Tp53* is mutated in mice, livers do not develop tumours unless further mutations or/and a damage are applied (Nantasanti et al. 2016; Dumble et al. 2001). This could represent a stark difference in how mouse and human livers respond to specific genes mutations. However, it is important to consider the model system used and to try to understand whether this difference is real or model system-dependent. Human liver organoids originate when ducts are placed in specific media conditions and start proliferating (Huch et al. 2014). *In vivo*, ductal proliferation (ductular reaction) is observed only after damage, and ducts are not actively proliferating in homeostasis conditions (Preisegger et al. 1999). Thus, taking into account the proliferation status of the culture, liver organoids could be considered as a model for damage-induced ductal proliferation. This could explain why one single mutation in a tumour suppressor might already induce phenotypical changes to organoid cultures that otherwise would not be observed in a homeostatic liver. However, to know whether this is true or the phenotype

observed is due to mouse-human differences, I have recently established mouse liver organoids from *tp53* mutant mice and I am currently assessing whether they would recapitulate what I have observed in the human system (malignant transformation) or they would instead remain normal.

Considering the positive results obtained from the *TP53* mutant model, I sought to explore whether the same strategy could be used to screen for genes that have only recently been found to have a role in cancer, namely *RNF43* and *ZNRF3* (R&Z) (Koo et al. 2012). Unfortunately, although being resistant to RSPO1 withdrawal and showing WNT target genes overexpression, *R&Z* double mutant clones had limited expansion potential, making it difficult to further analyse the effect of their deletion in this model system. Only one clone, $hR^{-/-}Z^{-/if}$-1, has survived so far up to passage 19, suggesting that at least one functional copy of *ZNRF3* is essential to allow organoids survival. However, this experiment needs to be repeated to confirm this result and, *RNF43* and *ZNRF3* single KO are needed to rule out whether the effect observed is ZNRF3-specific or whether it applies to RNF43 too. Importantly, when *R&Z* were mutated together with *TP53*, organoids acquired some of the features observed in tumoroids, including aneuploidy, and I have been able to expand the culture beyond passage 15. This data suggests that mutations in genes involved in different pathways might be needed to better recapitulate a tumour phenotype and might also help in preventing cell growth arrest caused by the deregulation of one of the pathway.

Taking into consideration all the data I have presented in this section, it is hard to suggest that using CRISPR/Cas9 system with human liver organoid culture is a valid replacement for current animal models and techniques. In order to delve deeper into this problem, full characterisation of mutant clones and more examples are needed to better understand any potential advantages this system may have. In addition, I have encountered a series of technical challenges that has made the system more difficult than expected. A key issue that arose from this work is that the transfection efficiency of liver organoids is very poor. I have tried several different methods to optimise the transfection of plasmids containing Cas9 and gRNAs into organoids. Lipofection using lipofectamine 3000 proved to be the best method with up to ~13% efficiency versus the ~2% and ~4% on average obtained with lipofectamine 2000 and electroporation respectively. However, the use of lipofectamine 3000 has been quite unreliable, with the efficiency often dropping as low as ~2%. The second major difficulty I have encountered is a potent growth arrest after introduction of the mutations. As

mentioned, *R&Z* KO clones have stopped growing around passage 9, while *TP53* and *TP53+R&Z* mutants, although being able to expand longer, suffer from a slower expansion rate over time. Whether this is mutation-dependent or due to technical issues is still to be established. One potential explanation is that throughout the transfection process cells undergo a series of steps that may induce cellular damage resulting in a permanent negative impact on their proliferative potential (two steps of single cells dissociation, FACS sorting). Finally, we need to consider that, after sorting, cells are grown clonally, which means that from one single mutated cell a new organoid line is derived. Although these cells come from the same starting culture, liver organoids exhibit some intrinsic heterogeneity and, by growing single cells clonally, cells with less proliferative potential might be selected, thus resulting in premature growth arrest.

Finally, we need to consider that, as organoids are composed by ductal/progenitor cells, they could be used to model CC (cholangiocyte-like tumour) using this system, but it might not be possible to model HCC (hepatocyte-like tumour). Deep analysis of mutant cultures is needed in order to assess whether specific mutations could drive cells towards a hepatocyte-like state and, only then, could be used to model HCC. Alternatively, a possible solution would be to induce the differentiation of the organoids into hepatocytes after the mutations have been introduced. In this case, if the mutation is tumorigenic, it might further push towards a HCC phenotype instead of a CC one.

It is then clear that, if this system is to be used to study gene function or, more specifically, the role of specific genes in cancer, further optimisation of the protocol to overcome the above issues is required. By increasing the transfection efficiency, an increased number of mutant clones can be generated, thus decreasing the chances of selecting less fit cells. If optimization of the protocol is achieved, then we may be able to uncover the true power of this system and correctly assess its potential against current animal models.

Future plans

Due to the difficulties above mentioned we have decided to stop this project until we can devise a better strategy for introducing mutation in human liver organoids without affecting their expansion potential.

6.3 R&Z as regulators of mouse liver homeostasis, metabolism and regeneration

The WNT signalling pathway is not only critical for liver development, but it has also been shown to have a key role in controlling liver regeneration and metabolic zonation (J. Yang et al. 2014). Liver-specific KO of β-catenin, the WNT pathway effector, results in decreased liver to body weight ratio and decreased cellular proliferation both in homeostasis and after partial hepatectomy, thus resulting in retarded activation and completion of the regenerative process (Tan et al. 2006). In addition, livers lacking β-catenin exhibit loss of expression of the metabolic genes GS and CYP2E1, showing the importance of the WNT signalling in regulating correct metabolic function of the liver (Sekine et al. 2006). Conversely, stabilisation of β-catenin results in increased proliferation and hepatomegaly without giving rise to cancer (Tan et al. 2005). In line with this, removal of a key suppressor of the WNT pathway *Apc*, also results in hepatomegaly and can give rise to HCC after >9 months from deletion (Colnot et al. 2004). Interestingly, APC has been suggested to be the guardian of liver zonation as its deletion induce decrease expression of periportal markers and increase of perivenous ones (Benhamouche et al. 2006). More recently, a new study has shown how global deletion of *R&Z*, driven by Rosa26-CreERT, results in increased proliferation as well as expansion of the GS and CYP2E1 positive regions after 10 days, suggesting R&Z as novel regulator of liver zonation and in line with their crucial role in regulating the WNT pathway (Planas-Paz et al. 2016). To further understand the implication of *R&Z* deletion in the liver, I have induced deletion either in the biliary compartment or in the hepatocytes and performed analysis at different time points during homeostasis and after damage.

R&Z conditional deletion in *Sox9* expressing cells (biliary ducts and hybrid periportal hepatocytes in the liver) did not result in any significant morphologic or structural alteration 40 days after induction of deletion, during homeostasis or after DDC-induced damage. Of note, mice fed with a DDC diet for 5 days developed ductular reactions and collagen deposition around the portal vein with no significant difference between KO and control mice at the time point analysed. As ductular reaction should resolve in a wild type setting, analysis at a later time point is needed in order to fully exclude a possible effect of *R&Z* deletion in the ducts. However, according to the data gathered so far, there seems to be no involvement of R&Z in regulating ductular reaction after acute DDC-induced damage.

The second approach to uncover the role of R&Z in the liver was to delete the two genes from the hepatocytes using an AlbCreERT2 line. Consistent with the already published data on the ablation of R&Z from the whole body, hepatocyte-specific *R&Z* deletion triggered an increase in proliferation and it also affected metabolic zonation by increasing the GS positive area around the CV. This abhorrent expression pattern of GS and the increased proliferation were maintained 7 months from the point of deletion. In agreement with what has been described after *Apc* KO or β-catenin stabilisation, hyperplasia was observed after deletion of *R&Z*. Interestingly, I observed increased expression of genes involved in beta oxidation, ketogenesis and fatty acid and cholesterol metabolism after 3 months and this expression pattern correlated with human steatosis. This was an interesting result as, how I observed at the later time point, *R&Z* KO in the liver eventually lead to sporadic focal fat accumulation and steatohepatic injury. This data suggests that R&Z are novel regulators of fat metabolism in the mouse liver.

Of note, as *R&Z* deletion causes an increased expression of metabolic genes localised around the CV and, considering that the CV is the zone where lipogenesis is localised, it is not surprising that the metabolic changes observed would result in fat accumulation in these livers. This data is in agreement with a recent paper showing that after suppression of the WNT pathway by liver-specific KO of *Tcf7l2* (encoding for TCF4, transcription factor involved in the WNT signalling) leads to an altered ability of these livers to metabolise fat and, as a result, to decreased fat accumulation (Boj et al. 2012). Furthermore, *Tcf7l2* KO was able also to affect glycogen storage and metabolism when mice were maintained on a high-fat diet. Therefore, it would be also interesting analysing the effect on gluconeogenesis in *R&Z* deleted livers, as well as other metabolic events localised at the PV.

I have also observed similar results when mice with hepatocyte-specific deletion of *R&Z* were treated with acute and chronic damage. However, while livers were able to recover completely after acute damage, they exhibited extensive alterations following chronic damage. For instance, regenerative nodules and mild fibrosis were readily observed at several time points after chronic damage. As the WNT pathway is involved in regeneration (J. Yang et al. 2014), it is possible that upon *R&Z* deletion, livers fail to regenerate properly. Of note, WNT pathway inactivation caused by removal of β-catenin results in a slower activation of the regenerative process after partial hepatectomy (Tan et al. 2006). Considering this, it would be expected an opposite

effect when the WNT pathway is instead activated by *R&Z* KO. However, chronically damaged *R&Z* deleted livers exhibit a higher extent of damage than the wild type littermate controls, suggesting impairment in regeneration after repetitive CCl4 injections. One hypothesis could be that the liver needs a balanced activation of the WNT pathway in order to properly regenerate after damage, thus either an excess or a shortage of WNT signal results in improper functioning of the regenerative machinery (Figure 6.1b). Furthermore, it is possible that the liver activates different regenerative mechanisms based on the kind of damage it experiences, thus different amounts of WNT activation might be required. Another possibility is that WNT is required for both the activation of the proliferative response to the damage as well as for the differentiation of the '*de novo'* produced hepatocytes (Figure 6.1b). Finally, we need to consider how the CCl4 damage works in relation to the phenotype that *R&Z* deletion triggers. Specifically, CCl4 kills the hepatocytes around the CV after being metabolised by the cytochrome P450. I have observed that *R&Z* deletion induces overexpression of CV specific genes, including *Cyp2E1*, encoding for the cytochrome P450 (Annex Figure 9.1). It is then possible that, due to more hepatocytes expressing the cytochrome, *R&Z* deleted livers are more susceptible to CCl4-induced damage (Figure 6.1a). Coupling the altered regeneration with the increased damage, *R&Z* deleted livers exhibit morphological changes otherwise not present in a wild type liver (regenerative nodules, mild fibrosis) (Figure 6.1c).

According to this data, it was clear that hepatocytes, lacking R&Z, were not able to fully repopulate the liver with functional new hepatocytes upon chronic damage. Interestingly, by allowing further recovery by increasing the time between the damage and the end of the experiment, *R&Z* KO livers did show partial regeneration. This regeneration was characterised by a milder phenotype with less GS, less Ki67 and less Sirius Red staining compared to an earlier time point. This suggests that although the regenerative machinery was not working properly, some regeneration was still taking place. For this reason, I have recently started to explore whether other regenerative mechanisms were being activated in order to help the regenerative process. In line with this, PCK staining, a marker for ductal cells, revealed the presence of extensive ductular reaction, with the presence of PCK positive cells far from the PV, their normal location (Annex Figure 9.2). Further analysis is needed to prove that this ductular reaction is responsible for the partial regeneration. Analysing how many hepatocytes have functional R&Z after partial regeneration could easily test this. These

hepatocytes could only arise from cells that avoided the initial deletion, such as ductal cells.

After long-term deletion of *R&Z*, the metabolic defects observed eventually lead to extensive cellular damage, sporadic foci of fat accumulation and steatohepatic injury. These features are commonly observed in patients suffering from non-alcoholic fatty liver disease (NAFLD). More specifically several cellular pathologies are used to diagnose the disease such as, steatosis, lobular inflammation, fibrosis and hepatocellular ballooning (Takahashi and Fukusato 2014), all of which are observed in *R&Z* KO livers. Although alterations in the WNT pathway are not usually associated with NAFLD, β-catenin is known for regulating many of the processes that lead to the establishment of the disease, including glucose and lipid metabolism. Also, I observed an increase of WNT related genes in a cohort of patients affected by either steatosis or non-alcoholic steatosis (NASH), a type of NAFLD. Thus, alteration of the WNT pathway and, in this case, of R&Z, can result in a series of metabolic alterations culminating in a NAFLD-like phenotype later in life.

Importantly, NAFLD and the chronic damage caused by the resulting steatohepatic injury and reactive oxygen species, can lead to cirrhosis, fibrosis and eventually to cancer (Takahashi and Fukusato 2014). Consistent with this, *R&Z* deletion also resulted in the establishment of early hepatocellular carcinoma (eHCC) after chronic damage. Whether these tumours arise as a direct consequence of the deletion in response to damage, or due to impaired regenerative mechanisms or steatohepatic injury or all of them together is still to be evaluated. Of note, *R&Z* deletion also resulted in focal nodular hyperplasia (FNH), which is a blood vessel response to impaired regeneration (J. Nault, Bioulac–Sage, and Zucman–Rossi 2013), further supporting the hypothesis of R&Z being important for liver regeneration. Further analysis of these lesions is needed in order to fully understand their origin. For example, I have observed no expression of *R&Z* in examples of both eHCC and FNH but, as I do not know whether these specific lesions initially express the two genes, it is difficult to say whether they originate from *R&Z* deleted cells or come from other cell populations in the liver. To answer this question, I am performing DNA analysis of the lesions and I will assess whether they have the deleted *R&Z* alleles. Also, *in situ* hybridization of deleted and undeleted form *R&Z* will help answer this question.

In conclusion, *R&Z* deletion in the liver triggers hepatomegaly and metabolic alteration similar to what observed upon manipulation of the WNT pathway using several other

mouse models that have already been described. These metabolic changes lead to alterations in fat metabolism and steatohepatic injury similar to what happens in NAFLD. When chronic damage is applied, R&Z deleted livers fail to fully activate or complete the regenerative mechanism and coupling this with the metabolic damage observed, it triggers establishment of lesions such as eHCC and FNH (Figure 6.1). Therefore, this work presents a novel role for R&Z in regulating not only liver metabolism but also regeneration after CCl4-induced damage.

Current work and future plans

- To understand the molecular mechanism underlying the phenotype observed, I have recently submitted samples, from all conditions at the different time points, for RNA sequencing. Analysis of this data will highlight possible pathways and processes involved in the mechanism of impaired regeneration, metabolism and cancer observed.

- To assess whether the results observed after chronic damage are due to the specific damage model or are due specifically to the lack of R&Z, I plan in testing different damage models. Chronic treatment with DDC diet could be used to confirm the results observed, as the cytochrome P450 is also involved in this chemical-induce damage. On the other hand, liver regeneration after physical injury like partial hepatectomy might provide answer regarding the specific effect of the deletion of R&Z, as cytochromes are not reported to be involved in the repair process following this kind of damage.

- To further assess the role or R&Z in regulating lipid metabolism, I aim at treating mice with a high-fat diet. In case of unbalanced metabolism, R&Z KO mice are expected to accumulate fat at higher rate than WT mice.

- Treatment of WT and R&Z organoids with free-fatty acids, both before and after differentiation, might be used to further corroborate a role for R&Z in lipid metabolism. In addition, this could be used as a model for steatosis *in vitro*, as also suggested by Kruitwagen et al. 2017.

- To test whether R&Z deletion might affect hepatocyte differentiation, I am planning of inducing differentiation into hepatocytes of WT and R&Z mutant liver organoids. Decreased cytochrome activity, LDL uptake and/or albumin secretion, might indicate that R&Z are required for complete maturation of hepatocytes and explain the retarded regeneration observed.

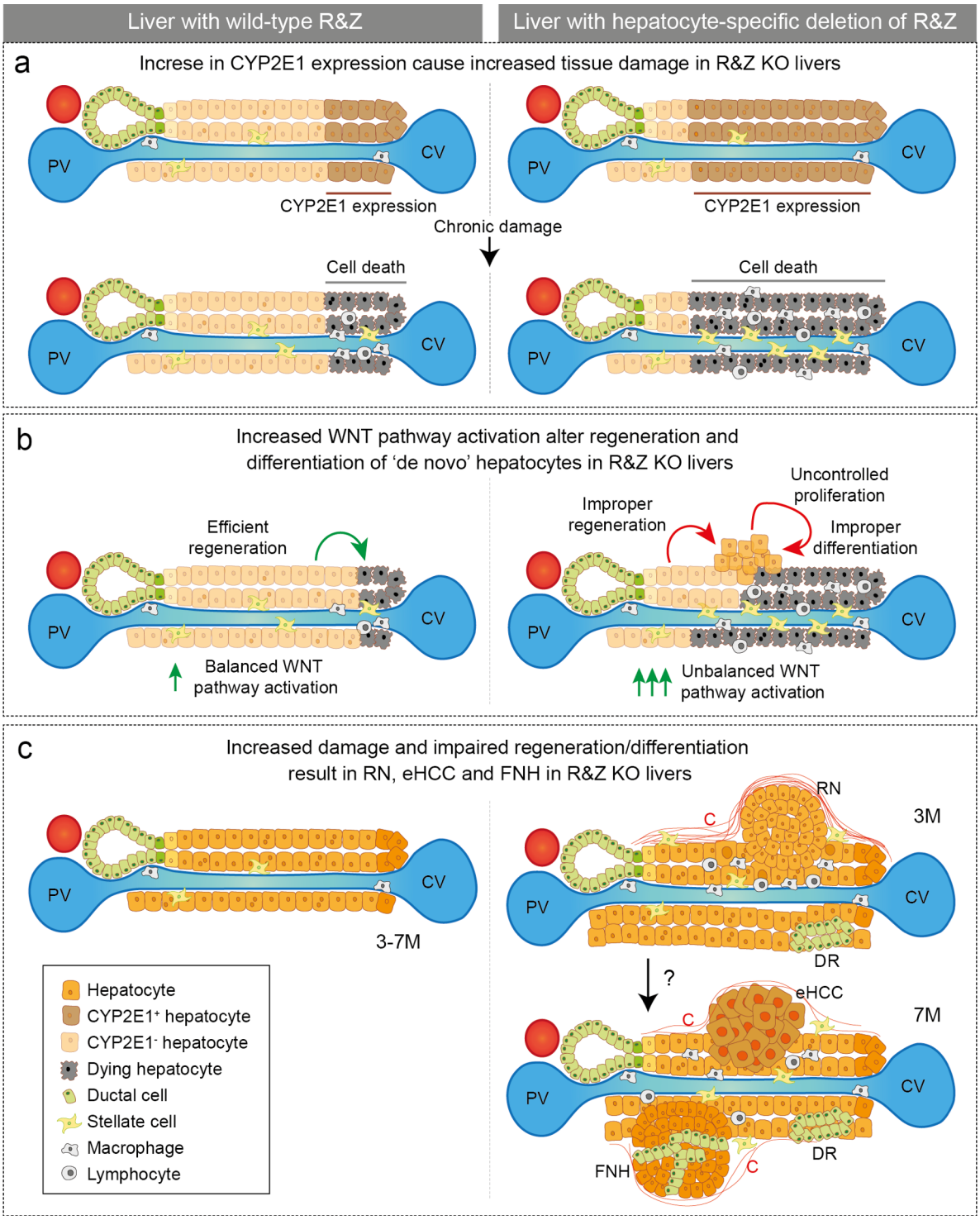

Figure 6.1. Proposed working model for the response to CD of livers with hepatocyte-specific deletion of *R&Z*. a) Deletion of *R&Z* drives increased expression of CYP2E1. Hepatocytes expressing the enzyme die after metabolising CCl4, thus *R&Z* deleted livers present a more extensive damage as more cells express CYP2E1. **b)** After CD, livers with wild type copies of *R&Z* are able to regenerate properly. Whereas, when the WNT pathway activation is increased due to *R&Z* deletion, hepatocytes are unable to properly initiate/complete the regenerative process. Also, newly formed hepatocytes fail to properly differentiate to become functional hepatocytes. This results in increased proliferation of cells to try to recover the damage. **c)** The increased damage and the improper regeneration and differentiation lead to formation of regenerative nodules, collagen deposition, ductular reaction, immunological infiltrate and giant hepatocytes. At 7 months, eHCC and FNH arise. It is unclear whether these lesions arise from the regenerative nodules observed at 3 months or originate from other cells. PV, portal vein; CV, central vein; M, month; C, collagen fibres; RN, regenerative nodule; DR, ductular reaction; eHCC, early HCC; FNH, focal nodular hyperplasia.

7. METHODS

7.1 *In vivo* experiments

7.1.1 Animals

All mouse experiments were conducted in accordance with procedures approved by the UK Home Office relating to the use of Animals in research (Animals Act 1986). Conditional knock-out mice for *Rnf43* and *Znrf3* were already available in the lab. Mice were generated as previously described (Koo et al. 2012). Briefly, exons encoding for the ring domain of RNF43 and ZNRF3 were flanked by *LoxP* sites to drive excision in presence of a CRE protein. RZ mice were crossed with either *Alb1-CreERT2* (Schuler et al. 2004) or *Sox9-CreERT2* (Jackson Laboratory JAX - http://jaxmice.jax.org/) to drive deletion in hepatocytes and cholangiocytes respectively. All experiments were started when mice were 7 weeks old. Primers used for genotyping are listed in Table 7.1. Immunocompromised NOD/Shi-scid/IL-2Rγnull (NSG) mice (Charles River) were used for xenotransplantation experiments.

Table 7.1. Primers used for genotyping

Gene	Forward primer	Reverse primer
Rnf43	ATTGGCATCGCAATTTTCTAA	TCGGTGTTCTTAACTGCTGA
Znrf3	GCAGTAATAAACAGGTAAAGAGCAAA	GCTGGAGAGACCGTTCATAAG
Cre	GCGGTCTGGCAGTAAAAACTATC	GTGAAACAGCATTGCTGTCACTT
Alb1-CreERT2	TATTTTGGGCACAACAGAGTC	TTCCGGTTATTCAACTTGCAC

7.1.2 Tamoxifen injections

Tamoxifen (Sigma-Aldrich) was dissolved in sunflower oil and was injected 200mg/kg intraperitoneally according to experimental protocol. Oil only was injected to control mice.

7.1.3 Damage experiments

Liver damage experiments were performed using toxic agents administrated IP (CCl4) or through diet (DDC). CCl4 (Sigma-Aldrich) was diluted in corn oil and administrated 1ml/kg one time for acute damage experiments (CCl4 dilution 1:10) or 500ul/kg ten times in 6 weeks for chronic damage experiments (CCl4 dilution 1:4). For DDC damage experiment, food was removed and replaced with DDC-supplemented diet for a total of 5 days after which normal food was restored. Mice weight was constantly monitored and measured once per week as a minimum. Mice were sacrificed by either cervical dislocation or carbon dioxide overdose. Liver, lungs and other relevant tissues were collected on ice and stored in PBS until fixed. Tail tip was collected to confirm genotype.

7.1.4 Xenograft

Xenotransplantation was performed by injecting dissociated organoids either subcutaneously or inside the kidney capsule. For subcutaneous graft, 1 million cells were injected into both flanks of NSG mice with or without BME2 (7mg/ml). Tumours size was measured weekly and mice were culled when the tumour reached limit end-point (size or necrosis). For kidney capsule graft, 500,000 cells were mixed with BME2 (7mg/ml) and implanted under the renal capsule of anesthetised NSG mice. These mice were then culled at different time point (0.5, 1, 2 and 3 month) by cervical dislocation and kidney and lung tissues were harvested to assess the growth and the metastatic potential of the grafted cells.

7.1.5 Liver perfusion, hepatocytes collection, macrophages and endothelial cells sorting

Mice were culled by carbon dioxide intoxication and head was removed to allow exsanguination. Livers were perfused inserting a small tube through the aorta and injecting 10ml of perfusion buffer (0.5mM EGTA in PBS), 10ml of perfusion buffer with BSA (Sigma-Aldrich) and 10ml of pre-warmed 0.5mg/ml Collagenase A (Sigma Aldrich) solution (HBSS 1x, 5mM CaCl2, 20mM HEPES). After 2 minutes incubation, livers were carefully removed, place in STOP solution (HBSS 1x, 5mM CaCl2, 20mM

HEPES, 0.5% BSA) and disaggregated using tweezers. Mixture was washed several times in STOP solution (50G for 2 minutes) and filtered with a 100µm strainer. Pellet containing hepatocytes was resuspended in RLT lysis buffer (Quiagen) and frozen at -80°C for RNA extraction. Supernatant was centrifuged again at 300g for 5 minutes to collect niche cells. Pellet containing niche cells was divided in two fractions and stained either with EpCAM-APC (eBioscience) and CD31-PE-Cy7 (AbCAM) antibodies or EpCam-APC and CD11b-PE-Cy7 (BD Bioscience) antibodies. Positive cells were sorted using a Flow Sorter MoFlo (Dako Colorado, Inc.), resuspended in RLT lysis buffer and stored at -80°C.

7.2 Immunohistochemistry

7.2.1 Tissue processing

Tissues were dissected and then fixed overnight in 10% buffered formalin (Sigma-Aldrich). The following day, tissues were divided in two parts to proceed to paraffin (Sigma-Aldrich) or OCT (VMR chemicals) embedding. For paraffin embedding, tissues were dehydrated in increasing concentration of ethanol (70%, 95% and 100% for 2h each) ending in xylene and then incubated overnight in paraffin. The following day, tissues were embedded in paraffin blocks and subsequently sectioned at a thickness of 5µm using a microtome. Sections were mounted onto SuperFrost Plus slides (ThermoFisher) and incubated from 3 to 12h at 60°C before staining. For OCT embedding, tissues were incubated in 30% sucrose PBS at 4°C overnight or until the tissue sunk, after which they were embedded in OCT blocks and frozen at -20°C. OCT blocks were sectioned at a thickness of 8µm using a Leica CM-3050S cryostat and mounted onto SuperFrost Plus slides for immunohistochemical analysis.

7.2.2 Immunohistochemistry of paraffin sections

After deparaffinising in two changes of xylene 5 minutes each, sections were rehydrated in descending grades of ethanol (100% 2x, 95%, 70%) 3-5 minutes each ending in water. Antigen retrieval was performed either enzymatically or heat-mediated based on primary antibody (see Table 7.2 for details). For enzymatic retrieval, sections were incubated 10 minutes at 37°C and 10 minutes at RT with TE buffer containing

0.5% Triton X-100 and 1/1000 proteinase K (800U/ml). For heat-mediated antigen retrieval, samples were incubated in either citrate buffer (10mM Sodium Citrate, pH 6) or Tris-EDTA buffer (10mM Tris base, 1mM EDTA solution, 0.05% Tween 20, pH 9.0), heated in a microwave to 95-98°C for 20 minutes and then cooled at RT for 20 minutes. After antigen retrieval, samples were blocked and permeabilized for 1.5 hours using TBS buffer containing 2% foetal bovine serum (FBS), 1% bovine serum albumin (BSA) and 1% or 0.1% of Triton x-100 based on antibody (see Table 7.2 for details). Samples were than incubated overnight with primary antibody at antibody-dependent concentration (see Table 7.2 for details). The following day, samples were washed in TBS and endogenous peroxidases were inactivating incubating 15 minutes in methanol containing 3% of hydrogen peroxide. Few drops of Poly-HRP-GAMs/Rb IgG (Immunologic) secondary antibody was added directly on the sections and incubated for 30 minutes. After washing, signal was developed using Bright Dab substrate kit (Immunologic) using manufacturer instruction. Sections were counterstained in hematoxylin for 5 minutes, dehydrated in ethanol (70%, 95% and 100% 2x) and in two changes of xylene 5 minutes each and finally mounted using xylene-based DPX mounting media (ThermoFisher). Slides were analysed using optical microscopy.

Table 7.2. Antibodies used for immunostaining

Antigen	Triton X-100	Retrieval	Concentration	Distributor
GS	0.1%	Citrate	1/800	BD
PCK	0.1%	Enzymatic	1/500	DAKO
Ki67	1%	Citrate	1/200	Invitrogen
CD34	0.1%	Citrate or Tris-EDTA	1/250	abcam
KRT19	-	Citrate	1/100	Atlas Antibody
CYP2E1	0.1%	Citrate	1/200	Atlas Antibody

7.2.3 Hematoxylin and eosin staining

Sections were deparaffinised and hydrated to water as previously and then stained with hematoxylin solution (Sigma-Aldrich) for 5 minutes and eosin solution (Sigma-Aldrich) from 30 seconds to 1 minute. Afterwards, sections were dehydrated to xylene

and mounted using xylene-based DPX mounting media (Fisher Scientific). Slides were analysed using optical microscopy.

7.2.4 Oil red O staining

Lipids were staining used oil red O staining kit (Sigma-Aldrich) following manufacturer protocol. Briefly, frozen sections were hydrated with water, rinsed with 60% isopropanol, stained with freshly prepared Oil Red O working solution for 15 minutes and rinsed again with 60% isopropanol. Slides were counterstained in hematoxylin for 5 minutes, washed and mounted using VectaShield mounting media (Vector lab). Slides were analysed using optical microscopy.

7.2.5 Picro-Sirius Red staining

Fibrosis was assessed staining collagen fibres using Picro-Sirius Red staining kit (AbCAM) following manufacturer instruction. Briefly, sections were deparaffinised, hydrated to water and stained with Picro-Sirius Red Solution for 60 minutes. Sections were rinsed quickly in 2 changes of acetic acid solution and then in absolute alcohol. Sections were cleared in two changes of xylene and mounted using xylene-based DPX mounting media (Fisher Scientific). Slides were analysed using optical microscopy.

7.3 RNA analysis

RNA was extracted from tissues, cells or organoid cultures using the RNeasy Mini RNA Extraction Kit (QIAGEN) according to the manufacturer's protocol and reverse-transcribed with the Moloney Murine Leukemia Virus reverse transcriptase (M-MLVRT) (Promega) as follows: 10 minutes at room temperature, 50 minutes at 50°C and 15 minutes at 70°C. The resulting cDNA was amplified with the iTaq™ Universal SYBR® Green Supermix (Bio-Rad) and a desired primer pair on the CFX Connect™ Real-Time PCR Detection System (Bio-Rad). The cycling conditions used were: 95°C for 3 minutes and 39 cycles of 95°C for 10 seconds and 55-60°C for 30 seconds (depending on the primer pair), followed by a melting curve (from 55-60°C to 95°C with an increase

of 0.5°C per cycle) to ensure amplicon specificity. Gene expression was normalised to the expression of the housekeeping gene *Hprt*. Primers used are listed in Table 7.3.

Table 7.3. List of primers used for qRT-PCR analysis.

Gene	Forward primer	Reverse primer
mRnf43	CCGTGTGTGCCATCTGTCTA	GTGGAGTCTTCTGCCTGGTTC
mZnrf3	GTACTCATCGGTTCCACAGGA	TAGTAGGGTAGGCTGGGATGG
mAxin2	TGTCCAGCAAAACTCTTC	CTTCTCTTGAAGGACCTGA
mLgr5	TCCAACCTCAGCGTCTTC	TGGGAATGTGTGTCAAAG
mHprt	AAGCTTGCTGGTGAAAAGGA	TTGCGCTCATCTTAGGCTTT
mSp5	ACTCACTGCAGGCCTTCCT	TCCAAGGGTGGAAAAGTCTG
mFasn	ACAGATGATGACAGGAGATGGAAG	GAGGCGTCGAACTTGGAGAG
mAcadl	TGCCCTATATTGCGAATTACG	AACACCTTGCTTCCATTGAG
mAcaa2	CCTCAGTTCTTGTCTGTTCAG	AGGTGTGCGGTGATTCTG
mAcaa1a	ATCAGAAATGGGTCTTATG	ACATTCTCCGAGGTCATC
mAcot4	TGCGGTACATGCTTCGACAT	TCCACTGAATGCAGAGCCATTG
mCyp2e1	CCCATCATTATCCCTTAC	AGTCAGATCTCGATACAG
mCyp2c39	CGCTAAAGAGATCACATATTC	ATAACTCCAGAAACCAGATG
mHmgcs2	TGAACGAGTGGATGAGATG	AGTCCCTATTTACTGCTGTG
mAqp9	TTTGGCATTTACTATGACGGACTC	GGCACCTGGCACGGATAC
mSlc17a2	ACAATCCAATCAAGACTCTAAGG	TCACCACGACAGGCTTTG
mCyp7a1	GCTGTGGTAGTGAGCTGTTG	GTTGTCCAAAGGAGGTTCACC
mAkr1b10	CTAGTGCCAAACCAGAGGACC	TCCTGTATTCGAGAAGGTGTCA
mFgf21	GTGTCAAAGCCTCTAGGTTTCTT	GGTACACATTGTAACCGTCCTC
mFads2	TCATCGGACACTATTCGGGAG	GGGCCAGCTCACCAATCAG
hRNF43	AAATTAATGCAGTCCCACCC	AAACTCCATCAGCTTCTCAG

hZNRF3	CATCGTCAACAAGCAGAAAGTG	GGAGACCACGACGAAGAAAG
hAXIN2	AGCTTACATGAGTAATGGGG	AATTCCATCTACACTGCTGTC
hLGR5	GACTTTAACTGGAGCACAGA	AGCTTTATTAGGGATGGCAA
hHPRT	AAGAGCTATTGTAATGACCAGT	CAAAGTCTGCATTGTTTTGC
hTNSFRS19	CAGGTGGCTGGGAAGAACTCTC	ACACAGTTTCCAGACCGATCC
hCDKN1A	GACTCTCAGGGTCGAAAACG	TAGGGCTTCCTCTTGGAGAA
hSOX9	GGAAGTCGGTGAAGAACGGG	TGTTGGAGATGACGTCGCTG
hKRT19	GTCATGGCCGAGCAGAAC	ACCTCCCGGTTCAATTCTTC
hCYP3A4	TGTGCCTGAGAACACCAGAG	GTGGTGGAAATAGTCCCGTG
hHNF4α	GTACTCCTGCAGATTTAGCC	CTGTCCTCATAGCTTGACCT
hALB	CTGCCTGCCTGTTGCCAAAGC	GGCAAGGTCCGCCCTGTCATC

7.4 Organoid cultures

7.4.1 Mouse liver organoids/ducts isolation

Mouse liver organoids were derived and cultured as previously described (Huch, Dorrell, et al. 2013). Livers were collected in PBS and dissociated using a collagenase solution (Collagenase type XI 0.012%, dispase 0.012%, FBS 1% in DMEM medium) and incubated for 3 to 4 hours at 37°C. Mixture was washed several times and ducts were hand-picked, mixed with Matrigel (BD Bioscience) and seeded in a 24 multi-well plate. After Matrigel had polymerized, culture medium was added. Culture conditions for expansion (EM) were based on AdDMEM/F12 (ThermoFisher) supplemented with 1% B27 (Invitrogen), 1% N2 (Invitrogen), 1.25mM N-acetylcysteine (Sigma-Aldrich), 10nM gastrin (Sigma-Aldrich), 50ng/ml mEGF (Peprotech), 5% RSPO1 conditioned medium (homemade), 100ng/ml Fgf10 (Peprotech), 10mM nicotinamide (Sigma-Aldrich) and 50ng/ml HGF (Peprotech). To establish the culture, for the first week media was supplemented with 25ng/ml Noggin (Peprotech), 30% Wnt conditioned media (homemade) and 10µm Rockinase inhibitor (Y27632, Sigma-Aldrich). Weekly,

organoids were removed from the matrigel, mechanically dissociated with a narrowed Pasteur pipette, and transferred to fresh matrix in a 1:4 split ratio.

7.4.2 Human specimens

Liver tumour biopsies (~1cm^3) were obtained from biopsies or resection performed at Erasmus Medical Center Rotterdam MEC-2013-143, Cambridge University Hospitals NHS Trust REC: 15/LO/0753 (Approval by NRES Committee London – Westminster) and The Royal Infirmary Hospital Edinburgh REC: 15/ES/0097. Healthy livers biopsies (~1cm^3) were obtained during liver transplantation performed at the Erasmus Medical Center, Rotterdam MEC-2014-060. All patients provided informed consent and samples were procured and studies were conducted under Institutional Review Board approval prior to tissue acquisition. Samples were confirmed to be tumour or normal based on pathological assessment. The histopathological diagnosis of each case was confirmed on routine hematoxylin and eosin stained slides and immunohistochemistry and analysed by an independent histopathologist.

7.4.3 Human liver donor and tumour-derived organoids isolation

Human liver donor organoids were derived using previously described protocol (Huch et al. 2014). Human liver biopsies (0.5–1 cm^3) were minced and incubated with digestion solution (2.5mg/ml collagenase D (Roche) in DMEM (Invitrogen), for 2 to 3h at 37°C. The digestion was stopped by adding cold DMEM with 1% FBS and the suspension was then filtered through a 100 µm Nylon cell strainer and spun 5 minutes at 400g. The pellet was washed in cold AdDMEM/F12 (ThermoFisher) then mixed with BME2 (Basement Membrane Extract, Type 2, Pathclear). 10,000-30,000 cells were seeded per well in a 24 multi-well plate.

After BME had solidified, donor samples were cultured in expansion medium (EM) based on AdDMEM/F12 (ThermoFisher) supplemented with 1% B27 (Invitrogen), 1% N2 (Invitrogen), 1.25mM N-acetylcysteine (Sigma-Aldrich), 10nM gastrin (Sigma-Aldrich), 50ng/ml hEGF (Peprotech), 10% RSPO1 conditioned medium (homemade), 100ng/ml Fgf10 (Peprotech), 10mM nicotinamide (Sigma-Aldrich), 25ng/ml HGF (Peprotech), 5µM A83.01 (Tocris) and 10µM FSK (Tocris). For the first week medium was supplemented with 25ng/ml Noggin (Peprotech), 30% Wnt CM (homemade) and 10µm Y27632 (Sigma-Aldrich). Same media was also used for establishment of all

tumoroid lines. In addition, tumoroids were also seeded in media with decreased concentration of RSPO1 (1%), to prevent growth of contaminating normal organoids originating from non-tumour tissue. For the establishment of the tumour culture, these media were kept the first 2 weeks after isolation then, changed into a classical human complete medium. For the establishment of the temporal cultures, Y27632 was kept until the first split. Medium was changed twice a week. For tumouroids cultures establishment, after 2-3 weeks in culture (depending on the sample) the growing structures were visually inspected and, if required, contaminating healthy organoids were hand-picked to prevent theses from outgrowing the tumouroids structures. Upon attainment of dense culture, passaging was performed by mechanical dissociation into small fragments via trituration with a glass Pasteur pipet, and transferred to fresh matrix. To prepare frozen stocks, organoid cultures were dissociated and mixed with recovery cell culture freezing medium (GIBCO) and frozen following standard procedures. When required, the cultures were thawed using standard thawing procedures and cultured as described above. For the 3-4 days (organoids) or first 2 weeks (tumouroids) after thawing, the culture medium was supplemented with Y-27632 (10μM). Organoid pictures were taken with either a Leica M80 stereoscope and Leica MC170 HD camera or with an inverted microscope Leica DMIL and Leica DFC 450C camera.

7.4.4 CRISPR/Cas9 genome engineering

Guide RNA (gRNA) were designed using the web tool accessible at crispr.mit.edu. Oligonucleotides were ordered from Sigma-Aldrich. Sequence and target region of gRNAs used can be found on Table 7.4. gRNAs were cloned either in pSpCas9(BB)-2A-GFP (PX458, Addgene) or pSpCas9n(BB)-2A-GFP (PX459, Addgene) as previously described(Ran, Hsu, Wright, et al. 2013). Briefly, 100μM of top and bottom strands were annealed and phosphorylated (T4 PNK, NEB) in a 2720 Thermal Cycler (Applied Biosystems) at 37°C for 30 minutes, 95 °C for 5 minutes then ramped down to 25°C for 5°C per minute. For cloning into the plasmid, annealed oligonucleotides were diluted 1:200 in water and incubated with 100ng plasmid, Tango buffer (Thermo fisher), 10mM DTT (Thermo fisher), 10mM ATP (NEB), restriction enzyme BbsI (NEB) and T7 ligase (NEB) at 37°C for 5 minutes followed by 21°C for 5 min for 6 cycles. The product was then treated with PlasmidSafe exonuclease (Epicentre) to digest any

residual linearized DNA. Plasmids were then incubated with 10G competent cells (Lucigen) 30 minutes on ice and heat-shocked 45 seconds at 42°C. Transformed cells were plated on ampicillin selection plates and incubated overnight at 37°C. The next day sample colonies were picked and plasmid DNA isolated using QIAprep spin miniprep (Quigen) kit according to the manufacturer's instructions. Plasmid DNA was sequenced to determine that guide RNA had correctly inserted into the plasmid. When deemed correct, QIAprep spin midiprep kit (Quigen) was used to extract purified DNA for subsequent transfection.

Table 7.4. Primer containing gRNA sequence used for cloning

Gene	gRNA target + PAM	Primer Top	Primer Bottom
RNF43	AGTCCGATGCTGATGTAACCAGG	CACCGAGTCCGATGCTGATGTAACC	AAACGGTTACATCAGCATCGGACTC
ZNRF3	GGACTTGTATGAATATGGCTGGG	CACCGGACTTGTATGAATATGGCT	AAACAGCCATATTCATACAAGTCC
TP53	TGTAACAGTTCCTGCATGGGTCGG	CACCGTGTAACAGTTCCTGCATGGG	AAACCCCATGCAGGAACTGTTACAC

7.4.5 Transfection

Transfection of liver organoids was performed using Lipofectamin 300 reagent (Thermo fisher). List of transfection performed and donor used can be found in Table 7.5. Organoids were expanded for 1 week and then dissociated to single cells after incubated with TrypLE Express for 5 minutes at 37°C. A total of 3 wells per transfection condition were used. Single cells were washed once, resuspended in 450µl of expansion medium supplemented with 25ng/ml Noggin (Peprotech), 30% Wnt CM (homemade) and 10 µM Y27632 (Sigma-Aldrich) and seeded in non-attaching 48 multi-well plate. Transfection mix containing 1.5µl of Lipofectamin, 1µl of P3000 reagent and 5µg of plasmid in Opti-MEM I Reduced Serum Media (Thermo fisher) were added to the cells. Plate was spun at 600g for 1h at 32°C and then incubated 4h at 37°C. After incubation, cells were mixed with BME2 and seeded in a 24 multi-well plate.

After 72 hours, cells were dissociated to single cells as before and resuspended in EM. Single cells were sorted for GFP fluorescence using a MoFlo cell sorter (Dako Colorado, Inc.). GFP positive cells were then seeded at clonal density in BME as described above and monitored for organoid formation. For the first 3 days media was supplemented with Wnt, noggin and ROCKi, before being changed for normal

complete medium. Once organoids were formed, these were hand-picked and clonally expanded for further characterisation.

Table 7.5. List of transfections and donor organoids used

gRNA transfected	Donor organoids used
TP53	Donor 5
RNF43 + ZNRF3	Donor 3
TP53 + RNF43 + ZNRF3	Donor 5

7.4.6 Organoids genotyping

To collect DNA organoids were collected, washed with cold PBS to remove matrigel or BME, disrupted by pipetting and incubated at 60C overnight with DirectPCR (Viagen) lysis buffer containing 1/100 of Proteinase K 800U/ml (NEB). On the following day, samples were spun 5 min at max speed and 1 or 2ul of supernatant containing DNA was used for PCR reaction. DNA was stored at 4C. To screen DNA for mutations, primers spanning the region of interested were designed using the web tool Primer3Plus (http://www.bioinformatics.nl/cgi-bin/primer3plus/primer3plus.cgi). Primers used are listed in Table 7.6. DNA was amplified using GoTaq® G2 DNA Polymerase (Promega) using standard protocol. Amplicons were purified using QIAquick PCR Purification Kit (Quiagen) and sequence was analysed by Sanger sequencing by Beckman Coulter Genomics services. The free web tool TIDE (https://tide.nki.nl/) was used to screen for CRISPR/Cas9 mutations. In case of presence of different mutated alleles, PCR amplicons were cloned using a pGEM®-T Easy Vector Systems (Promega) and transformed into DH5α™ Competent Cells (Thermo fisher). Colonies were hand-picked and incubated for 1h at 37°C in 100ul of lysogeny broth (LB) medium. 2ul of the bacterial cultures were used in a PCR reaction and amplicons were sequenced as previously described.

Table 7.6. List of primers used for organoid genotyping

Gene	Primer FWD	Primer REV
RNF43	AGCTAAGTGCAAAATCCAGGTC	TTACATTTTGAATGACGCTTCC
ZNRF3	GATCACCATCACTTACAAGG	CATGTCTCTTGGAGGTTACT
TP53	AGGAAATTTGCGTGTGGAGTAT	CACAGGTTAAGAGGTCCCAAAG

7.4.7 Organoid formation efficiency and drug resistance

For organoid formation efficiency quantification, organoid cultures were dissociated to single cells after incubation with TrypLE Express (Thermo fisher) for 5min at 37C. Cell were counted using counting chambers and a total of 1000 or 500 cells were seeded per well. A total of 3 wells per condition were used. For the first three days, medium was supplemented with 25ng/ml Noggin (Peprotech), 30% Wnt CM (homemade) and 10 µm Y27632 (Sigma-Aldrich), then changed to normal expansion medium. Medium was changed every three day and organoid number was counted using optical microscopy 1-2 week after seeding. For drug resistance experiment, medium was supplemented with either 5µm Nutiln3 (Cayman chemical), 3µm IWP2 (Tocris) or 5µm Gefitinib. Control cells were treated with DMSO (Sigma-Aldrich) only.

8. REFERENCES

Akhurst, B, E J Croager, C A Farley-Roche, J K Ong, M L Dumble, B Knight, and G C Yeoh. 2001. “A Modified Choline-Deficient, Ethionine-Supplemented Diet Protocol Effectively Induces Oval Cells in Mouse Liver.” *Hepatology* 34 (3):519–22. https://doi.org/10.1053/jhep.2001.26751.

Arendt, Bianca M., Elena M. Comelli, David W.L. Ma, Wendy Lou, Anastasia Teterina, TaeHyung Kim, Scott K. Fung, et al. 2015. “Altered Hepatic Gene Expression in Nonalcoholic Fatty Liver Disease Is Associated with Lower Hepatic N-3 and N-6 Polyunsaturated Fatty Acids.” *Hepatology* 61 (5):1565–78. https://doi.org/10.1002/hep.27695.

Barker, Nick, Johan H. van Es, Jeroen Kuipers, Pekka Kujala, Maaike van den Born, Miranda Cozijnsen, Andrea Haegebarth, et al. 2007. “Identification of Stem Cells in Small Intestine and Colon by Marker Gene Lgr5.” *Nature* 449 (7165):1003–7. https://doi.org/10.1038/nature06196.

Barker, Nick, Meritxell Huch, Pekka Kujala, Marc van de Wetering, Hugo J Snippert, Johan H van Es, Toshiro Sato, et al. 2010. “Lgr5(+ve) Stem Cells Drive Self-Renewal in the Stomach and Build Long-Lived Gastric Units in Vitro.” *Cell Stem Cell* 6 (1):25–36. https://doi.org/10.1016/j.stem.2009.11.013.

Bartfeld, Sina, Tülay Bayram, Marc van de Wetering, Meritxell Huch, Harry Begthel, Pekka Kujala, Robert Vries, Peter J Peters, and Hans Clevers. 2014. “In Vitro Expansion of Human Gastric Epithelial Stem Cells and Their Responses to Bacterial Infection.” *Gastroenterology* 148 (1):126–136.e6. https://doi.org/10.1053/j.gastro.2014.09.042.

Beer, Shelly, Kimberly Komatsubara, David I. Bellovin, Masashi Kurobe, Karl Sylvester, and Dean W. Felsher. 2008. “Hepatotoxin-Induced Changes in the Adult Murine Liver Promote MYC-Induced Tumorigenesis.” Edited by Juha Klefstrom. *PLoS ONE* 3 (6). Public Library of Science:e2493. https://doi.org/10.1371/journal.pone.0002493.

Bellentani, Stefano. 2017. “The Epidemiology of Non-Alcoholic Fatty Liver Disease.” *Liver International*. https://doi.org/10.1111/liv.13299.

Benhamouche, Samira, Thomas Decaens, Cécile Godard, Régine Chambrey, David S Rickman, Christophe Moinard, Mireille Vasseur-Cognet, et al. 2006. “Apc Tumor Suppressor Gene Is the "zonation-Keeper" of Mouse Liver.” *Developmental Cell* 10 (6):759–70. https://doi.org/10.1016/j.devcel.2006.03.015.

Best, Jan, Clemens Schotten, Jens M Theysohn, Axel Wetter, Stefan Müller, Sonia Radünz, Maren Schulze, Ali Canbay, Alexander Dechêne, and Guido Gerken. 2016. “Novel Implications in the Treatment of Hepatocellular Carcinoma.” *Annals of Gastroenterology* 30 (1):23–32. https://doi.org/10.20524/aog.2016.0092.

Birchmeier, Walter. 2016. “Orchestrating Wnt Signalling for Metabolic Liver Zonation.” *Nature Cell Biology* 18 (5). Nature Research:463–65. https://doi.org/10.1038/ncb3349.

Bitler, Benjamin G, Katherine M Aird, Azat Garipov, Hua Li, Michael Amatangelo, Andrew V Kossenkov, David C Schultz, et al. 2015. “Synthetic Lethality by Targeting EZH2 Methyltransferase Activity in ARID1A-Mutated Cancers.” *Nature Medicine* 21 (3). Nature Research:231. https://doi.org/10.1038/nm.3799.

Blokzijl, Francis, Joep de Ligt, Myrthe Jager, Valentina Sasselli, Sophie Roerink, Nobuo Sasaki, Meritxell Huch, et al. 2016. “Tissue-Specific Mutation Accumulation in Human Adult Stem Cells during Life.” *Nature* 538 (7624). Nature Research:260–64. https://doi.org/10.1038/nature19768.

Boj, Sylvia F., Chang-Il Hwang, Lindsey A. Baker, Iok In Christine Chio, Dannielle D. Engle, Vincenzo Corbo, Myrthe Jager, et al. 2014. “Organoid Models of Human and Mouse Ductal Pancreatic Cancer.” *Cell*, December. https://doi.org/10.1016/j.cell.2014.12.021.

Boj, Sylvia F, Johan H van Es, Meritxell Huch, Vivian S W Li, Anabel José, Pantelis Hatzis, Michal Mokry, et al. 2012. “Diabetes Risk Gene and Wnt Effector Tcf7l2/TCF4 Controls Hepatic Response to Perinatal and Adult Metabolic Demand.” *Cell* 151 (7). Elsevier:1595–1607. https://doi.org/10.1016/j.cell.2012.10.053.

Bokhari, Maria, Ross J. Carnachan, Neil R. Cameron, and Stefan A. Przyborski. 2007. “Culture of HepG2 Liver Cells on Three Dimensional Polystyrene Scaffolds Enhances Cell Structure and Function during Toxicological Challenge.” *Journal*

of Anatomy 0 (0). Blackwell Publishing Ltd:070816212604002–??? https://doi.org/10.1111/j.1469-7580.2007.00778.x.

Bosch, F Xavier, Josepa Ribes, Mireia Díaz, and Ramon Cléries. 2004. “Primary Liver Cancer: Worldwide Incidence and Trends.” *Gastroenterology* 127 (5 Suppl 1):S5–16. http://www.ncbi.nlm.nih.gov/pubmed/15508102.

Bruna, Alejandra, Oscar M. Rueda, Wendy Greenwood, Ankita Sati Batra, Maurizio Callari, Rajbir Nath Batra, Katherine Pogrebniak, et al. 2016. “A Biobank of Breast Cancer Explants with Preserved Intra-Tumor Heterogeneity to Screen Anticancer Compounds.” *Cell* 167 (1):260–274.e22. https://doi.org/10.1016/j.cell.2016.08.041.

Bucher, Nancy L. R., and Ronald A. Malt. 1971. *Regeneration of Liver and Kidney*. Little, Brown.

Cajuso, Tatiana, Ulrika A Hänninen, Johanna Kondelin, Alexandra E Gylfe, Tomas Tanskanen, Riku Katainen, Esa Pitkänen, et al. 2014. “Exome Sequencing Reveals Frequent Inactivating Mutations in ARID1A, ARID1B, ARID2 and ARID4A in Microsatellite Unstable Colorectal Cancer.” *International Journal of Cancer. Journal International Du Cancer* 135 (3):611–23. https://doi.org/10.1002/ijc.28705.

Cavalloni, Giuliana, Caterina Peraldo-Neia, Chiara Varamo, Laura Casorzo, Carmine Dell’Aglio, Paola Bernabei, Giovanna Chiorino, Massimo Aglietta, and Francesco Leone. 2016. “Establishment and Characterization of a Human Intrahepatic Cholangiocarcinoma Cell Line Derived from an Italian Patient.” *Tumor Biology* 37 (3):4041–52. https://doi.org/10.1007/s13277-015-4215-3.

Chua, Christelle En Lin, Shu Ning Chan, and Bor Luen Tang. 2014. “Non-Cell Autonomous or Secretory Tumor Suppression.” *Journal of Cellular Physiology* 229 (10):1346–52. https://doi.org/10.1002/jcp.24574.

Clevers, Hans, and Roel Nusse. 2012. “Wnt/β-Catenin Signaling and Disease.” *Cell* 149 (6):1192–1205. https://doi.org/10.1016/j.cell.2012.05.012.

Colnot, S., T. Decaens, M. Niwa-Kawakita, C. Godard, G. Hamard, A. Kahn, M. Giovannini, and C. Perret. 2004. “Liver-Targeted Disruption of Apc in Mice

Activates -Catenin Signaling and Leads to Hepatocellular Carcinomas." *Proceedings of the National Academy of Sciences* 101 (49):17216–21. https://doi.org/10.1073/pnas.0404761101.

Confer, David B., and Richard J. Stenger. 1966. "Nodules in the Livers of C3H Mice after Long-Term Carbon Tetrachloride Administration: A Light and Electron Microscopic Study." *Cancer Research* 26 (5).

Cruciat, Cristina-Maria, and Christof Niehrs. 2013. "Secreted and Transmembrane Wnt Inhibitors and Activators." *Cold Spring Harbor Perspectives in Biology* 5 (3). Cold Spring Harbor Laboratory Press:a015081. https://doi.org/10.1101/cshperspect.a015081.

Delire, Bénédicte, Peter Stärkel, and Isabelle Leclercq. 2015. "Animal Models for Fibrotic Liver Diseases: What We Have, What We Need, and What Is under Development." *Journal of Clinical and Translational Hepatology* 3 (1). Xia & He Publishing Inc. (USA):53–66. https://doi.org/10.14218/JCTH.2014.00035.

Dong, Bingning, Ju-Seog Lee, Yun-Yong Park, Feng Yang, Ganyu Xu, Wendong Huang, Milton J. Finegold, and David D. Moore. 2015. "Activating CAR and β-Catenin Induces Uncontrolled Liver Growth and Tumorigenesis." *Nature Communications* 6 (February):5944. https://doi.org/10.1038/ncomms6944.

Drost, Jarno, Richard H. van Jaarsveld, Bas Ponsioen, Cheryl Zimberlin, Ruben van Boxtel, Arjan Buijs, Norman Sachs, et al. 2015. "Sequential Cancer Mutations in Cultured Human Intestinal Stem Cells." *Nature* 521 (7550):43–47. https://doi.org/10.1038/nature14415.

Dumble, M L, B Knight, E A Quail, and G C Yeoh. 2001. "Hepatoblast-like Cells Populate the Adult p53 Knockout Mouse Liver: Evidence for a Hyperproliferative Maturation-Arrested Stem Cell Compartment." *Cell Growth & Differentiation : The Molecular Biology Journal of the American Association for Cancer Research* 12 (5):223–31. http://www.ncbi.nlm.nih.gov/pubmed/11373269.

Duncan, Andrew W., Craig Dorrell, and Markus Grompe. 2009. "Stem Cells and Liver Regeneration." *Gastroenterology* 137 (2):466–81. https://doi.org/10.1053/j.gastro.2009.05.044.

El-Serag, Hashem B, and K Lenhard Rudolph. 2007. “Hepatocellular Carcinoma: Epidemiology and Molecular Carcinogenesis.” *Gastroenterology* 132 (7):2557–76. https://doi.org/10.1053/j.gastro.2007.04.061.

Fan, Biao, Yann Malato, Diego F Calvisi, Syed Naqvi, Nataliya Razumilava, Silvia Ribback, Gregory J Gores, et al. 2012. “Cholangiocarcinomas Can Originate from Hepatocytes in Mice.” *The Journal of Clinical Investigation*. https://doi.org/10.1172/JCI63212.

Fausto, Nelson, and Jean S. Campbell. 2003. “The Role of Hepatocytes and Oval Cells in Liver Regeneration and Repopulation.” *Mechanisms of Development* 120 (1):117–30. https://doi.org/10.1016/S0925-4773(02)00338-6.

Fickert, Peter, Ulrike Stöger, Andrea Fuchsbichler, Tarek Moustafa, Hanns-Ulrich Marschall, Andreas H Weiglein, Oleksiy Tsybrovskyy, et al. 2007. “A New Xenobiotic-Induced Mouse Model of Sclerosing Cholangitis and Biliary Fibrosis.” *The American Journal of Pathology* 171 (2). American Society for Investigative Pathology:525–36. https://doi.org/10.2353/ajpath.2007.061133.

Font-Burgada, Joan, Shabnam Shalapour, Suvasini Ramaswamy, Brian Hsueh, David Rossell, Atsushi Umemura, Koji Taniguchi, et al. 2015. “Hybrid Periportal Hepatocytes Regenerate the Injured Liver without Giving Rise to Cancer.” *Cell* 162 (4):766–79. https://doi.org/10.1016/j.cell.2015.07.026.

Fujimoto, Akihiro, Yasushi Totoki, Tetsuo Abe, Keith A Boroevich, Fumie Hosoda, Ha Hai Nguyen, Masayuki Aoki, et al. 2012. “Whole-Genome Sequencing of Liver Cancers Identifies Etiological Influences on Mutation Patterns and Recurrent Mutations in Chromatin Regulators.” *Nature Genetics* 44 (7):760–64. https://doi.org/10.1038/ng.2291.

Furukawa, Toru, Yuko Kuboki, Etsuko Tanji, Shoko Yoshida, Takashi Hatori, Masakazu Yamamoto, Noriyuki Shibata, Kyoko Shimizu, Naoyuki Kamatani, and Keiko Shiratori. 2011. “Whole-Exome Sequencing Uncovers Frequent GNAS Mutations in Intraductal Papillary Mucinous Neoplasms of the Pancreas.” *Scientific Reports* 1 (January):161. https://doi.org/10.1038/srep00161.

Gao, Dong, Ian Vela, Andrea Sboner, Phillip J. Iaquinta, Wouter R. Karthaus, Anuradha Gopalan, Catherine Dowling, et al. 2014. “Organoid Cultures Derived

from Patients with Advanced Prostate Cancer." *Cell* 159 (1):176–87. https://doi.org/10.1016/j.cell.2014.08.016.

Gebhardt, Rolf. 2014. "Liver Zonation: Novel Aspects of Its Regulation and Its Impact on Homeostasis." *World Journal of Gastroenterology* 20 (26):8491. https://doi.org/10.3748/wjg.v20.i26.8491.

Gehart, Helmuth, and Hans Clevers. 2015. "Repairing Organs: Lessons from Intestine and Liver." *Trends in Genetics* 31 (6):344–51. https://doi.org/10.1016/j.tig.2015.04.005.

Giannakis, Marios, Eran Hodis, Xinmeng Jasmine Mu, Mai Yamauchi, Joseph Rosenbluh, Kristian Cibulskis, Gordon Saksena, et al. 2014. "RNF43 Is Frequently Mutated in Colorectal and Endometrial Cancers." *Nature Genetics* 46 (12):1264–66. https://doi.org/10.1038/ng.3127.

Gu, Qingyang, Bin Zhang, Hongye Sun, Qiang Xu, Yexiong Tan, Guan Wang, Qin Luo, et al. 2015. "Genomic Characterization of a Large Panel of Patient-Derived Hepatocellular Carcinoma Xenograft Tumor Models for Preclinical Development." *Oncotarget* 6 (24). Impact Journals:20160–76. https://doi.org/10.18632/oncotarget.3969.

Guglielmi, Alfredo, Andrea Ruzzenente, Tommaso Campagnaro, Silvia Pachera, Alessandro Valdegamberi, Paola Nicoli, Alessandro Cappellani, Giulio Malfermoni, and Calogero Iacono. 2009. "Intrahepatic Cholangiocarcinoma: Prognostic Factors after Surgical Resection." *World Journal of Surgery* 33 (6):1247–54. https://doi.org/10.1007/s00268-009-9970-0.

Guichard, Cécile, Giuliana Amaddeo, Sandrine Imbeaud, Yannick Ladeiro, Laura Pelletier, Ichrafe Ben Maad, Julien Calderaro, et al. 2012. "Integrated Analysis of Somatic Mutations and Focal Copy-Number Changes Identifies Key Genes and Pathways in Hepatocellular Carcinoma." *Nature Genetics* 44 (6):694–98. https://doi.org/10.1038/ng.2256.

Hao, Huai-Xiang, Yang Xie, Yue Zhang, Olga Charlat, Emma Oster, Monika Avello, Hong Lei, et al. 2012. "ZNRF3 Promotes Wnt Receptor Turnover in an R-Spondin-Sensitive Manner." *Nature* 485 (7397):195–200. https://doi.org/10.1038/nature11019.

Hardcastle, I.R. 2007. “Inhibitors of the MDM2-p53 Interaction as Anticancer Drugs.” Drugs of the Future. 2007. https://doi.org/10.1358/dof.2007.032.10.1131965.

He, Li, De-An Tian, Pei-Yuan Li, Xing-Xing He, Li He, De-An Tian, Pei-Yuan Li, and Xing-Xing He. 2015. “Mouse Models of Liver Cancer: Progress and Recommendations.” *Oncotarget* 6 (27). Impact Journals:23306–22. https://doi.org/10.18632/oncotarget.4202.

Heindryckx, Femke, Isabelle Colle, and Hans Van Vlierberghe. 2009. “Experimental Mouse Models for Hepatocellular Carcinoma Research.” *International Journal of Experimental Pathology* 90 (4):367–86. https://doi.org/10.1111/j.1365-2613.2009.00656.x.

Helming, Katherine C, Xiaofeng Wang, and Charles W M Roberts. 2014. “Vulnerabilities of Mutant SWI/SNF Complexes in Cancer.” *Cancer Cell* 26 (3):309–17. https://doi.org/10.1016/j.ccr.2014.07.018.

Helming, Katherine C, Xiaofeng Wang, Boris G Wilson, Francisca Vazquez, Jeffrey R Haswell, Haley E Manchester, Youngha Kim, et al. 2014. “ARID1B Is a Specific Vulnerability in ARID1A-Mutant Cancers.” *Nature Medicine* 20 (3):251–54. https://doi.org/10.1038/nm.3480.

Hidalgo, Manuel, Frederic Amant, Andrew V. Biankin, Eva Budinská, Annette T. Byrne, Carlos Caldas, Robert B. Clarke, et al. 2014. “Patient-Derived Xenograft Models: An Emerging Platform for Translational Cancer Research.” *Cancer Discovery*. http://cancerdiscovery.aacrjournals.org/content/early/2014/07/15/2159-8290.CD-14-0001.

Hindley, Christopher J, Lucía Cordero-Espinoza, and Meritxell Huch. 2016. “Organoids from Adult Liver and Pancreas: Stem Cell Biology and Biomedical Utility.” https://doi.org/10.1016/j.ydbio.2016.06.039.

Hindley, Christopher J, Gianmarco Mastrogiovanni, and Meritxell Huch. 2014. “The Plastic Liver: Differentiated Cells, Stem Cells, Every Cell?” *The Journal of Clinical Investigation* 124 (12):5099–5102. https://doi.org/10.1172/JCI78372.

Horie, Yasuo, Akira Suzuki, Ei Kataoka, Takehiko Sasaki, Koichi Hamada, Junko

Sasaki, Katsunori Mizuno, et al. 2004. “Hepatocyte-Specific Pten Deficiency Results in Steatohepatitis and Hepatocellular Carcinomas.” *Journal of Clinical Investigation* 113 (12):1774–83. https://doi.org/10.1172/JCI200420513.

Huch, Meritxell, Paola Bonfanti, Sylvia F Boj, Toshiro Sato, Cindy J M Loomans, Marc van de Wetering, Mozhdeh Sojoodi, et al. 2013. “Unlimited in Vitro Expansion of Adult Bi-Potent Pancreas Progenitors through the Lgr5/R-Spondin Axis.” *The EMBO Journal* 32 (20):2708–21. https://doi.org/10.1038/emboj.2013.204.

Huch, Meritxell, Craig Dorrell, Sylvia F Boj, Johan H van Es, Vivian S W Li, Marc van de Wetering, Toshiro Sato, et al. 2013. “In Vitro Expansion of Single Lgr5+ Liver Stem Cells Induced by Wnt-Driven Regeneration.” *Nature* 494 (7436):247–50. https://doi.org/10.1038/nature11826.

Huch, Meritxell, Helmuth Gehart, Ruben van Boxtel, Karien Hamer, Francis Blokzijl, Monique M.A. Verstegen, Ewa Ellis, et al. 2014. “Long-Term Culture of Genome-Stable Bipotent Stem Cells from Adult Human Liver.” *Cell*, December. https://doi.org/10.1016/j.cell.2014.11.050.

Huch, Meritxell, and Bon-Kyoung Koo. 2015. “Modeling Mouse and Human Development Using Organoid Cultures.” *Development (Cambridge, England)* 142 (18):3113–25. https://doi.org/10.1242/dev.118570.

Jaks, Viljar, Nick Barker, Maria Kasper, Johan H van Es, Hugo J Snippert, Hans Clevers, and Rune Toftgård. 2008. “Lgr5 Marks Cycling, yet Long-Lived, Hair Follicle Stem Cells.” *Nature Genetics* 40 (11):1291–99. https://doi.org/10.1038/ng.239.

Jiao, Yuchen, Timothy M Pawlik, Robert A Anders, Florin M Selaru, Mirte M Streppel, Donald J Lucas, Noushin Niknafs, et al. 2013. “Exome Sequencing Identifies Frequent Inactivating Mutations in BAP1, ARID1A and PBRM1 in Intrahepatic Cholangiocarcinomas.” *Nature Genetics* 45 (12):1470–73. https://doi.org/10.1038/ng.2813.

Jones, Siân, Tian-Li Wang, Ie-Ming Shih, Tsui-Lien Mao, Kentaro Nakayama, Richard Roden, Ruth Glas, et al. 2010. “Frequent Mutations of Chromatin Remodeling Gene ARID1A in Ovarian Clear Cell Carcinoma.” *Science (New*

York, N.Y.) 330 (6001):228–31. https://doi.org/10.1126/science.1196333.

Juhlin, C Christofer, Gerald Goh, James M Healy, Annabelle L Fonseca, Ute I Scholl, Adam Stenman, John W Kunstman, et al. 2014. “Whole-Exome Sequencing Characterizes the Landscape of Somatic Mutations and Copy Number Alterations in Adrenocortical Carcinoma.” *The Journal of Clinical Endocrinology and Metabolism*, December, jc20143282. https://doi.org/10.1210/jc.2014-3282.

Jusakul, Apinya, Sarinya Kongpetch, and Bin Tean Teh. 2015. “Genetics of Opisthorchis Viverrini-Related Cholangiocarcinoma.” *Current Opinion in Gastroenterology* 31 (3):258–63. https://doi.org/10.1097/MOG.0000000000000162.

Khan, Shahid A, Howard C Thomas, Brian R Davidson, and Simon D Taylor-Robinson. 2005. “Cholangiocarcinoma.” *Lancet* 366 (9493):1303–14. https://doi.org/10.1016/S0140-6736(05)67530-7.

Kim, Chang-Min, Kazuhiko Koike, Izumu Saito, Tatsuo Miyamura, and Gilbert Jay. 1991. “HBx Gene of Hepatitis B Virus Induces Liver Cancer in Transgenic Mice.” *Nature* 351 (6324). Nature Publishing Group:317–20. https://doi.org/10.1038/351317a0.

Koo, Bon-Kyoung, Johan H van Es, Maaike van den Born, and Hans Clevers. 2015. “Porcupine Inhibitor Suppresses Paracrine Wnt-Driven Growth of Rnf43;Znrf3-Mutant Neoplasia.” *Proceedings of the National Academy of Sciences of the United States of America* 112 (24):7548–50. https://doi.org/10.1073/pnas.1508113112.

Koo, Bon-Kyoung, Maureen Spit, Ingrid Jordens, Teck Y Low, Daniel E Stange, Marc van de Wetering, Johan H van Es, et al. 2012. “Tumour Suppressor RNF43 Is a Stem-Cell E3 Ligase That Induces Endocytosis of Wnt Receptors.” *Nature* 488 (7413). Nature Publishing Group:665–69. https://doi.org/10.1038/nature11308.

Kopp, Janel L, Claire L Dubois, Ashleigh E Schaffer, Ergeng Hao, Hung Ping Shih, Philip A Seymour, Jenny Ma, and Maike Sander. 2011. “Sox9+ Ductal Cells Are Multipotent Progenitors throughout Development but Do Not Produce New Endocrine Cells in the Normal or Injured Adult Pancreas.” *Development* 138 (4). Oxford University Press for The Company of Biologists Limited:653–65.

https://doi.org/10.1242/dev.056499.

Kordes, Claus, Iris Sawitza, Silke Götze, Diran Herebian, and Dieter Häussinger. 2014. “Hepatic Stellate Cells Contribute to Progenitor Cells and Liver Regeneration.” *Journal of Clinical Investigation* 124 (12):5503–15. https://doi.org/10.1172/JCI74119.

Kruitwagen, Hedwig S, Loes A Oosterhoff, Ingrid G W H Vernooij, Ingrid M Schrall, Monique E van Wolferen, Farah Bannink, Camille Roesch, et al. 2017. “Long-Term Adult Feline Liver Organoid Cultures for Disease Modeling of Hepatic Steatosis.” *Stem Cell Reports* 8 (4). Elsevier:822–30. https://doi.org/10.1016/j.stemcr.2017.02.015.

Ku, J-L, K-A Yoon, I-J Kim, W-H Kim, J-Y Jang, K-S Suh, S-W Kim, et al. 2002. “Establishment and Characterisation of Six Human Biliary Tract Cancer Cell Lines.” *British Journal of Cancer* 87 (2):187–93. https://doi.org/10.1038/sj.bjc.6600440.

Kudo, M. 2013. “Early Hepatocellular Carcinoma: Definition and Diagnosis.” *Liver Cancer* 2 (2). Karger Publishers:69–72. https://doi.org/10.1159/000343842.

Kurinna, Svitlana, Sabrina A Stratton, Zeynep Coban, Jill M Schumacher, Markus Grompe, Andrew W Duncan, and Michelle Craig Barton. 2013. “p53 Regulates a Mitotic Transcription Program and Determines Ploidy in Normal Mouse Liver.” *Hepatology (Baltimore, Md.)* 57 (5):2004–13. https://doi.org/10.1002/hep.26233.

Lau, Wim de, Weng Chuan Peng, Piet Gros, and Hans Clevers. 2014. “The R-spondin/Lgr5/Rnf43 Module: Regulator of Wnt Signal Strength.” *Genes & Development* 28 (4). Cold Spring Harbor Laboratory Press:305–16. https://doi.org/10.1101/gad.235473.113.

Li, Xingnan, Lincoln Nadauld, Akifumi Ootani, David C Corney, Reetesh K Pai, Olivier Gevaert, Michael A Cantrell, et al. 2014. “Oncogenic Transformation of Diverse Gastrointestinal Tissues in Primary Organoid Culture.” *Nature Medicine* 20 (7):769–77. https://doi.org/10.1038/nm.3585.

Lin, Zhiwu, and Yvonne Will. 2012. “Evaluation of Drugs with Specific Organ Toxicities in Organ-Specific Cell Lines.” *Toxicological Sciences : An Official*

Journal of the Society of Toxicology 126 (1). Oxford University Press:114–27. https://doi.org/10.1093/toxsci/kfr339.

Liu, L., Y. Cao, C. Chen, X. Zhang, A. McNabola, D. Wilkie, S. Wilhelm, M. Lynch, and C. Carter. 2006. “Sorafenib Blocks the RAF/MEK/ERK Pathway, Inhibits Tumor Angiogenesis, and Induces Tumor Cell Apoptosis in Hepatocellular Carcinoma Model PLC/PRF/5.” *Cancer Research* 66 (24):11851–58. https://doi.org/10.1158/0008-5472.CAN-06-1377.

Llovet, Josep M., Sergio Ricci, Vincenzo Mazzaferro, Philip Hilgard, Edward Gane, Jean-Frédéric Blanc, Andre Cosme de Oliveira, et al. 2008. “Sorafenib in Advanced Hepatocellular Carcinoma.” *New England Journal of Medicine* 359 (4):378–90. https://doi.org/10.1056/NEJMoa0708857.

Lonardo, Amedeo, Fabio Nascimbeni, Mauro Maurantonio, Alessandra Marrazzo, Luca Rinaldi, and Luigi Elio Adinolfi. 2017. “Nonalcoholic Fatty Liver Disease: Evolving Paradigms.” *World Journal of Gastroenterology* 23 (36):6571–92. https://doi.org/10.3748/wjg.v23.i36.6571.

Lu, Wei-Yu, Thomas G. Bird, Luke Boulter, Atsunori Tsuchiya, Alicia M. Cole, Trevor Hay, Rachel V. Guest, et al. 2015. “Hepatic Progenitor Cells of Biliary Origin with Liver Repopulation Capacity.” *Nature Cell Biology* 17 (8). Nature Research:971–83. https://doi.org/10.1038/ncb3203.

Lujambio, Amaia, Leila Akkari, Janelle Simon, Danielle Grace, Darjus F Tschaharganeh, Jessica E Bolden, Zhen Zhao, et al. 2013. “Non-Cell-Autonomous Tumor Suppression by p53.” *Cell* 153 (2):449–60. https://doi.org/10.1016/j.cell.2013.03.020.

Lukacs-Kornek, Veronika, and Frank Lammert. 2017. “The Progenitor Cell Dilemma: Cellular and Functional Heterogeneity in Assistance or Escalation of Liver Injury.” https://doi.org/10.1016/j.jhep.2016.10.033.

Marquardt, Jens U., Jesper B. Andersen, and Snorri S. Thorgeirsson. 2015. “Functional and Genetic Deconstruction of the Cellular Origin in Liver Cancer.” *Nature Reviews Cancer* 15 (11). Nature Research:653–67. https://doi.org/10.1038/nrc4017.

Masuzaki, Ryota, Seth J Karp, and Masao Omata. 2016. “NAFLD as a Risk Factor for HCC: New Rules of Engagement?” *Hepatology International* 10 (4). Springer:533–34. https://doi.org/10.1007/s12072-016-9731-8.

Matano, Mami, Shoichi Date, Mariko Shimokawa, Ai Takano, Masayuki Fujii, Yuki Ohta, Toshiaki Watanabe, Takanori Kanai, and Toshiro Sato. 2015. “Modeling Colorectal Cancer Using CRISPR-Cas9–mediated Engineering of Human Intestinal Organoids.” *Nature Medicine* 21 (3):256–62. https://doi.org/10.1038/nm.3802.

Maximin, Suresh, Dhakshina Moorthy Ganeshan, Alampady K Shanbhogue, Manjiri K Dighe, Matthew M Yeh, Orpheus Kolokythas, Puneet Bhargava, and Neeraj Lalwani. 2014. “Current Update on Combined Hepatocellular-Cholangiocarcinoma.” *European Journal of Radiology Open* 1:40–48. https://doi.org/10.1016/j.ejro.2014.07.001.

Mederacke, Ingmar, Christine C. Hsu, Juliane S. Troeger, Peter Huebener, Xueru Mu, Dianne H. Dapito, Jean-Philippe Pradere, and Robert F. Schwabe. 2013. “Fate Tracing Reveals Hepatic Stellate Cells as Dominant Contributors to Liver Fibrosis Independent of Its Aetiology.” *Nature Communications* 4 (November):2823. https://doi.org/10.1038/ncomms3823.

Meng, Xuan, Derek A Franklin, Jiahong Dong, and Yanping Zhang. 2014. “MDM2-p53 Pathway in Hepatocellular Carcinoma.” *Cancer Research* 74 (24):7161–67. https://doi.org/10.1158/0008-5472.CAN-14-1446.

Michalopoulos, G K, and M C DeFrances. 1997. “Liver Regeneration.” *Science (New York, N.Y.)* 276 (5309):60–66. http://www.ncbi.nlm.nih.gov/pubmed/9082986.

Moeini, Agrin, Daniela Sia, Zhongyang Zhang, Genis Camprecios, Ashley Stueck, Hui Dong, Robert Montal, et al. 2017. “Mixed Hepatocellular-Cholangiocarcinoma Tumors: Cholangiolocellular Carcinoma Is a Distinct Molecular Entity.” *Journal of Hepatology*, January. https://doi.org/10.1016/j.jhep.2017.01.010.

Mueller, Daniel, Anika Koetemann, and Fozia Noor. 2011. “Organotypic Cultures of Hepg2 Cells for In Vitro Toxicity Studies.” *Journal of Bioengineering and Biomedical Sciences* 1 (S2). OMICS International. https://doi.org/10.4172/2155-

9538.S2-002.

Nantasanti, Sathidpak, Mathilda J. M. Toussaint, Sameh A. Youssef, Peter C. J. Tooten, Alain de Bruin, and CA Reed. 2016. “Rb and p53 Liver Functions Are Essential for Xenobiotic Metabolism and Tumor Suppression.” Edited by Matias A Avila. *PLOS ONE* 11 (3). CRC press:e0150064. https://doi.org/10.1371/journal.pone.0150064.

Nault, Jean-Charles, and Jessica Zucman-Rossi. 2016. “TERT Promoter Mutations in Primary Liver Tumors.” *Clinics and Research in Hepatology and Gastroenterology* 40 (1):9–14. https://doi.org/10.1016/j.clinre.2015.07.006.

Nault, Jean–Charles, Paulette Bioulac–Sage, and Jessica Zucman–Rossi. 2013. “Hepatocellular Benign Tumors—From Molecular Classification to Personalized Clinical Care.” *Gastroenterology* 144 (5):888–902. https://doi.org/10.1053/j.gastro.2013.02.032.

Ong, Choon Kiat, Chutima Subimerb, Chawalit Pairojkul, Sopit Wongkham, Ioana Cutcutache, Willie Yu, John R McPherson, et al. 2012. “Exome Sequencing of Liver Fluke-Associated Cholangiocarcinoma.” *Nature Genetics* 44 (6):690–93. https://doi.org/10.1038/ng.2273.

Park, Young Nyun, and Massimo Roncalli. n.d. “Large Liver Cell Dysplasia: A Controversial Entity.” Accessed May 16, 2017. https://doi.org/10.1016/j.jhep.2006.08.002.

Pinter, Matthias, Michael Trauner, Markus Peck-Radosavljevic, and Wolfgang Sieghart. 2016. “Cancer and Liver Cirrhosis: Implications on Prognosis and Management.” *ESMO Open* 1 (2):e000042. https://doi.org/10.1136/esmoopen-2016-000042.

Piscaglia, Fabio, Gianluca Svegliati-Baroni, Andrea Barchetti, Anna Pecorelli, Sara Marinelli, Claudio Tiribelli, Stefano Bellentani, and HCC-NAFLD Italian Study Group. 2016. “Clinical Patterns of Hepatocellular Carcinoma in Nonalcoholic Fatty Liver Disease: A Multicenter Prospective Study.” *Hepatology* 63 (3):827–38. https://doi.org/10.1002/hep.28368.

Planas-Paz, Lara, Vanessa Orsini, Luke Boulter, Diego Calabrese, Monika Pikiolek,

Florian Nigsch, Yang Xie, et al. 2016. “The RSPO–LGR4/5–ZNRF3/RNF43 Module Controls Liver Zonation and Size.” *Nat Cell Biol* 18 (5). https://doi.org/10.1038/ncb3337.

Platt, Randall J, Sidi Chen, Yang Zhou, Michael J Yim, Lukasz Swiech, Hannah R Kempton, James E Dahlman, et al. 2014. “CRISPR-Cas9 Knockin Mice for Genome Editing and Cancer Modeling.” *Cell* 159 (2). NIH Public Access:440–55. https://doi.org/10.1016/j.cell.2014.09.014.

Preisegger, K H, V M Factor, A Fuchsbichler, C Stumptner, H Denk, and S S Thorgeirsson. 1999. “Atypical Ductular Proliferation and Its Inhibition by Transforming Growth Factor beta1 in the 3,5-Diethoxycarbonyl-1,4-Dihydrocollidine Mouse Model for Chronic Alcoholic Liver Disease.” *Laboratory Investigation; a Journal of Technical Methods and Pathology* 79 (2):103–9. http://www.ncbi.nlm.nih.gov/pubmed/10068199.

Ran, F Ann, Patrick D Hsu, Chie-Yu Lin, Jonathan S Gootenberg, Silvana Konermann, Alexandro E Trevino, David A Scott, et al. 2013. “Double Nicking by RNA-Guided CRISPR Cas9 for Enhanced Genome Editing Specificity.” *Cell* 154 (6). Elsevier:1380–89. https://doi.org/10.1016/j.cell.2013.08.021.

Ran, F Ann, Patrick D Hsu, Jason Wright, Vineeta Agarwala, David A Scott, and Feng Zhang. 2013. “Genome Engineering Using the CRISPR-Cas9 System.” *Nature Protocols* 8 (11):2281–2308. https://doi.org/10.1038/nprot.2013.143.

Reiberger, Thomas, Yunching Chen, Rakesh R Ramjiawan, Tai Hato, Christopher Fan, Rekha Samuel, Sylvie Roberge, et al. 2015. “An Orthotopic Mouse Model of Hepatocellular Carcinoma with Underlying Liver Cirrhosis.” *Nature Protocols* 10 (8). Nature Research:1264–74. https://doi.org/10.1038/nprot.2015.080.

Reisman, D, S Glaros, and E A Thompson. 2009. “The SWI/SNF Complex and Cancer.” *Oncogene* 28 (14):1653–68. https://doi.org/10.1038/onc.2009.4.

Saha, Supriya K., Christine A. Parachoniak, Krishna S. Ghanta, Julien Fitamant, Kenneth N. Ross, Mortada S. Najem, Sushma Gurumurthy, et al. 2014. “Mutant IDH Inhibits HNF-4α to Block Hepatocyte Differentiation and Promote Biliary Cancer.” *Nature* 513 (7516). Nature Research:110–14. https://doi.org/10.1038/nature13441.

Sansom, Owen J, Karen R Reed, Anthony J Hayes, Heather Ireland, Hannah Brinkmann, Ian P Newton, Eduard Batlle, et al. 2004. “Loss of Apc in Vivo Immediately Perturbs Wnt Signaling, Differentiation, and Migration.” *Genes & Development* 18 (12):1385–90. https://doi.org/10.1101/gad.287404.

Sato, Toshiro, Daniel E. Stange, Marc Ferrante, Robert G.J. Vries, Johan H. van Es, Stieneke van den Brink, Winan J. van Houdt, et al. 2011. “Long-Term Expansion of Epithelial Organoids From Human Colon, Adenoma, Adenocarcinoma, and Barrett’s Epithelium.” *Gastroenterology* 141 (5):1762–72. https://doi.org/10.1053/j.gastro.2011.07.050.

Sato, Toshiro, Robert G Vries, Hugo J Snippert, Marc van de Wetering, Nick Barker, Daniel E Stange, Johan H van Es, et al. 2009. “Single Lgr5 Stem Cells Build Crypt-Villus Structures in Vitro without a Mesenchymal Niche.” *Nature* 459 (7244):262–65. https://doi.org/10.1038/nature07935.

Schug, Thaddeus T. 2009. “Awakening p53 in Senescent Cells Using Nutlin-3.” *Aging* 1 (10):842–44. http://www.pubmedcentral.nih.gov/articlerender.fcgi?artid=2815727&tool=pmcentrez&rendertype=abstract.

Schuler, Michael, Andrée Dierich, Pierre Chambon, and Daniel Metzger. 2004. “Efficient Temporally Controlled Targeted Somatic Mutagenesis in Hepatocytes of the Mouse.” *Genesis (New York, N.Y. : 2000)* 39 (3):167–72. https://doi.org/10.1002/gene.20039.

Schulze, Kornelius, Sandrine Imbeaud, Eric Letouzé, Ludmil B Alexandrov, Julien Calderaro, Sandra Rebouissou, Gabrielle Couchy, et al. 2015. “Exome Sequencing of Hepatocellular Carcinomas Identifies New Mutational Signatures and Potential Therapeutic Targets.” *Nature Genetics* 47 (5). Nature Research:505–11. https://doi.org/10.1038/ng.3252.

Schwank, Gerald, Bon-Kyoung Koo, Valentina Sasselli, Johanna F Dekkers, Inha Heo, Turan Demircan, Nobuo Sasaki, et al. 2013. “Functional Repair of CFTR by CRISPR/Cas9 in Intestinal Stem Cell Organoids of Cystic Fibrosis Patients.” *Cell Stem Cell* 13 (6):653–58. https://doi.org/10.1016/j.stem.2013.11.002.

Sekine, Shigeki, Billy Yu-Ang Lan, Melanie Bedolli, Sandy Feng, and Matthias

Hebrok. 2006. “Liver-Specific Loss of β-Catenin Blocks Glutamine Synthesis Pathway Activity and Cytochrome p450 Expression in Mice.” *Hepatology* 43 (4):817–25. https://doi.org/10.1002/hep.21131.

Shaib, Yasser H, Jessica A Davila, Kathryn McGlynn, and Hashem B El-Serag. 2004. “Rising Incidence of Intrahepatic Cholangiocarcinoma in the United States: A True Increase?” *Journal of Hepatology* 40 (3):472–77. https://doi.org/10.1016/j.jhep.2003.11.030.

Sharma, Sreenath V, Daniel A Haber, and Jeff Settleman. 2010. “Cell Line-Based Platforms to Evaluate the Therapeutic Efficacy of Candidate Anticancer Agents.” https://doi.org/10.1038/nrc2820.

Sia, D, V Tovar, A Moeini, and J M Llovet. 2013. “Intrahepatic Cholangiocarcinoma: Pathogenesis and Rationale for Molecular Therapies.” *Oncogene* 32 (41):4861–70. https://doi.org/10.1038/onc.2012.617.

Siegel, Rebecca, Jiemin Ma, Zhaohui Zou, and Ahmedin Jemal. “Cancer Statistics, 2014.” *CA: A Cancer Journal for Clinicians* 64 (1):9–29. https://doi.org/10.3322/caac.21208.

Simmini, Salvatore, Monika Bialecka, Meritxell Huch, Lennart Kester, Marc van de Wetering, Toshiro Sato, Felix Beck, Alexander van Oudenaarden, Hans Clevers, and Jacqueline Deschamps. 2014. “Transformation of Intestinal Stem Cells into Gastric Stem Cells on Loss of Transcription Factor Cdx2.” *Nature Communications* 5 (January):5728. https://doi.org/10.1038/ncomms6728.

Stange, Daniel E, Bon-Kyoung Koo, Meritxell Huch, Greg Sibbel, Onur Basak, Anna Lyubimova, Pekka Kujala, et al. 2013. “Differentiated Troy+ Chief Cells Act as Reserve Stem Cells to Generate All Lineages of the Stomach Epithelium.” *Cell* 155 (2):357–68. https://doi.org/10.1016/j.cell.2013.09.008.

Takahashi, Yoshihisa, and Toshio Fukusato. 2014. “Histopathology of Nonalcoholic Fatty Liver Disease/nonalcoholic Steatohepatitis.” *World Journal of Gastroenterology* 20 (42). Baishideng Publishing Group Inc:15539–48. https://doi.org/10.3748/wjg.v20.i42.15539.

Talabnin, Chutima, Patcharee Janthavon, Sunisa Thongsom, Wipa Suginta, Krajang

Talabnin, and Sopit Wongkham. 2016. “Ring Finger Protein 43 Expression Is Associated with Genetic Alteration Status and Poor Prognosis among Patients with Intrahepatic Cholangiocarcinoma.” *Human Pathology* 52 (June):47–54. https://doi.org/10.1016/j.humpath.2015.12.027.

Tan, Xinping, Udayan Apte, Amanda Micsenyi, Emorphia Kotsagrelos, Jian-Hua Luo, Sarangarajan Ranganathan, Dulabh K Monga, Aaron Bell, George K Michalopoulos, and Satdarshan P S Monga. 2005. “Epidermal Growth Factor Receptor: A Novel Target of the Wnt/beta-Catenin Pathway in Liver.” *Gastroenterology* 129 (1):285–302. http://www.ncbi.nlm.nih.gov/pubmed/16012954.

Tan, Xinping, Jaideep Behari, Benjamin Cieply, George K. Michalopoulos, and Satdarshan P.S. Monga. 2006. “Conditional Deletion of β-Catenin Reveals Its Role in Liver Growth and Regeneration.” *Gastroenterology* 131 (5):1561–72. https://doi.org/10.1053/j.gastro.2006.08.042.

Tolba, R, T Kraus, C Liedtke, M Schwarz, and R Weiskirchen. 2015. “Diethylnitrosamine (DEN)-Induced Carcinogenic Liver Injury in Mice.” *Laboratory Animals* 49 (1_suppl):59–69. https://doi.org/10.1177/0023677215570086.

Tostões, Rui M., Sofia B. Leite, Margarida Serra, Janne Jensen, Petter Björquist, Manuel J. T. Carrondo, Catarina Brito, and Paula M. Alves. 2012. “Human Liver Cell Spheroids in Extended Perfusion Bioreactor Culture for Repeated-Dose Drug Testing.” *Hepatology* 55 (4). Wiley Subscription Services, Inc., A Wiley Company:1227–36. https://doi.org/10.1002/hep.24760.

Tyson, Gia L, and Hashem B El-Serag. 2011. “Risk Factors for Cholangiocarcinoma.” *Hepatology (Baltimore, Md.)* 54 (1). NIH Public Access:173–84. https://doi.org/10.1002/hep.24351.

Uehara, T., G. R. Ainslie, K. Kutanzi, I. P. Pogribny, L. Muskhelishvili, T. Izawa, J. Yamate, et al. 2013. “Molecular Mechanisms of Fibrosis-Associated Promotion of Liver Carcinogenesis.” *Toxicological Sciences* 132 (1):53–63. https://doi.org/10.1093/toxsci/kfs342.

Uehara, Takeki, Igor P Pogribny, and Ivan Rusyn. n.d. “The DEN and CCl 4 -Induced

Mouse Model of Fibrosis and Inflammation-Associated Hepatocellular Carcinoma." https://doi.org/10.1002/0471141755.ph1430s66.

Vassilev, Lyubomir T, Binh T Vu, Bradford Graves, Daisy Carvajal, Frank Podlaski, Zoran Filipovic, Norman Kong, et al. 2004. "In Vivo Activation of the p53 Pathway by Small-Molecule Antagonists of MDM2." *Science (New York, N.Y.)* 303 (5659):844–48. https://doi.org/10.1126/science.1092472.

Wang, Bruce, Ludan Zhao, Matt Fish, Catriona Y. Logan, and Roel Nusse. 2015. "Self-Renewing Diploid Axin2+ Cells Fuel Homeostatic Renewal of the Liver." *Nature* 524 (7564). Nature Research:180–85. https://doi.org/10.1038/nature14863.

Wang, Kai, Siu Tsan Yuen, Jiangchun Xu, Siu Po Lee, Helen H N Yan, Stephanie T Shi, Hoi Cheong Siu, et al. 2014. "Whole-Genome Sequencing and Comprehensive Molecular Profiling Identify New Driver Mutations in Gastric Cancer." *Nature Genetics* 46 (6):573–82. https://doi.org/10.1038/ng.2983.

Wend, Peter, Jane D Holland, Ulrike Ziebold, and Walter Birchmeier. 2010. "Wnt Signaling in Stem and Cancer Stem Cells." *Seminars in Cell & Developmental Biology* 21 (8):855–63. https://doi.org/10.1016/j.semcdb.2010.09.004.

Wetering, Marc van de, Hayley E Francies, Joshua M Francis, Gergana Bounova, Francesco Iorio, Apollo Pronk, Winan van Houdt, et al. 2015. "Prospective Derivation of a Living Organoid Biobank of Colorectal Cancer Patients." *Cell* 161 (4):933–45. https://doi.org/10.1016/j.cell.2015.03.053.

White, Donna L., Fasiha Kanwal, and Hashem B. El–Serag. 2012. "Association Between Nonalcoholic Fatty Liver Disease and Risk for Hepatocellular Cancer, Based on Systematic Review." *Clinical Gastroenterology and Hepatology* 10 (12):1342–1359.e2. https://doi.org/10.1016/j.cgh.2012.10.001.

Wiegand, Kimberly C, Sohrab P Shah, Osama M Al-Agha, Yongjun Zhao, Kane Tse, Thomas Zeng, Janine Senz, et al. 2010. "ARID1A Mutations in Endometriosis-Associated Ovarian Carcinomas." *The New England Journal of Medicine* 363 (16):1532–43. https://doi.org/10.1056/NEJMoa1008433.

Wilhelm, Scott M., Christopher Carter, LiYa Tang, Dean Wilkie, Angela McNabola,

Hong Rong, Charles Chen, et al. 2004. “BAY 43-9006 Exhibits Broad Spectrum Oral Antitumor Activity and Targets the RAF/MEK/ERK Pathway and Receptor Tyrosine Kinases Involved in Tumor Progression and Angiogenesis.” *Cancer Research* 64 (19):7099–7109. https://doi.org/10.1158/0008-5472.CAN-04-1443.

Williamson, Chris T., Rowan Miller, Helen N. Pemberton, Samuel E. Jones, James Campbell, Asha Konde, Nicholas Badham, et al. 2016. “ATR Inhibitors as a Synthetic Lethal Therapy for Tumours Deficient in ARID1A.” *Nature Communications* 7 (December). Nature Publishing Group:13837. https://doi.org/10.1038/ncomms13837.

Wolpin, Brian M, Cosmeri Rizzato, Peter Kraft, Charles Kooperberg, Gloria M Petersen, Zhaoming Wang, Alan A Arslan, et al. 2014. “Genome-Wide Association Study Identifies Multiple Susceptibility Loci for Pancreatic Cancer.” *Nature Genetics* 46 (9):994–1000. https://doi.org/10.1038/ng.3052.

Wu, Jennifer N, and Charles W M Roberts. 2013. “ARID1A Mutations in Cancer: Another Epigenetic Tumor Suppressor?” *Cancer Discovery* 3 (1):35–43. https://doi.org/10.1158/2159-8290.CD-12-0361.

Wu, Jian, Yuchen Jiao, Marco Dal Molin, Anirban Maitra, Roeland F de Wilde, Laura D Wood, James R Eshleman, et al. 2011. “Whole-Exome Sequencing of Neoplastic Cysts of the Pancreas Reveals Recurrent Mutations in Components of Ubiquitin-Dependent Pathways.” *Proceedings of the National Academy of Sciences of the United States of America* 108 (52):21188–93. https://doi.org/10.1073/pnas.1118046108.

Yang, Jing, Laura E. Mowry, Kari Nichole Nejak-Bowen, Hirohisa Okabe, Cassandra R. Diegel, Richard A. Lang, Bart O. Williams, and Satdarshan P. Monga. 2014. “Beta-Catenin Signaling in Murine Liver Zonation and Regeneration: A Wnt-Wnt Situation!” *Hepatology* 60 (3):964–76. https://doi.org/10.1002/hep.27082.

Yang, Liu, Youngmi Jung, Alessia Omenetti, Rafal P. Witek, Steve Choi, Hendrika M. Vandongen, Jiawen Huang, Gianfranco D. Alpini, and Anna Mae Diehl. 2008. “Fate-Mapping Evidence That Hepatic Stellate Cells Are Epithelial Progenitors in Adult Mouse Livers.” *Stem Cells* 26 (8):2104–13. https://doi.org/10.1634/stemcells.2008-0115.

Yanger, Kilangsungla, David Knigin, Yiwei Zong, Lara Maggs, Guoqiang Gu, Haruhiko Akiyama, Eli Pikarsky, and Ben Z. Stanger. 2014. “Adult Hepatocytes Are Generated by Self-Duplication Rather than Stem Cell Differentiation.” *Cell Stem Cell* 15 (3):340–49. https://doi.org/10.1016/j.stem.2014.06.003.

Yoo, Kyo-Sang, Woo Taek Lim, and Ho Soon Choi. 2016. “Biology of Cholangiocytes: From Bench to Bedside.” *Gut and Liver* 10 (5):687–98. https://doi.org/10.5009/gnl16033.

Yu, Jia, and David M Virshup. 2014. “Updating the Wnt Pathways.” *Bioscience Reports* 34 (5). Portland Press Ltd.:593–607. https://doi.org/10.1042/BSR20140119.

Zender, Steffen, Irina Nickeleit, Torsten Wuestefeld, Inga Sörensen, Daniel Dauch, Przemyslaw Bozko, Mona El-Khatib, et al. 2013. “A Critical Role for Notch Signaling in the Formation of Cholangiocellular Carcinomas.” *Cancer Cell* 23 (6):784–95. https://doi.org/10.1016/j.ccr.2013.04.019.

Zhang, Jian, Jing Zhao, Wen-jie Jiang, Xi-wei Shan, Xiao-mei Yang, and Jian-gang Gao. 2012. “Conditional Gene Manipulation: Cre-Ating a New Biological Era.” *Journal of Zhejiang University. Science. B* 13 (7):511–24. https://doi.org/10.1631/jzus.B1200042.

Zhao, Hong, Jian Wang, Yongqing Han, Zhen Huang, Jianming Ying, Xinyu Bi, Jianjun Zhao, et al. 2011. “ARID2: A New Tumor Suppressor Gene in Hepatocellular Carcinoma.” *Oncotarget* 2 (11):886–91. http://www.pubmedcentral.nih.gov/articlerender.fcgi?artid=3259997&tool=pmcentrez&rendertype=abstract.

Zhou, Yehui, Jing Lan, Wei Wang, Qin Shi, Yang Lan, Zhiyi Cheng, and Honggeng Guan. 2013. “ZNRF3 Acts as a Tumour Suppressor by the Wnt Signalling Pathway in Human Gastric Adenocarcinoma.” *Journal of Molecular Histology* 44 (5):555–63. https://doi.org/10.1007/s10735-013-9504-9.

Zou, Shanshan, Jiarui Li, Huabang Zhou, Christian Frech, Xiaolan Jiang, Jeffrey S. C. Chu, Xinyin Zhao, et al. 2014. “Mutational Landscape of Intrahepatic Cholangiocarcinoma.” *Nature Communications* 5 (December):5696. https://doi.org/10.1038/ncomms6696.

9. ANNEX

Table 9.1. List of tissues from donors and patients used for isolation.

Sample	Gender	Age	Nodal Metastasis	Histological grade	Ki67 staining	Organoid growth	Organoid expansion	Derivation rate (%)	Expansion rate (%)
CC-1	F	34	Yes	CC mod/well diff.	++++	✓	✓	100%	88%
CC-2	M	68	No	CC mod diff.	+++	✓	✓		
CC-3	M	64	No	CC poorly diff.	+++	✓	✓		
CHC-1	F	56	No	CHC - Classical	++	✓	✓		
CHC-2	F	61	Yes	CHC - SC	++++	✓	✓		
HCC-1	M	69	No	HCC mod/well diff.	+++	✓	✓		
HCC-2	M	52	No	HCC mod/well diff.	+++	✓	✗		
HCC-3	F	71	N/A	HCC mod diff.	+++	✓	✓		
wCC-1	F	54	No	CC well diff.	+/-	✗	✗	0%	0%
wHCC-1	M	78	No	HCC well diff.	+/-	✗	✗		
wHCC-2	M	57	No	HCC well diff.	+/-	✗	✗		
wHCC-3	M	77	No	HCC well diff.	+/-	✗	✗		
wHCC-4	F	70	No	HCC well diff.	+/-	✗	✗		
wHCC-5	M	76	No	HCC well diff.	+/-	✗	✗		
wHCC-6	M	75	No	HCC well diff.	+/-	✗	✗		
wHCC-7	M	72	No	HCC well diff.	+/-	✗	✗		
wHCC-8	M	66	No	HCC well diff.	+/-	✗	✗		
Healthy-1	M	23	Healthy liver; biopsy obtained from donor tissue used for transplantation			✓	✓	100%	100%
Healthy-2	F	44				✓	✓		
Healthy-3	M	50				✓	✓		

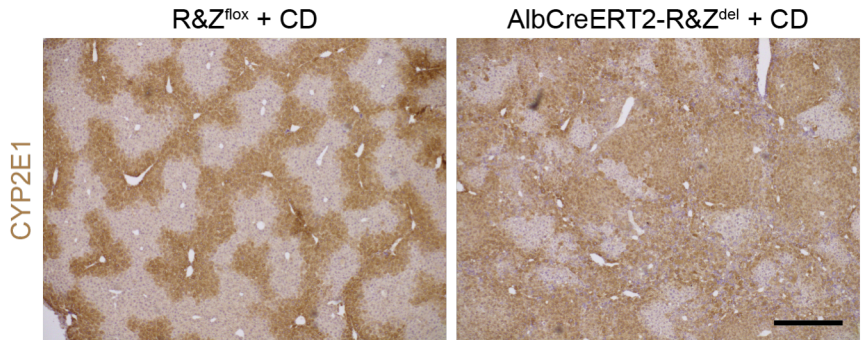

Figure 9.1. CYP2E1 immunostaining. Immunostaining of CYP2E1 on R&Z control and deleted livers following CD. Liver were collected 3 months after the first tamoxifen injection. Scale bar, 500 µm.

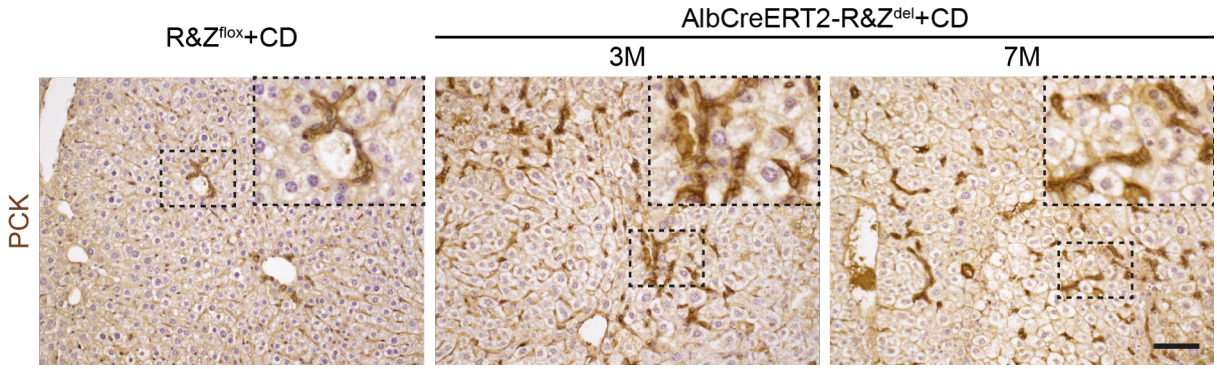

Figure 9.2. PCK immunostaining. Immunostaining of PCK on R&Z control and deleted livers following CD. Liver were collected 3 and 7 months after the first tamoxifen injection. Scale bar, 100µm.

10. AKNOWLEDGEMNTS

To begin, I would like to express my sincerest gratitude to my supervisors, to Dr. Bon-Kyoung Koo, for giving me the opportunity to undertake this arduous but rewarding experience here at Cambridge, and to Dr. Meritxell Huch, for the steadfast supervision and continual support during many challenging times.

And a special “thank you” to Dr. Laura Broutier for her excellent work with the tumoroid project and for making our collaboration very successful — and, even more importantly, for her moral and scientific support since she joined the lab.

Thanks to my PhD advisor, Dr. Christine Farr, for the advice and feedback she provided during my assessments and for always being available for discussion. Thanks to Robert Arnes for the essential help with tissue sectioning and staining. Thanks to Mikel Mckie for proofreading the manuscript and always being ready to help. Thanks to Dr. Susan Davies for pathological examination of the tissue samples used in the project.

I would also like to thank all the members of the Huch lab — especially Lucia, for our many important life discussions and her weirdness; Luigi, for our enlightening scientific discussion and precious advice; Chris, because he was my primary source of knowledge when I first joined the lab; Daisy, for her unique ‘daisy-ness’; Nicole, for being my PhD rock; and everybody else in the lab, for always being ready for a night at the pub whenever it was needed.

Also, thanks to Alessa’, for her constant physical and ‘telephonic’ presence; Timo, for being a redoubtable opponent; Michael, for precious help with Illustrator.

Finally, I would like to thank the ITN Marie Curie WntsApp FP7 Programme for their generous funding and all at The Wellcome/CRUK Gurdon Institute and Wellcome/MRC Cambridge Stem Cell Institute, with special mention to the biofacilities staff.

Last but not the least, I would like to thank my family: my parents and my brothers and sister for supporting me mentally and emotionally throughout writing this thesis and throughout my life in general.

INDEX